Université de Montréal

Bayesian Modeling of Biological Motion Perception in Sport

Modélisation bayésienne de la perception du mouvement biologique dans le sport

par Khashayar Misaghian

École d'optométrie

Thèse présentée
en vue de l'obtention du grade de doctorat
en Sciences de la Vision
option Neurosciences de la vision et psychophysique

Janvier 2020

Résumé

La perception d'un mouvement biologique correspond à l'aptitude à recueillir des informations (comme par exemple, le type d'activité) issues d'un objet animé en mouvement à partir d'indices visuels restreints. Cette méthode a été élaborée et instaurée par Johansson en 1973, à l'aide de simples points lumineux placés sur des individus, à des endroits stratégiques de leurs articulations. Il a été démontré que la perception, ou reconnaissance, du mouvement biologique joue un rôle déterminant dans des activités cruciales pour la survie et la vie sociale des humains et des primates. Par conséquent, l'étude de l'analyse visuelle de l'action chez l'Homme a retenu l'attention des scientifiques pendant plusieurs décennies. Ces études sont essentiellement axées sur informations cinématiques en provenance de différents mouvements (comme le type d'activité ou les états émotionnels), le rôle moteur dans la perception des actions ainsi que les mécanismes sous-jacents et les substrats neurobiologiques associés.

Ces derniers constituent le principal centre d'intérêt de la présente étude, dans laquelle nous proposons un nouveau modèle descriptif de simulation bayésienne avec minimisation du risque. Ce modèle est capable de distinguer la direction d'un ballon à partir d'un mouvement biologique complexe correspondant à un tir de soccer.

Ce modèle de simulation est inspiré de précédents modèles, neurophysiologiquement possibles, de la perception du mouvement biologique ainsi que de récentes études. De ce fait, le modèle présenté ici ne s'intéresse qu'à la voie dorsale qui traite les informations visuelles relatives au mouvement, conformément à la théorie des deux voies visuelles. Les stimuli visuels utilisés, quant à eux, proviennent d'une précédente étude psychophysique menée dans notre laboratoire chez des athlètes. En utilisant les données psychophysiques de cette étude antérieure

et en ajustant une série de paramètres, le modèle proposé a été capable de simuler la fonction psychométrique ainsi que le temps de réaction moyen mesurés expérimentalement chez les athlètes.

Bien qu'il ait été établi que le système visuel intègre de manière optimale l'ensemble des indices visuels pendant le processus de prise de décision, les résultats obtenus sont en lien avec l'hypothèse selon laquelle les indices de mouvement sont plus importants que la forme dynamique dans le traitement des informations relatives au mouvement.

Les simulations étant concluantes, le présent modèle permet non seulement de mieux comprendre le sujet en question, mais s'avère également prometteur pour le secteur de l'industrie. Il permettrait, par exemple, de prédire l'impact des distorsions optiques, induites par la conception de verres progressifs, sur la prise de décision chez l'Homme.

Mots-clés : Mouvement biologique, Bayésien, Voie dorsale, Modèle de simulation hiérarchique, Fonction psychométrique, Temps de réaction

Abstract

The ability to recover information (e.g., identity or type of activity) about a moving living object from a sparse input is known as Biological Motion perception. This sparse input has been created and introduced by Johansson in 1973, using only light points placed on an individual's strategic joints. Biological motion perception/recognition proves to play a significant role in activities that are critical to the survival and social life of humans and primates. In this regard, the study of visual analysis of human action had the attention of scientists for decades. These studies are mainly focused on: kinematics information of the different movements (such as type of activity, emotional states), motor role in the perception of actions and underlying mechanisms, and associated neurobiological substrates.

The latter being the main focus of the present study, a new descriptive risk-averse Bayesian simulation model, capable of discerning the ball's direction from a set of complex biological motion soccer-kick stimuli is proposed.

Inspired by the previous, neurophysiologically plausible, biological motion perception models and recent studies, the simulation model only represents the dorsal pathway as a motion information processing section of the visual system according to the two-stream theory, while the stimuli used have been obtained from a previous psychophysical study on athletes. Moreover, using the psychophysical data from the same study and tuning a set of parameters, the model could successfully simulate the psychometric function and average reaction time of the athlete participants of the aforementioned study.

Although it is established that the visual system optimally integrates all available visual cues in the decision-making process, the results conform to the speculations favouring motion cue importance over dynamic form by only depending on motion information processing.

As a functioning simulator, the present simulation model not only introduces some insight into the subject at hand but also shows promise for industry use. For example, predicting the impact of the lens-induced distortions, caused by various lens designs, on human decision-making.

Keywords : Biological motion, Bayesian, Dorsal pathway, Hierarchical simulation model, Psychometric function, Reaction time

Table des matières

Liste des tableaux

Liste des figures

Liste des sigles

3D : Three Dimensional

STS : Superior Temporal Sulcus

V1/2 : Visual Areas 1 and 2

MT : Medial Temproal Area

MST : Medial Superior Temporal

KO : Kinetic Occipital

V3B : Ventral 3 Area B

SD: Standard Deviation

RDM: Random Dot Movement

To My Dear Family, and in the Memory of Flight #PS752

Remerciements

First off, I would like to express my deepest gratitude to my advisor Prof. Jocelyn Faubert for his trust and continuous support, none of this would have had happened without him. His mentorship not only helped me in my research but also guided me in all other areas of my life. I could not have imagined having a better advisor and mentor for my PhD study.

Additionally, I must thank my other dear advisor, Dr. Eduardo Lugo, for his encouragement, patience and specifically his immense knowledge. His counsel was integral to the existence of the present study.

Maman, Baba and Parisi, thanks for all the love you have given me since Day One, Without your support, doing this doctorate would not have been possible. I love you all.

I will be forever grateful to the fellows from the lab for their support, especially: Dr. Delphine Bernardin, Raphael Doti, Vadim Sutyuchev, Marie Maze, Sergio Mejia, Yannick Roy, Thomas Romeas, Robyn Lahiji, Laura Mikula. Also, friends and fellows from the department: dearest Umit Keysan, Bruno Oliveira, Nelson Cortes, Sabine Demosthènes, Sylvie Beaudoin.

Last but not least, my greatest love and appreciation to my friends who were there for me during this journey: Marie-Claude Légaré, Sajjad Ghaemi, Amir Pourmorteza, Ali Seyedi, Behzad Barzegar, Reza Maghsoudi.

Introduction

Early Inspirations for Computational Brain Models

In 1973 Alan Newell argued that the scientific trend in the field of psychology and cognitive science must reach beyond mere reductionism. Despite all functional aspects of reductionism, he believed that endeavours should lead to a unified knowledge integrated into a unified human-information processing model that could perform generalized tasks and could explain the exploitation and the synergy of the brain's sub-functions (Kriegeskorte & Douglas, 2018; Newell, 1994).

On the other hand, the advent of ground-breaking imaging techniques like fMRI gave rise to the field of cognitive neuroscience, which succeeded in mapping the global functional layout of the brain, initially by associating task-related activations to the brain regions.

Despite its high importance, one could not discover the related cognitive mechanism and subfunctions of the brain using such experimental manipulations in imaging. The reason is implicit in the *reverse-inference* problem which states that, since a variety of processes could be employed in the brain to accomplish a particular task, one could not infer the underlying cognitive processes based on an experimental manipulation or, in simple words, there is more than one cause for the same effect (Poldrack, 2006). So, no matter how advanced or high resolution the brain maps are, they could not unveil the underlying computational mechanisms due to the nature of the *reverse-inference* problem.

Ultimately, a computational brain model could be envisioned as a model made up of biologically plausible components, which perform complicated cognitive tasks to re-enact behavior while using data from cognitive science or psychophysical experiments as criteria to corroborate, reject or fine-tune its foundations and functions.

How to Tackle the Problem of Computational Modeling?

Marr introduced the notion of *levels of analysis,* stating that the analysis (?) of a complex system should be conducted at different levels: computational, algorithmic and at an implementation level. Also, Marr believed that one should not proceed to a higher (?) level of analysis unless the system has been characterized at its introductory level.

At the computational level, the concern is focused on the function of the system (definition of the task) and why it is necessary to execute such a function or performance (the goal of computation). Then, at the algorithmic or representational level, one must investigate *how* the system executes what it executes, in other words, how inputs are being represented and then manipulated to the outputs. Furthermore, at the implementation level, the question is how to materialize what we learned on the algorithmic level to replicate the function of the system (Kriegeskorte & Douglas, 2018; Marr & Poggio, 1976).

Generally, Marr's taxonomy provided a robust framework for intuitively describing models of perception and cognition. This is because, first, the insights from a higher level keep the researcher from pursuing redundant questions on lower levels and, second, studying the system on all levels in this way embodies the connection between experimental and theoretical findings in neuroscience (Poggio, 2012).

Subsequently, Poggio, the coauthor of the original hypothesis, made an amendment to the tri-level manifesto of the late Marr, arguing that to understand and be able to describe how an organism learns from its experience in the real world might be even more critical and insightful than the characterization of what that organism has learned in detail. Therefore, he proposed a new level to be added above the computational level, called learning (Poggio, 2012).

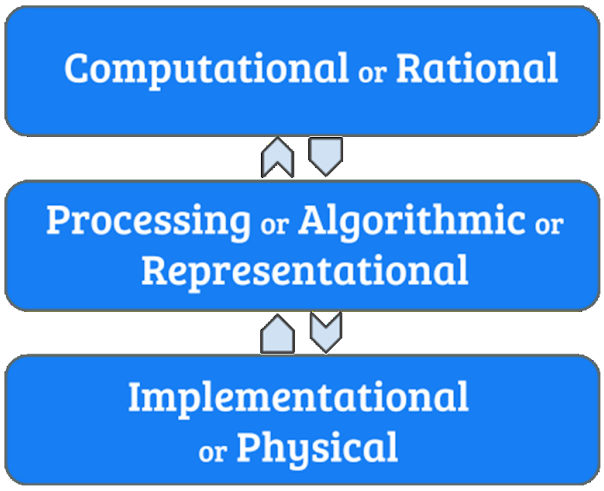

Figure 1-1: Marr's levels of analysis (Commons, 2018)

Implementation Level

In order to create a realistic neural code from this viewpoint, one must consider the fact that neurons work together. So, to discover a neural code close to realism means to reveal how these neurons co-function. Observations of stereotyped patterns across the cortex which lead to the theory of repeated motifs of cortical microcircuits (Creutzfeldt, 1977) inspired some models that tried to explain the dynamics of a population of neurons, namely, mean field and neural mass models which were, in fact, systems of ordinary differential equations (Coombes, 2010).

One of the more recent and more realistic neural-population dynamic models of this kind is the canonical microcircuit model that incorporates more details such as local recurrences in its dynamic (Bastos et al., 2012).

One common exciting fact about all these models, from the most simple to the most complex, is the importance of the balance of inhibition and excitation between neurons which appeared to be a theme in the more recent studies, suggesting that an efficient neural code essentially requires a tight excitation and inhibition balance (Denève & Machens, 2016).

However population-dynamics models are not showing much promise when it comes to explaining the interactions between cortical regions. Therefore, neuroscience resorts to connectivity models such as structural connectivity and functional connectivity models from which the graph-theoretic measures could be generated using thresholding, which shows the connection hubs between different regions of the brain. However, such models can not include latencies as well as indirect connectivities between brain regions (Sporns, 2007).

Finally, effective connectivity methods are biologically plausible; they take latencies and indirect inter-regional connections into account. The idea is that one biophysical model like the canonical microcircuit and one measurement model like lead field model (if we are dealing with EEG data) is being assigned to each region under investigation, and from that a wide range of dynamics in EEG, fMRI and other forms of data could be described or generated. Nonetheless, they are built on mean overall activations of the regions and generally are not suitable to perform actual cognitive tasks (Stephan & Friston, 2010).

Representational and Algorithm Level.

While the traditional analyses are focused on the change in the overall activity of a region throughout a task, representational models seek to explain how brain activity patterns are related

to cognitive processes, responses or even stimuli. In other words, the objective is how neurons *represent* and process the information. In that regard encoding and decoding models exist: encoding models use the features from the stimuli to predict the brain responses, whereas decoding models try to predict the aspects of the stimuli from brain activation patterns. Other than stimulus reconstruction, a decoding model could contribute to understanding the representational content of a fine grain pattern or shed light on which areas between task and response contain mutual information (Diedrichsen & Kriegeskorte, 2017).

Moreover, algorithm-based models like, neural network models, reinforcement learning, Bayesian models also belong to this level of analysis. Neural networks have been used as brain computational models in recent years to explain or predict human behaviour and brain activity data and to perform high-level tasks (Kriegeskorte, 2015). The convolutional recurrent network which incorporated long-range connections into its architecture inspired by structural connectivities in the brain to model object recognition in the visual system (Nayebi et al., 2018), and canonical microcircuit based models within Bayesian framework in the work of (Moran, Pinotsis, & Friston, 2013) are two more recent examples.

Modeling Circuit Mechanisms and Neural Dynamics of Decision-making

Decision Making as a Proof of Life

Biologists make the assertion that "life is irritable." Therefore, an entity is considered a living organism as long as it creates a purposeful response to the environment's stress that impacts it. One thoughtful, resolute response to a situation indeed entails the concept of decision making. According to this view, the act of decision making is one common thing among all living things (Dobransky, 1999).

Unlike a rock that does nothing actively in response to its surroundings, a frog decides to hop away from the predator, a tree grows its branches towards light and not the shade, and these are all decisions made in response to what presented by the environment. On the human level, decisions are what renders each person's identity without equal on earth and that identity comes from nothing but the sum of all and every single decision ever made until that time point by that person (Dobransky, 1999).

The above could shed some light on the importance of decisions and, consequently, their mechanisms in every aspect of the lives of living organisms.

There Will Be Uncertainty

Decision-making could be viewed as an act of finding a solution to a problem (presented by the environment). The solution has to be satisfactory or even better: optimal. Such a process could be based on the agent's knowledge of explicit or tacit nature, while the result would be rational or irrational (Brockmann & Anthony, 2002). Furthermore, finding a solution could be construed as a simple act of choosing an alternative among multiple alternatives. Reality dictates that different circumstances could lead to different results and, the more of them there are, the less certain would the agent be about the outcomes. So, one could say that the nature of the events in our universe begets uncertainty in making a decision, and that is why choice under uncertainty is the core of decision theory.

Decision theory dates back to the 17th century when Pascal introduced the notion of expected value as a criterion for making a decision in the sense that, by knowing the value of each outcome and its probability and by multiplying these two numbers, one has the expected value of each result and could simply choose the one with the highest value as the winning alternative. In the following century, Bernoulli, using the St. Petersburg Paradox, argued that such a solution to the problem of decision making is suboptimal and, to resolve this conundrum, he introduced the expected utility hypothesis which asserts that only counting on expected value would not suffice and other factors like the agent's wealth, the diminishing marginal benefit and the cost of entering the game must be taken into consideration in the form of one utility function. Thereupon, the agent could make an optimal decision (Schoemaker, 1982).

The resurfacing of the Bayesian probability theory in the 20th century extended the capacities of the expected utility theory and "expected utility maximization" was able to explain some rational behaviours, (Von Neumann, Morgenstern, & Kuhn, 2007). Later, Maurice Allais and Daniel Ellsberg demonstrated systematic deviation from expected-utility maximization in many human behaviors. After that, the prospect theory renewed the experimental economic behavior studies, introducing three distinct regularities in human decision making (Allais & Hagen, 2013):

1. Losses appear larger than gains

2. The agent has more focus on changes in the utility rather than the actual utilities

3. The initial piece of information offered to the agent at the beginning of the process critically affects its estimation of subjective probabilities

Ultimately, it is safe to say that the process of decision making is a statistical phenomenon and any effort to explain or model such a process must indeed capture its essence of randomness.

Brain: Our Statistical Decision-Making Machine

So far, we believe that our nervous system, with the brain as its chief, is in charge of the decisions that we make. Even though establishing decision-making as a statistical process does not entail that decision-making happens in the same fashion in the brain, a wide range of evidence and the hypotheses built upon it consolidates the idea that the brain is, in fact, a statistical computation machine. For instance, using the logarithm of the likelihood ratio of alternatives as a single quantity that could incorporate many aspects of a statistical decision variable over time, researchers have proposed neural computations that could explain the categorical decisions about sensory stimuli and their substrata in the brain based on electrophysiological studies (Gold & Shadlen, 2001, 2007).

As another example, one recent study suggests that the feeling that one gets after making any decision is called "confidence" in the decision. The results indicate that despite the subjective essence of this notion of confidence, as a matter of fact, it depends on objective statistical calculations (Sanders, Hangya, & Kepecs, 2016).

These are just two primary examples of how the neural computations taking place in the brain are parallel to statistical calculations. Therefore, not only that uncertainty is a significant natural element embedded in the decision-making process but, also, the agent, being the brain, calculates probabilities to achieve a final decision. Considering these notions, the path to model the decision making on any level is clearer. However, to make a good start, one should examine the process on a deeper level.

More Practical Definition of Decision-Making

When it comes to defining the process of decision-making, everyone automatically recalls only the act of choosing, but this process in living creatures in its entirety is a concept beyond that. A good explanation of the organic process of decision-making is: forming a

judgment about an issue of certain difficulty under various conditions of exigency and risk. In other words, the decision-maker happens to make the right decision about an identical problem for a different range of urgency and risk situations. For example, one has to cross a highway with fast-moving cars while being chased by wild dogs or has to pass the very same road with the same fast cars being rewarded for the most nimble performance at its best convenience.

Moreover, a long history of behavioral studies corroborates this intuitive notion that decisions are less accurate when conditions side with speed and are more accurate when they favour accuracy, also referred to as speed-accuracy trade-off (SAT)(Fitts, 1966; Standage, Blohm, & Dorris, 2014; Wickelgren, 1977). At the same time, there is often the element of risk involved in every quotidian decision and, not surprisingly, has been a matter of investigation in a whole diverse spectrum of subjects from cognitive studies to neuro-economics (Braun, Nagengast, & Wolpert, 2011; Dayan & Niv, 2008; Nagengast, Braun, & Wolpert, 2010; Niv, Edlund, Dayan, & O'Doherty, 2012; Shen, Tobia, Sommer, & Obermayer, 2014).

The more elaborate the definition is, the clearer are the features that need to be addressed by proposed models. It also shows what would be the next step towards a more general model beyond what already exists.

Having a rather good definition of the decision-making process facilitates discussion of the ways to model it. First, at the representational level and from there, we could gradually proceed to the implementation level.

Modeling of Decision Making

Given levels of abstraction in modeling, models of decision making are accordingly categorized into algorithmic (representational) and implementation levels (Marr, 1982). Intuitively, all proposed models always fall somewhere between these two ends of the modeling spectrum (Standage et al., 2014). Moreover, interestingly, analytic studies demonstrate that under certain conditions and assumptions, implementation-level models could be deemed equivalent to algorithmic models, which provides a massive degree of flexibility when it comes to having a neural code (Bogacz, Brown, Moehlis, Holmes, & Cohen, 2006).

The most extensively adhered-to hypothesis in decision making is the bounded integration framework. According to this framework, the decision-making agent integrates the available noisy evidence of different alternatives in various specific fashions until the

aggregating total meets a criterion level. The aggregating amount is referred to as a decision variable, while the criterion level is referred to as bound. A higher bound allows for a longer time of evidence integration, which could lead to more accurate decisions due to more information. More precisely, integration low-pass filtering quality helps with averaging the accumulating evidence in the presence of noise either in the neural processes or the evidence itself. So, clearly the more prolonged the integration time, the better the average and the higher the chance of accurate decision (Bogacz, Wagenmakers, Forstmann, & Nieuwenhuis, 2010; Ratcliff & McKoon, 2008; P. L. Smith & Ratcliff, 2004; Standage et al., 2014).

It was mentioned previously that the integration of evidence from alternatives by the model could be conducted in different fashions and that is one ground on which the families of bounded integration algorithmic models are categorized;

- **Race models:** when the evidence of each alternative is integrated independently from the others
- **Drift diffusion models (DDM):** when the evidence for each choice serves as evidence against the other (two alternative tasks) (Fig 1-2).
- **Competing accumulator models:** considered as arbitration between models above; this time, each decision variable associated with its respective alternative gets subtracted by other weighted decision variables.

Only by changing the weights in Competing accumulator models, one could transition from pure race models to absolute DDMs. More importantly, this class of models incorporates multi alternative tasks while it serves as a gateway where the algorithmic level could be interpreted into implementation level (Standage et al., 2014).

It is beneficial to emphasize several points before moving further with the bounded integration modeling at the implementation level: Firstly, the decision variable is not necessarily made up of the input associated with evidence, and, in reality, there exist other inputs besides evidence. For example, inputs that modulate prior probabilities of the evidence. This notion elucidates the distinction between the decision variable and the amount of integrated modulated evidence, albeit the implications in defining the bounded integration framework in which evidence of an alternative and the decision variable seemed interchangeable (Standage et al., 2014); Secondly, it was mentioned that the integration helps with noise reduction but, in reality,

noise is not always white. In other words, the autocorrelation of the noise signal, in reality, is not zero and there would be a correlation time, that could only mean that the benefits of integration depend on the timescale of noise correlations (Standage et al., 2014). Finally, although integration operation pertains to the continuous-time domain, for simplicity here, accumulation of evidence in discrete time is being referred to as integration.

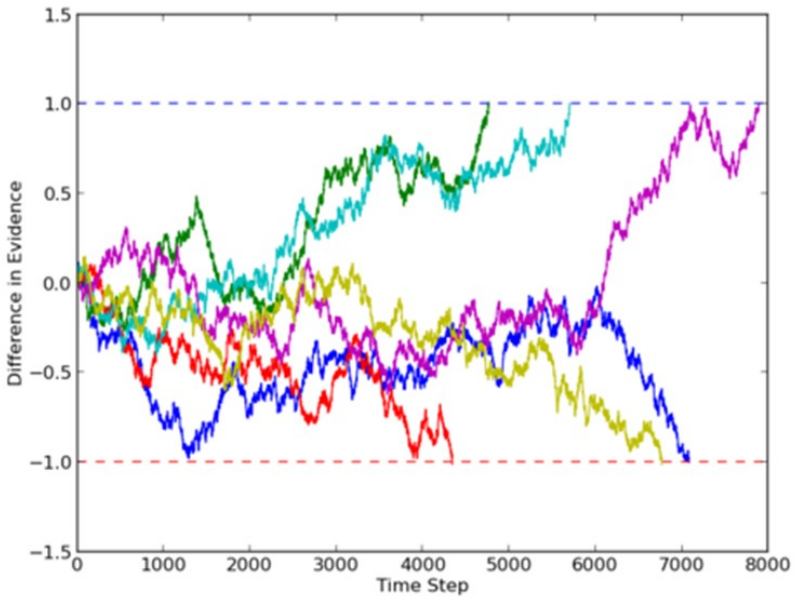

Figure 1-2: Example graph of accumulation of evidence in a Drift-Diffusion Model, with a source at 100% noise (Commons, 2017)

Now that some light has been shed on the body of work trying to characterize the computations underlying decision making (Ratcliff & McKoon, 2008; P. L. Smith & Ratcliff, 2004), the leading existing hypotheses on identification of neural correlates of these computations may be examined further (Gold & Shadlen, 2007; Kable & Glimcher, 2009; Schall, 2001).

Neural Correlates of Decision Making

Signal Detection Theory and Sequential Analysis

It has been highlighted above that multiple pieces of evidence shall come together in time, for an agent, in order to pick an alternative. This could be all substantiated within *sequential analysis* as an extension to *signal detection theory*. According to *signal detection theory*, to infer whether the signal is present or not makes up two hypotheses: h_1, the signal is present, and h_2, the signal is not present. Now, evidence e bears on the likelihood of each h_1 and h_2 to be true. Likelihood of h_1 states how likely it is that the $h_1$is true, given e, ($P(h_1|e)$).

The good news is that, in order to decide which hypothesis is true, we do not necessarily need the exact level of likelihood, but that only the ratio of the two likelihoods, LR, would suffice to come up with a decision (Gold & Shadlen, 2001, 2007).

$$LR_{1,2|e} = \frac{P(h_1|e)}{P(h_2|e)} \tag{1.1}$$

Therefore, if $LR_{1,2|e} > 1$, the agent would decide that the signal is present and it is not present, if the other way around (in case $LR_{1,2|e} = 1$, it will randomly pick one of the hypotheses).

Now, if there exists any knowledge on the likelihood of the events prior to the presence of evidence or, in general, any external factor that affects the likelihoods, it is best to adjust the previous formula into a general one (*sequential analysis* formalization) capable of incorporating such factors. Therefore, the decision goes to $h_1$if (Gold & Shadlen, 2001, 2007):

$$LR_{1,2|e}\ \frac{P(h_1)}{P(h_2)} = \frac{P(h_1|e)P(h_1)}{P(h_2|e)P(h_2)} > 1 \tag{1.2}$$

where $P(h_1)$ and $P(h_2)$ are the prior probabilities of the two hypotheses before presenting the agent with any evidence. More interestingly, the rule allows for the integration of multiple independent observations (e_1, e_2, …, e_n) (Gold & Shadlen, 2001, 2007):

$$LR_{1,2|e_1,e_2,\ldots,e_n} = LR_{1,2|e_1} \cdot LR_{1,2|e_2} \cdot \ldots \cdot LR_{1,2|e_n} \tag{1.3}$$

Ultimately, to factor in the cost or benefits affiliated with the choices, one would choose the h_1 when (Gold & Shadlen, 2001):

$$LR_{1,2|e} > \frac{V_{22} - V_{21}}{V_{11} - V_{12}} \quad (1.4)$$

where, $V_{ij}$is the expected cost of choosing h_j when h_i is true (when $i = j$ it is a positive reward, and it is a negative cost when $i \neq j$). Combining all three equations above that incorporate prior knowledge and cost computing into the process of decision making, the result is (Gold & Shadlen, 2001; D. M. Green & Swets, 1966):

$$LR_{1,2|e_1} \cdot LR_{1,2|e_2} \cdot \ldots \cdot LR_{1,2|e_n} \cdot \frac{P(h_1)}{P(h_2)} \cdot \frac{V_{11} - V_{12}}{V_{22} - V_{21}} > 1 \quad (1.5)$$

Here the left side of the equation is what we mathematically refer to as the decision variable and, as one can see, it is not only comprised of likelihood ratios of pieces of evidence.

It is worth mentioning that the formalization is not only limited to two-choice tasks. Instead, it applies to multi-alternative scenarios by calculation and comparison of all the likelihood ratios (D. M. Green & Swets, 1966).

Furthermore, given that applying a monotonic kernel holds the inequality, taking the logarithms of the previous equation yields:

$$logLR_{1,2|e_1} + logLR_{1,2|e_2} + \cdots + logLR_{1,2|e_n} + log\left[\frac{P(h_1)}{P(h_2)}\right] + log\left[\frac{V_{11} - V_{12}}{V_{22} - V_{21}}\right] > 0 \quad (1.6)$$

This form of the decision rule shows how pieces of evidence could be accumulated towards a final decision by simple summation. That is to say, while a positive value is in favour of accepting the h_1 , a negative value weakens this hypothesis.

To summarize, the LR allows for information from various sources to combine and accumulate over time, making up the evolving decision variable (besides other terms). Given a criterion value, the decision-making agent arrives at a perceptual judgment upon the act of comparison with criterion value (Carpenter & Williams, 1995).

Where Is This Log LR in the Brain?

The reason behind highlighting the practicality of *log* LR is that neurons could approximate these quantities (Gold & Shadlen, 2001). Imagine a light-sensitive neuron with a higher rate of spikes when light is present and vice versa. Two probability density functions,

$f(e|\, h_1)$ and $f(e|\, h_2)$ characterize the neuron's output under two conditions of the presence (h_1) or absence of light (h_2); therefore, to have an output instance of the neuron (or the group of neurons), y, would mathematically suffice to decide whether there were light or not, but implementational-wise, it predicates on neurons stored knowledge of the two distributions that open doors to a whole lot other new conditions and distributions that the brain must know.

It would be much easier to have an equivalent decision rule that circumvents the dependency on the probability distribution functions. Following that logic and remembering that using monotonically changing kernels (i.e., *log()*) will not affect the decision rule, let us assume that a sensory neuron (or batch of neurons) respond to two conditions (h_1: light, h_2: no light) with different rates of discharge following two normal distributions of different means, $\mu_1 > \mu_2$, and the same standard deviation, σ, respectively. Subsequently,(Gold & Shadlen, 2001)*:*

$$LR_{1,2|y} = \frac{\exp\left[-\frac{1}{2\sigma^2}(y-\mu_1)^2\right]}{\exp\left[-\frac{1}{2\sigma^2}(y-\mu_2)^2\right]} \tag{1.7}$$

y, being the spike rate response of the neuron (or pool of neurons), then:

$$logLR_{1,2|y} = -\frac{1}{2\sigma^2}\left[(y-\mu_1)^2-(y-\mu_2)^2\right] = -\frac{1}{2\sigma^2}\left[2y(\mu_2-\mu_1)+\mu_1^2-\mu_2^2\right] \tag{1.8}$$

Now, it is clear that the *log* LR is linearly related to the output activity of the neuron, the decision rule (*log* LR > 0 then h_1 is true) would become, $y > \frac{(\mu_1+\mu_2)}{2}$ then h_1 is true.

As one could see, the rule comes down to comparing the neuron's response with criterion value. It is true that there is no necessity to know the probability densities but yet with this new criterion, $\frac{(\mu_1+\mu_2)}{2}$, the brain has to know the averages and consider any changes that affect them, which is not very probable.

There must be a better biological solution to this, and there is: the antagonistic acting neuron (or group of neurons) which responses exactly in opposite manner of the original neuron (or group of neurons), these neurons that have been dubbed "antineurons" by Gold and Shadlen, respond with an average rate of μ_2 when $h_1$is the condition and with an average rate of μ_1 when h_2 is the case.

A good example would be the combination of a sensitive to the rightward motion neuron and its antineuron, a left-motion-sensitive neuron. Hereafter, the *log* LR of the antineuron with the output spike rate, y', in favor of $h_1$would be(Gold & Shadlen, 2001):

$$logLR_{1,2|y'} = -\frac{1}{2\sigma^2}[2y'(\mu_1 - \mu_2) + \mu_2^2 - \mu_1^2] \tag{1.9}$$

Now, the *log* LR given two outputs would be the summation of the two *log* LRs:

$$logLR_{1,2|y,y'} = \frac{\mu_1 - \mu_2}{\sigma^2}(y - y') \tag{1.10}$$

With the new output y', the decision only depends on whether the sign of $(y - y')$ is positive or negative because it is the only decisive term for the decision rule ($logLR_{1,2|y,y'} > 0$ then h_1 is true) (Gold & Shadlen, 2001).

Therefore, introducing adversarial evidence from another group of neurons eliminated the need to know the distributions or averages and being responsive to all the factors that affect them by the brain.

So far, the introduced platform explains how a categorical decision is being made through the calculation of the decision variable, which is the estimate of the natural logarithm of the likelihood ratio of one hypothesis over another one or all other hypotheses. Moreover, the nature of the logarithm provides a framework that allows the incorporation of sensory evidence from different sources and different time points, in combination with prior and expected costs or rewards. After that, it has been shown under normal (distribution) assumption for likelihoods the estimate of *log*LRs would reduce to a comparison between spike rates from two pools of sensory neurons, each favouring one of the hypotheses (Gold & Shadlen, 2001).

There is experimental evidence that neurons in action-planning structures in the brain calculate the aforementioned decision variable. The sensory information essential to form the decision variable lies in the responses of neurons in these structures. Additionally, the body of evidence shows that prior knowledge, along with costs and rewards, affect the neural responses in those structures (Gold & Shadlen, 2001).

It Is Teamwork and It Is Hierarchical to Form the Decision Variable.

The neural processing stages required to form a perceptual decision could not be fewer than two levels. For at least, sensory neurons must encode the stimulus information and a second group of neurons must be capable of computing the decision variable from the responses of the previous group. It is worth emphasizing that the two stages are the minimum number required while, in reality, there are hierarchies of neural processing for most tasks (Graham, 1989).

It turns out that the special neuron groups residing in the sensory cortex are doing a pretty good job encoding sensory stimuli: extrastriate visual cortex neurons sensitive to motion and somatosensory cortex neurons responsive to the vibration frequency in a tactile stimulus are examples found through lesion and electrophysiological studies (Albright, 1993; Britten, Shadlen, Newsome, & Movshon, 1992; Mountcastle, Talbot, Sakata, & Hyvärinen, 1969; Newsome & Pare, 1988; Parker & Newsome, 1998; Romo, Hernández, Zainos, Brody, & Lemus, 2000; Romo, Hernández, Zainos, & Salinas, 1998; Salzman, Murasugi, Britten, & Newsome, 1992). Yet, the neural responses from the sensory neurons are merely momentary, when, in fact, making decisions relies on a more continuous type of neural activity; that is to say, there is a demand for the accumulation of the sensory responses from sensory neuronal pools over time that apparently is not occurring in those very sensory neurons (Deneve, Latham, & Pouget, 1999; Johnson, 1980a, 1980b; Recanzone, Guard, & Phan, 2000; Seung & Sompolinsky, 1993; Shadlen & Newsome, 1996).

For instance, representational models of motion discrimination tasks are only able to explain the performance accuracy by the accumulation of the moment-to-moment responses of sensory neurons (Gold & Shadlen, 2000; Parker & Newsome, 1998; Shadlen & Newsome, 1996). Also, explaining the discrimination of sequential stimuli could only be achieved when there exists a more persistent representation of sensory information (Boussaoud & Wise, 1993; Miller, Erickson, & Desimone, 1996; Romo, Brody, Hernández, & Lemus, 1999).

The neuronal signal of such a sustained nature that bears sensory representations in addition to forthcoming action planning information has been detected in parietal and frontal lobes of the association cortex through physiological and anatomical studies (Bruce & Goldberg, 1985; Colby & Goldberg, 1999; Schall & Bichot, 1998; Snyder, Batista, & Andersen, 2000). One good example would be the recordings from frontal eye field (FEF) neurons in monkeys

shifting their gaze towards visual targets; these single-neuron responses not only discriminate the target from the distractor but also carry information due to the onset of saccadic movements (Bichot & Schall, 1999). All in all, these qualities made these type of neurons eligible to be hypothesized as evidence accumulators in the decision-making process (Gold & Shadlen, 2001).

Thus far, the discussion has focused on how neural responses representative of sensory evidence contribute to the formation of a decision, but as discussed before, a decision variable also encompasses psychological aspects such as priors and anticipated costs. Fortunately, under the *Log* LR regime, it is only a question of adding those factors to the sensory representations to contain those aspects. Thus, it is not difficult to assume that the same circuits which process sensory pieces of information would also encode those other factors involved in a decision variable (Gold & Shadlen, 2001).

Neural correlates modulating prior probabilities have been reported in the oculomotor-signal-generating circuits in visually guided eye movement tasks. By biasing the frequency of target appearance in specific locations in blocks of trials (Dorris & Munoz, 1998; Platt & Glimcher, 1999) or tampering with the number of possible target locations (Basso & Wurtz, 1997, 1998), neurons in LIP (Platt & Glimcher, 1999) and superior colliculus (Basso & Wurtz, 1997, 1998; Dorris & Munoz, 1998) have shown offset in their responses before and during saccade target presence.

Similarly, it turns out that varying the reward according to the responses in visual tasks would affect the activity of neurons in LIP (Platt & Glimcher, 1999). Comparable to the function of agonist and antagonistic sensory neurons for estimating the *Log* LR, a continuous evaluation of the difference between the predicted reward and actual reward could count for the calculation of the term, $log\left[\frac{V_{11}-V_{12}}{V_{22}-V_{21}}\right]$, in our previous decision rule equations (Gold & Shadlen, 2001).

Despite the effectiveness and reliability of this framework on explaining the neural code of decision variables and how pieces of evidence accumulate in time, it is still missing some elements to account for the mechanisms which ultimately could explain the decision process in its wholeness which must be able to implement the SAT (Standage et al., 2014) or explain how the commitment to choice is manifested at the neuronal level.

Bounded Integrator Models in Implementation Level.

The bounded integration framework must be further explored in order to have a more inclusive code at the implementation level. It is helpful to define the counterparts of the bounded integration parameters in the neuronal terms, beforehand:

1. **Noisy evidence**: The response of the sensory neurons to task-relevant stimuli, i.e., neurons' response in the medial temporal area (MT) of monkeys to the movement of the dots in RDM tasks (Britten et al., 1992; Britten, Shadlen, Newsome, & Movshon, 1993).
2. **Decision variable**: the activity of down-stream neuron populations that are believed to integrate the stimuli-relevant activity of the sensory neurons or other factors, a more detailed definition of decision variables at the neuronal level will be discussed in the next section; i.e., the building up type activity in lateral intraparietal area (LIP) which responds to the chosen target, namely, target-in neurons (Churchland, Kiani, & Shadlen, 2008; Roitman & Shadlen, 2002), activities of the same nature also have been recorded in dorsolateral prefrontal cortex (dlPFC) (Kim & Shadlen, 1999) and the frontal eye fields (FEF) (Ding & Gold, 2012) cortical areas.
3. **The starting point of the decision variable**: the baseline level activity of the integrator neurons before the onset of evidence is deemed to be the starting point of the decision variable (Bogacz et al., 2010).
4. **The Decision criterion**: the rate of the activity of the integrator neurons at the time of commitment to a choice (Bogacz et al., 2010).

Also, the fact that MT area projects to LIP gives rise to the idea that the building up activity in LIP is the integration of the modulated evidence that has been supplied by MT and will successively project to the circuits which mediate the movements of the eyes or, in other words, action circuitry. It is worth noting that, at the implementation level, different stages of the process are taking place in different physical stages as well (Gold & Shadlen, 2007; Shadlen & Kiani, 2013).

Previously, it was asserted that one category of bounded rationality, the competing accumulator model is the gateway from algorithmic to implementation level; therefore, for the next step, it would be beneficial to find the correspondences of that framework within the implementation level. While the rate of activity in neurons responsive to the chosen target

(target-in neurons) is high, the neurons that are responsive to the not chosen target (target-out neurons) demonstrate noticeably lower than target-in activity before commitment to choice (Bollimunta & Ditterich, 2011; Ding & Gold, 2012; Roitman & Shadlen, 2002). This dynamic of enhanced activity in the target-in and suppressed activity in the target-out neurons could be construed as an interaction between decision variables that have a competitive nature (Albantakis & Deco, 2009; Standage & Paré, 2011; Usher & McClelland, 2001; X. J. Wang, 2002).

It Runs on Inter-Inhibition, Intra-excitation, and Leakage.

Such a dynamic could be interpreted as a competing accumulator model: for each alternative, a population of neurons would act as the evidence accumulator or the implementation-level decision variable, while the degree of inhibition between these groups could be thought of as the weight of subtraction in the competing accumulator model (Standage et al., 2014).

Nevertheless, to incorporate only the inhibition parameter would not suffice to make this neural code function. That is, the competing accumulator model needs more parameters to achieve decision-making capability in neural terms. While the inhibition parameter is about the interplay between target-in and target-out groups of neurons, leakage and recurrent excitations govern the dynamics within each of those groups.

First, the membrane potential and synaptic activation decline over time; this is known as leakage. The leakage-time constants are of the order of tens of milliseconds, whereas it takes around 500 to 1200 milliseconds to accomplish a perceptual decision. Such short time-constants could not maintain the temporal integration of hundreds of milliseconds (Standage et al., 2014).

The above arguments necessitate the existence of some other dynamics to render the long integrations possible. That dynamic is believed to be composed of the recurrent excitations between individual neurons of a population responsive to a given alternative, which occurs through synaptic connectivities (X. J. Wang, 2002). Therefore, the strength of recurrent excitation from other neurons within a population along with the leakage and inhibitory synaptic currents as the linear inputs of the individual neuron could administrate the length of time for evidence integration (limited by the neuron's maximum firing rate) (Standage et al., 2014).

It is the network dynamics of the competing neural population that regulates the time length over which the evidence could be integrated. However, it is the local-circuit dynamics that put a constraint on how long a population could maintain integration (Standage et al., 2014).

State-Space Interpretation. From the state-space perspective, the rise of activity of the winning integrator population to the final high-rate state concurrent with the suppression of the other populations associated with not-chosen alternatives through recurrent inhibition corresponds to the network's state transition from an unstable steady state (emergent of the onset of evidence as an initial condition) to one possible attractor of the system (picture below) (Standage et al., 2014).

System attractors are the stable states of one system that the state of that system will eventually transit to and stay there under a set of conditions unless the conditions change. Usually, the state evolves slowly from the unstable steady state, which is in accord with the demand for a longer interval for integration. We refer to this time over which the integration is maintained, as the effective time constant of the network (Wong, Haith, & Krakauer, 2015).

As discussed before, it is the recurrent dynamics that support the time for integration, and the strength of the dynamics would control the effective time constant. Unsurprisingly, with very weak recurrent dynamics, the effective time constant of the system would decline to the order of neurons' leakage time constants (Standage et al., 2014).

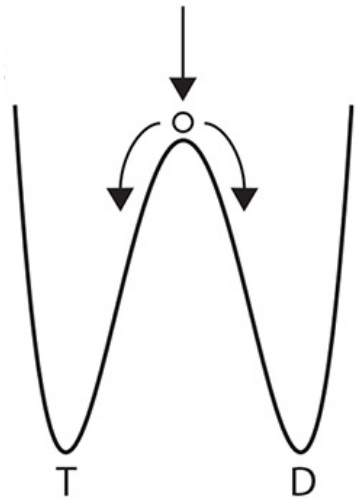

Figure 1-3: The ball is the current state of the system, and the curve is the energy landscape of the neural model, T is the target the low-energy, attractor and D is the other low-energy attractor, the distractor. The vertical arrow represents the onset of the stimulus and how this change could drive the system towards each of these steady-state attractors (Standage et al., 2014)

The Processing Stages of Decision Making. In the preceding section, we mentioned that a perceptual decision could not be formed with less than two stages: one stage for encoding the stimulus information and one stage for computing the decision variable from the first stage (Graham, 1989); But a more elaborate way to categorize the successive processing stages of decisions is depicted below:

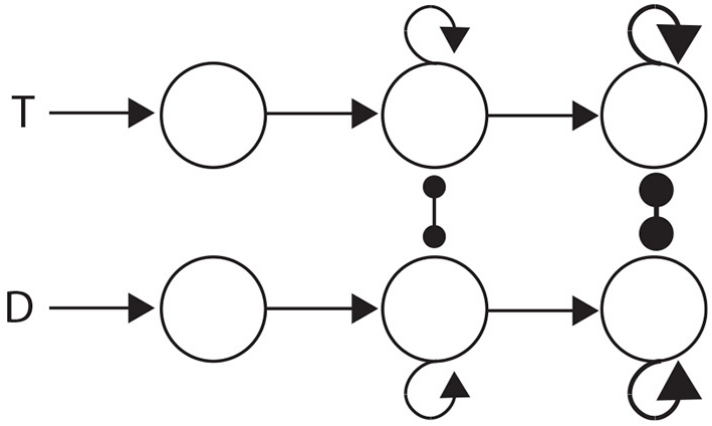

Figure 1-4: From left to right, 1. The evidence-encoding stage, 2. The integration stage, 3. The Thresholding Stage (Standage et al., 2014)

From left to right:

1. The first stage is the evidence-encoding stage, comprised of groups of target-responsive or distractor-responsive populations of neurons (Target and distractor stimuli are specified with letters T and D in the picture above, respectively). Weak recurrent dynamics prevail on this level, which means the effective time constant is governed by leakage (leakage regime), which is far shorter than the time constant required to support evidence integration.
2. The integration of encoded evidence by integrator neural populations occurs at the second stage: there exist moderate to strong dynamics (recurrent excitatory connectivities and inhibition between populations), which set the stage to support the integration of encoded evidence projected from the first stage. Moreover, to control the strength of the dynamics means controlling the SAT (decision regime).
3. The last stage is the choosing stage that has very strong dynamics (shown by thick connectivities), which has a short effective time constant (little support for evidence integration) to an input with a critical level in the winner-take-all fashion; also called thresholding circuitry (Simen, 2012).

These three stages composed of neuron populations with different dynamics embody the different phases of bounded rationalization in representational (algorithmic) level, which are: 1. to acquire pieces of evidence, 2. to integrate the pieces of evidence, and 3. finally, to commit to a choice (Standage et al., 2014).

Hypotheses on Modeling SAT at the Implementation Level.

In light of the three stages described above, it is time to advance to the hypotheses describing the speed-accuracy trade-off, as one salient feature of the perceptual decision-making process.

There are three classes of hypotheses on the implementation of the SAT, depending on which stage out of three is being modulated (Standage et al., 2014). There exist revealing electrophysiological data (Heitz & Schall, 2012) supporting the occurrence of all three classes

of hypotheses, which merely demonstrate that these hypotheses are not mutually exclusive (Standage et al., 2014).

Modulation of the encoding of evidence. Data from a study in 2012 show that the baseline rates of visual neurons regardless of being target-in or target-out were higher under speed and lower under accuracy conditions before the onset of the stimulus (Heitz & Schall, 2012). The hypothesis suggests that, under the speed condition, all visual neurons receive a spatially non-selective common excitatory cognitive signal that increases their baseline activity. The increase in the baseline rate is equivalent to having a lower decision threshold, and consequently, accuracy conditions call for a weaker common signal; such a mechanism is referred to as gain modulation in attractor models.

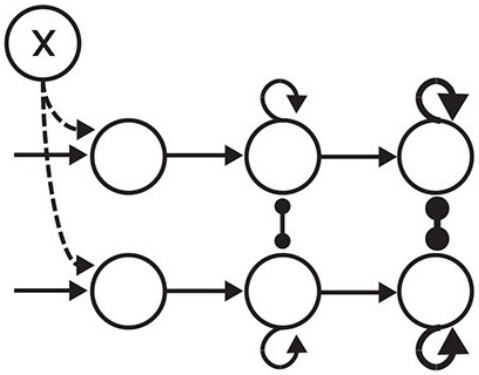

Figure 1-5: Modulation of the encoding of the evidence (Standage et al., 2014)

Modulation of the Integration of Evidence, Encoded by the Previous Stage This class of hypotheses has three sub-classes: 1. Modulation of the rate of integration, 2. Modulation of the onset of integration, and 3. Modulation of the sensitivity of the integration circuits.

Evidence for the first sub-class abounds, demonstrating the change in the rate of rising in the integrators according to speed or accuracy conditions (Heitz & Schall, 2012).

There are also two hypotheses explaining the modulation of the rate of integration:

a) A spatially non-selective stationary excitatory cognitive signal applied to the integrators controls the strength of recurrent dynamics (gain modulation). Expectedly, stronger persistent spatially non-selective spike-trains result in faster but less accurate choices

and the opposite happens for the weaker signals (Furman & Wang, 2008; Roxin & Ledberg, 2008).

b) A time-dependent ramp signal (linearly increasing as time elapses) called the *urgency signal* applied to the integrators would control the ramp of the sigmoid gain function associated with the recurrent dynamics governing the support for integration and affecting the effective time constant (Standage et al., 2014).

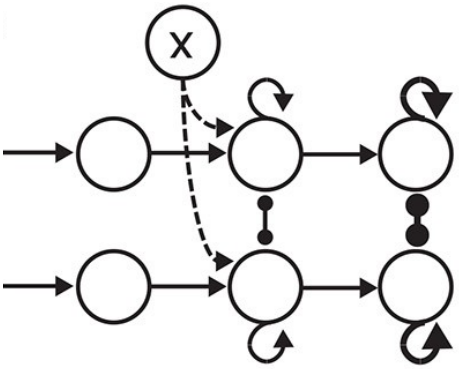

Figure 1-6: Modulation of the rate of integration of evidence (Standage et al., 2014)

The other subclass, modulation of the onset of integration, states that one inhibitory gate adjusts the onset of the integration which, as mentioned, equates adjusting the bound (Purcell, Hair, & Mills, 2012).

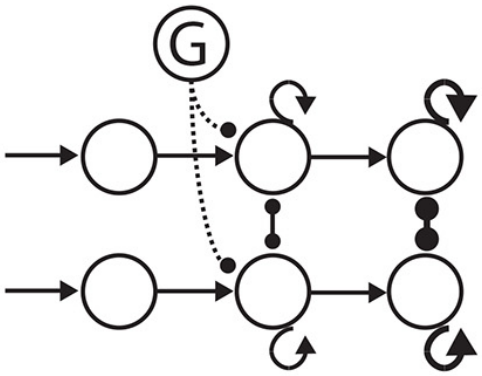

Figure 1-7: Modulation of the onset of integration (Standage et al., 2014)

Finally, the last subclass of this category assumes that, depending on speed or accuracy condition, integrators select different sub-populations of evidence-encoding neurons (black and gray arrows representing two separate sets of encoded-evidence for two-speed and accuracy conditions) (Scolari, Byers, & Serences, 2012).

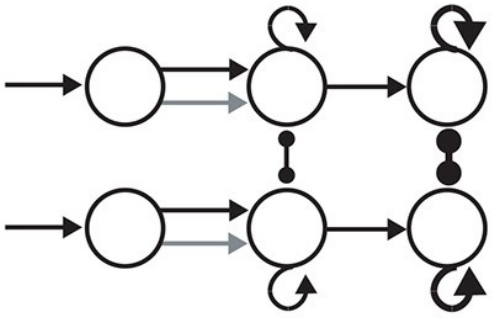

Figure01-8: Modulation of the Sensitivity to the Evidence (Standage et al., 2014)

Modulation of the Amount of integrated evidence Adequate for Commitment to Choice. The hypotheses in this class are categorized into two subclasses, 1. Adjustment to the cognitive input added to the thresholding circuit input, and 2. Modulation of the connectivity strength between integrators and thresholding circuitry (Standage et al., 2014).

1. Modulation of non-selective input to thresholding circuitry: such a top-down, spatially non-selective signal does not have the same effective time constant adjustment characteristic as before (being applied to the integrator populations). The reason is that

the dynamics in thresholding circuits are already strong; instead, if to commit to a choice entails a fixed level of activity from the previous stage (integrators), then the amount of the non-selective signal dictates how much of integrated evidence is required to make a decision. Under speed conditions, a higher level of the top-down signal allows for a faster but less accurate decision due to less available information (Forstmann et al., 2010; Frank, 2006; N. Green, Biele, & Heekeren, 2012; Simen, Cohen, & Holmes, 2006).

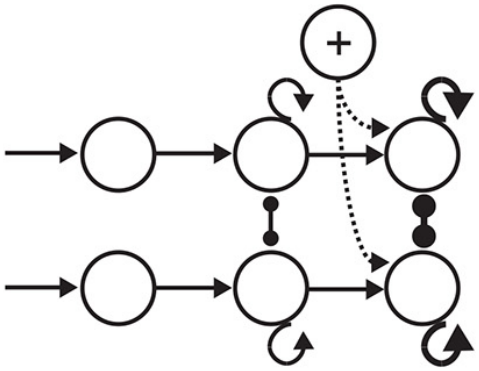

Figure 1-9: Modulation of the non-integrator signal into the thresholding circuitry (Standage et al., 2014)

2. Adjusting the strength of connectivity between integrators and thresholding populations, is a hypothesis proposed in a biophisacally-based model for saccadic decisions (Lo & Wang, 2006).

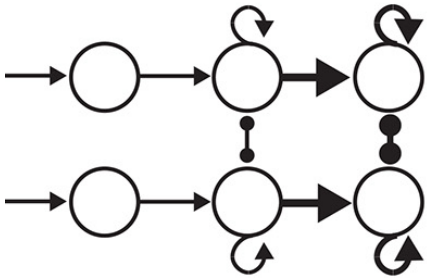

Figure 1-10: Connectivity Modulation between Integrators and Thresholding stage (Standage et al., 2014)

Modeling Behaviour.

The ultimate goal of all the efforts to find neural correlates of the decision making representational models in the brain is to model the behavior of the brain in a natural context. All the proof of concept and ideal-observer studies sets the stage to launch into modeling the behaviour. Many studies that have suggested the mechanistic hypothesis were trying to explain some behavioural data of the subjects doing RDM tasks (Xiao Jing Wang, 2008, 2012).

Evidently, to model behaviour in its true definition is a daunting challenge because it has to go beyond research paradigms towards natural, richer scenarios, let alone all the existing predicaments. In other words, going towards more real brain modeling predicates: 1. modeling real behavior, and 2. modeling the behavior in scenarios closer to real situations.

Present Study

The present study tries to make a step in this direction. Therefore, it was decided to model the behavior of a group of elite athletes as epitomes of the human brain in the face of a biological motion detection task representing a situation closer to reality (Romeas & Faubert, 2015).

Why Biological Motion?

The ability to recover information like identity or the type of activity of a moving living object from a sparse input is known as Biological Motion perception. This sparse input has been created and introduced by Johansson in 1973, using only light points placed on the individual's strategic joints (Johansson, 1973). Below one can see one frame of a person kicking an invisible ball in a soccer kick biological motion stimulus (Figure 1-11):

Figure 1-11: A frame from a soccer kick biological motion stimulus

Moreover, it has been shown that athletes show superior levels of perceptual-cognitive capacities in biological motion perception not only in tasks within sports contexts but also, surprisingly, in non-sport related tasks. Results demonstrated that athletes' performance in general tasks like point-light walker direction detection was more accurate and robust compared to non-athletes (Romeas & Faubert, 2015).

Additionally, one other compelling study has shown that athletes' ability to read and make decisions in dynamic visual sports scenes, within which the biological motion information is a key element, can be enhanced with a non-contextual, perceptual-cognitive training task called "3D Multiple Object Tracking". It is safe to say that this may be the first evidence of transference where non-contextual perceptual-cognitive training could contribute to the enhancement of biological motion perception (Romeas, Guldner, & Faubert, 2016).

The above led to the idea that whatever is happening inside the brain that results in the betterment of the subjects' performance could have less to do with the actual soccer-related experiences and more to do with pure perceptual aspects of this process. It would be desirable to have an implementational-level model that could explain this biological motion detection that could be manipulated.

In addition, implementing a genuinely functional framework could provide a powerful tool to explore, test and design other aspects, hypotheses and new experiments, respectively.

Present State of Modeling of Biological Motion?

The study of visual analysis of human action as a significant role-player in the survival and social life of humans and primates had the attention of scientists for decades (Giese & Poggio, 2003).

The main themes of these studies are as follows (Blake & Shiffrar, 2007):

1. Kinematics information of the different movements (such as the type of activity and emotional states)
2. Motor role in the perception of actions
3. Neural mechanisms

Therefore, to date, a multitude of psychophysical, neurophysiological and functional imaging experiments have been conducted on movement perception/recognition leading to the procurement of a wide range of experimental data. For instance, the prominent cortical areas involved in biological motion perception/cognition have been identified:

1. The dorsal pathway, specialized in motion information processing, is a substantial contributor to the perception of biological motion (Mather, Radford, & West, 1992)
2. Recognition of gait movements from stimuli stripped of motion cues also points to the fact that the ventral pathway, in charge of form perception, could also be involved (Beintema & Lappe, 2002)

Accumulation of a significant amount of experimental data and the demand for a useful tool to put some of the possible explanations to the test made devising a computational model for the biological motion perception inevitable (Blake & Shiffrar, 2007).

A model based on four assumptions was proposed in 2003(Giese & Poggio, 2003):

1. The model entails two parallel processing modules simulating the ventral (form) and dorsal streams (Optic flow).
2. Both pathways consist of hierarchies of neural detectors to extract form or optic-flow features.
3. This model adopts a predominantly feed-forward architecture for both pathways.

4. The visual system stores prototypical patterns and uses them for perception/cognition.

This study concluded that local motion analysis taking place in the dorsal pathway is the most influential one, contradicting an earlier study by Beintema and Lappe (2002) (Beintema & Lappe, 2002). Later, Blake and Shiffrar suggested that a multitude of contingencies, including both local motion or dynamic form processing, could be deployed to make the perception/recognition of the actions as robust as possible, with the internal and external noise present (Blake & Shiffrar, 2007).

Behavioural evidence entails the existence of low-level motion-capturing filters for biological motion detection (Chang & Troje, 2008; Troje & Westhoff, 2006). However, other than developmental studies showing the presence of some sort of natural predisposition towards biological motion in human infants and newborn chicks, no study points to a similar sensitivity to biological form cues. That implicitly suggested that there is no specialized substrate in the brain for dealing explicitly with biological form (Bardi, Regolin, & Simion, 2011; Vallortigara, Regolin, & Marconato, 2005).

Therefore, in 2014, Thurman and Lu proposed a Bayesian template-matching model that integrated form features of the stimuli using a weighting system, suggesting that the dynamic form analysis pathway works for both biological and non-biological motion in a Bayesian fashion (Thurman & Lu, 2014).

Investigations of the neural correlates involved in the body movement perception implicate a vast cortical network (Grosbras, Beaton, & Eickhoff, 2012). Even though the biological motion stimuli activate both form-related and motion-related cortical regions, the causal nature of those areas' contributions is under question (Gilaie-Dotan, Saygin, Lorenzi, Rees, & Behrmann, 2015; Kourtzi, Krekelberg, & Van Wezel, 2008). Recently, one exciting study investigated whether the activations of the ventral pathway in the event of biological motion detection are functionally essential to the perception process. The study showed that six patients with a focally injured ventral visual cortex in multiple regions managed to recognize the point-light stimuli with thresholds similar to those of the control groups while outperforming the subjects with compromised regions critical to biological motion perception other than ventral pathway (Gilaie-Dotan et al., 2015).

Studies and simulations above with all their assumptions and limitations were our starting point for designing our own biologically plausible simulation model capable of discerning human biological motion.

Subsequently, it was **hypothesized** that, with an implementational-level model that processes motion features of a complex biological motion stimulus (our case: a manifold of soccer kicks to the left or right of the observer) we could affirm that:

1. Motion feature processing could undertake the whole process on its own. (The speculation of the (Gilaie-Dotan et al., 2015) and (Casile & Giese, 2005) studies).
2. If so, certain aspects of motion are more significant than other elements of motion to biological motion detection (i.e., expansions versus rotations)
3. It is a risk-averse process due to the nature of natural reinforcement when (?) learning happens in a living thing.
4. The thresholding circuitry must reflect a mutual inhibition dynamic to enact human behavior (Wilson, 1999).

Present Work.

Initially, the capability of the (Casile & Giese, 2005) implementational-level model as the closest existing platform, which conformed to our hypothesis, was investigated. The present model was implemented only the motion pathway and got good results for the biological motion stimuli of walking.

The integration circuitry of the model was the well-known one-dimensional mean-field array of template-matching neurons and the templates were radial basis functions, that is, Gaussian kernels of different stages of a walking movement in time to the left and right directions.

The thresholding circuitry was also of the same dynamic but with faster effective time. So, the inhibitions between decision-making neurons (or group of neurons) were analogous to the integration circuitry of their model.

While the stimuli were produced by rotating a pre-captured biological motion of an actual human kick with an invisible ball around its Z-axis (Fig 1-), the task was to detect the direction of the ball (left or right side of the observer).

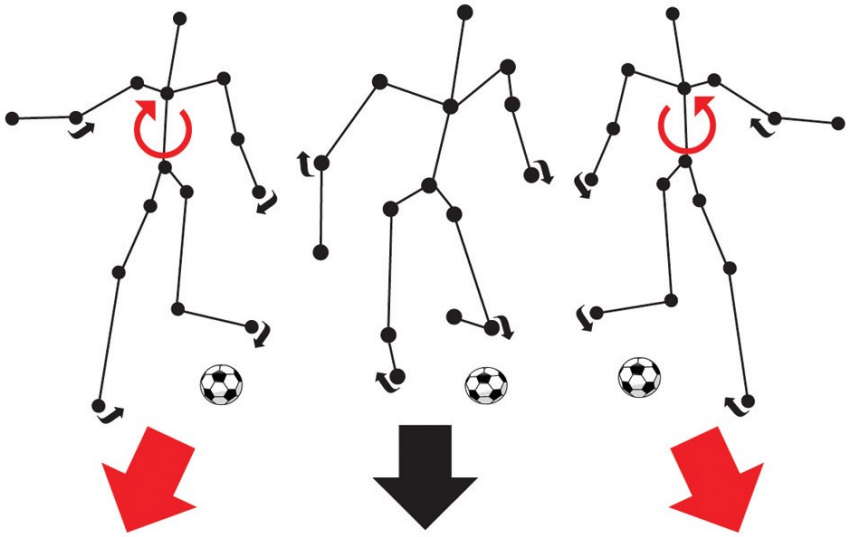

Figure01-12: Schematics of how the stimuli were produced. The connecting lines or the ball were not present at the actual stimuli (Romeas & Faubert, 2015)

After implementing, adjusting and tuning their integration stage to as many feasible Gaussian kernels using the stimuli, an acceptable response was not achievable. It is conceivable that the reason lies in the fact that the original integration stage was purported to be tuned to temporal templates of two leftward and rightward walking stimuli, as opposed to the problem at hand that was 40 kicking stimuli (all angles from 20° to the left to 20° to the right).

The Anatomy of the Model. A brief outline of the implementational level decision-making model is listed below:

1. Local motion energy detectors (the first stage of the encoding of evidence)
2. Opponent motion detectors (the second stage of the encoding of evidence)
3. Complex global optic flow patterns (the integration of evidence stage)
4. Complete biological motion pattern detectors (thresholding stage)

Local motion energy detectors. The presence of neurons with small receptive fields and sensitive to the direction of motion has been reported in the monkey visual cortex in area V1/2 and area MT (A. T. Smith & Snowden, 1994). The evidence being the direction of the motion, these neurons characterize "the evidence encoding stage" of our model (Figure 1-13). These pieces of evidence are still too high-dimensional to be fed to the integration stage. Instead, they will be processed by the next hierarchy of neurons: the opponent-motion detectors.

To implement this level, like in the work of Giese and Poggio (2003) and Casile and Giese (2005), the optical flow of every two consecutive frames has been calculated and gives a vector field (Casile & Giese, 2005; Giese & Poggio, 2003). As a result, using the vector field, the activity of all the detectors at each time point (every 500 msec) is approximated.

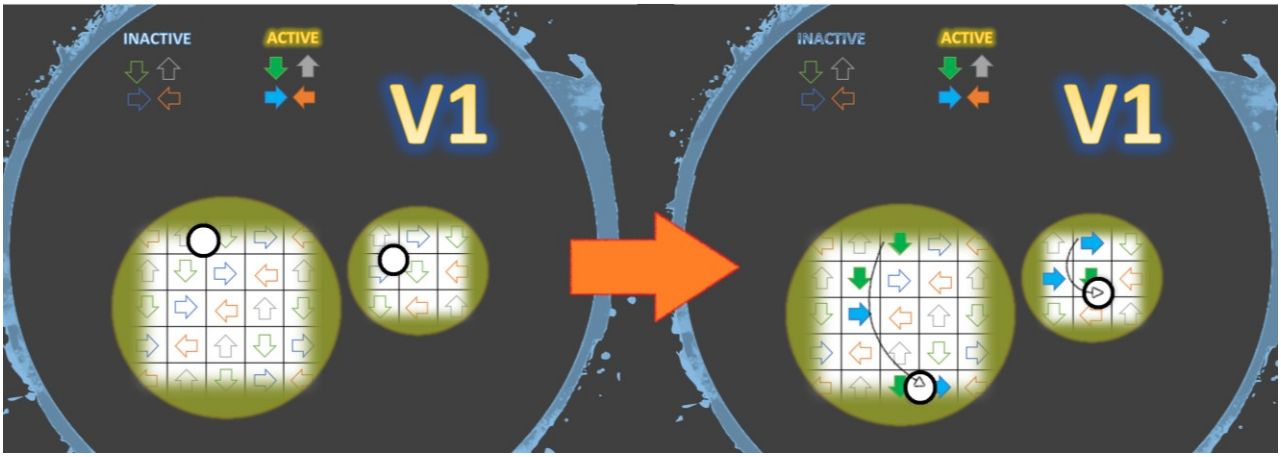

Figure 1-13: Each white square with an arrow represents a neuron sensitive to the direction that its arrow direction. Two areas show the reflection of two moving dots on the retina and, therefore, on V1. As the dots pave their paths, if there exists a sensitive neuron would fire and get deactivated as the stimulus passes. Here, for the sake of demonstration, we kept all the stimulated neurons active on the right side of the picture.

Opponent-motion detector expansions, contractions, and rotations are what is deemed as the opponent motions. Imaging studies suggest the existence of the neurons sensitive to these type of motions in the kinetic occipital area (KO/V3B) of humans (Orban et al., 1995; Orban et al., 1992)

An expansion-type opponent motion detector pools the responses of the local motion detectors of the same direction preference into one subfield using a maximum operator. Then, it does the same to the other subfield but, this time, for the opposite direction and finally creates an output from the multiplication of these pooled quantities (Allman, Miezin, & McGuinness, 1985). The counter clock-wise rotation opponent motion detector has been depicted below (Figure 1-14):

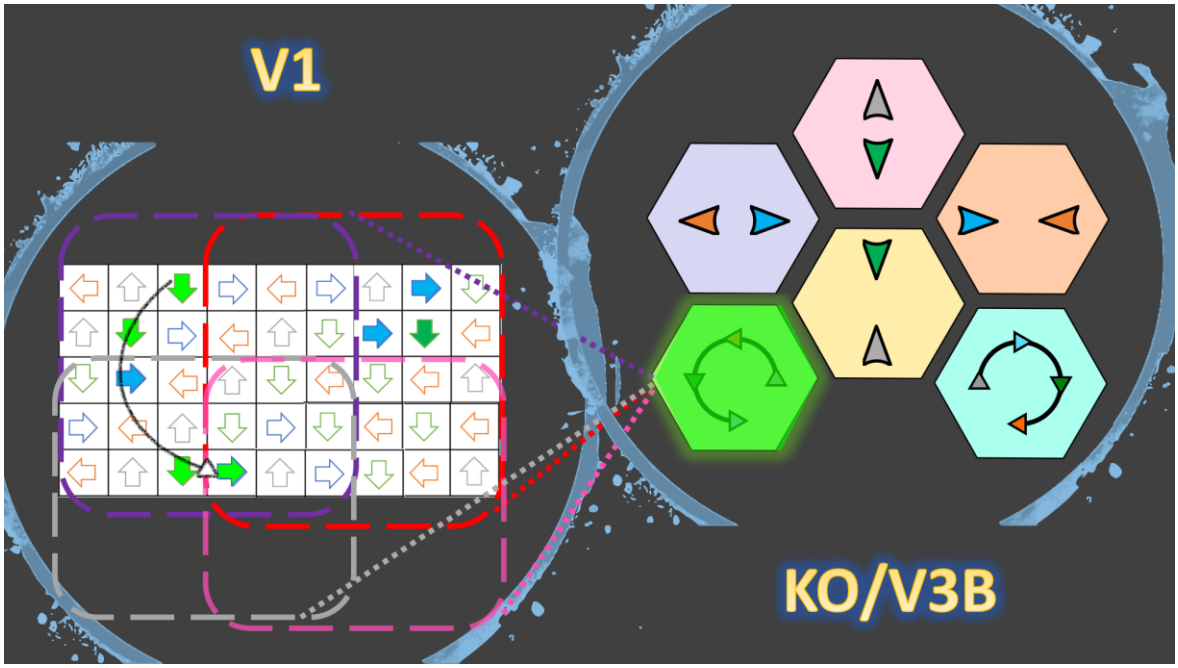

Figure 1-14: The color-filled arrows in the white square boxes demonstrate the activated local motion detectors at one point in time. The hexagons on the right represent an ensemble of opponent motion detectors at a higher level in the visual system. The counter clock-wise opponent motion detector is the only one firing (shown by neon green) because its subfields (depicted by dotted lines) are experiencing the anticipated motions at this point in time, in this example.

Opponent motion detectors in the proposed network establish the evidence encoding stage that passes a 100- to 140-element feature vector as the evidence to the integration stage at each time point.

Complex global optic flow patterns. At the integration stage, each neuron embodies a template that is tuned to a template that represents a specific interval of the stimuli sequence; for example, the second neuron has a template that represents the features of the seconds 11 to 20 of all the right-side kicks (all 20 angles). In other words, the templates are temporal.

At each time point, the evidence feature-vector gets passed to all the integration stage neurons at the same time and the template matching process happens in every neuron providing each one with its required instantaneous feed-forward input.

In the Casile and Giese (2005) model, the instantaneous feed-forward input to the mean-field integration network is produced from the template-matching of the tuned Gaussian kernels (templates) against the evidence (Casile & Giese, 2005). The feed-forward input of the present model is a product of a multiclass Bayesian classification scheme that will be thoroughly discussed in the upcoming chapters.

It is believed that the complex optic flow pattern neurons are to be found in diverse areas of the superior temporal sulcus (STS) (Decety & Grèzes, 1999; Oram & Perrett, 1994; Perrett et al., 1985; Vaina, Solomon, Chowdhury, Sinha, & Belliveau, 2001)

To give the reader a clearer mental image, the cartoon below demonstrates the mechanics of such a process (Figure 1-15):

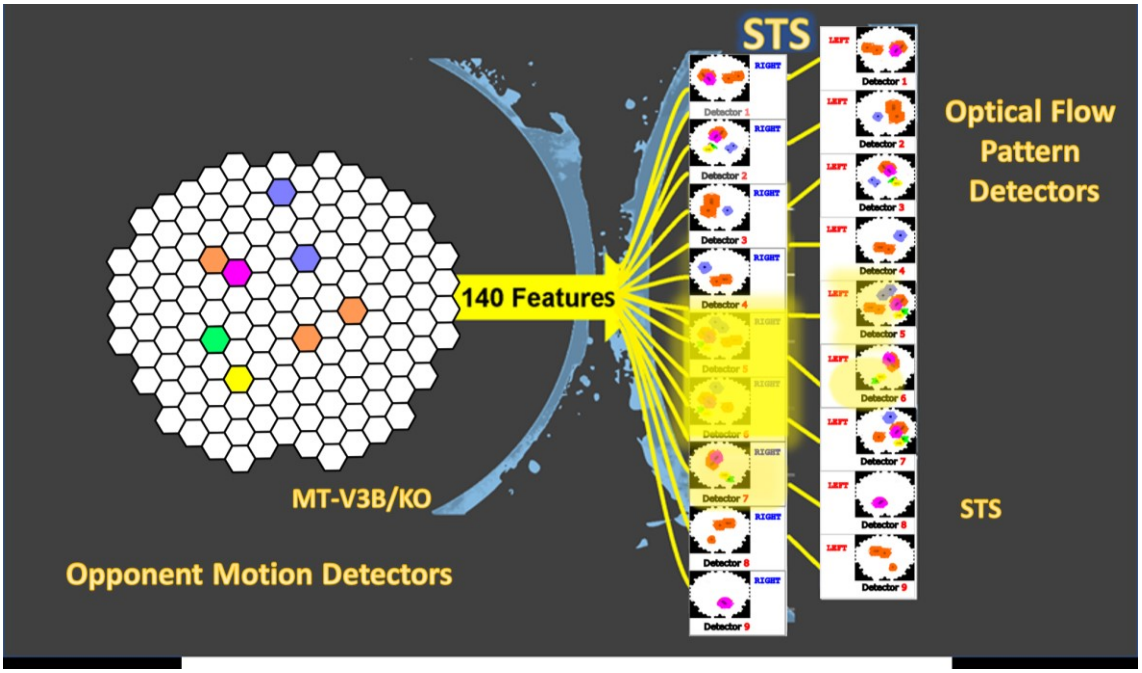

Figure 1-15: On the right, there is an exemplary 140-element feature vector made by opponent motion neurons in which white means no activity and colors represent different quantities (sparse for the demonstration purposes). On the right, there are 18 complex global flow pattern detectors 9 for the right kicks and 9 for the left kicks inside each of these neurons; there is a template stored. The more similar the input is to the templates the larger is the feed-forward input of that neuron (depicted by neon yellows of different intensity). From the picture one could assume that the presented feature vector represents the seconds 41 to 50 of the right side kick stimulus sequence (the detector 4 of the right kick group has the most intense yellow) while the detector 4 of the left kick group falsely shows some activity. It is up to the thresholding stage to receive the integrated evidence to make the final decision.

Complete biological motion pattern detectors. As expected, the integration-like activity from the right-kick group of neurons (optic-flow pattern detectors) goes to a right-kick thresholding neuron (or group of neurons) and the activity from the left-kick group of neurons to a left-kick thresholding neuron (or group of neurons).

According to imaging studies, the whereabouts of these specialized biological motion decision making neurons are likely to be in STS (Grossman et al., 2000; Vaina et al., 2001), and perhaps also in FFA (Grossman et al., 2000).

As mentioned earlier, a mutual inhibition dynamic was adopted and modified to model the dynamic of these two neurons (groups of neurons). The anatomy of their interaction is depicted below but further details will be discussed further in the next chapters (Figure 1-16).

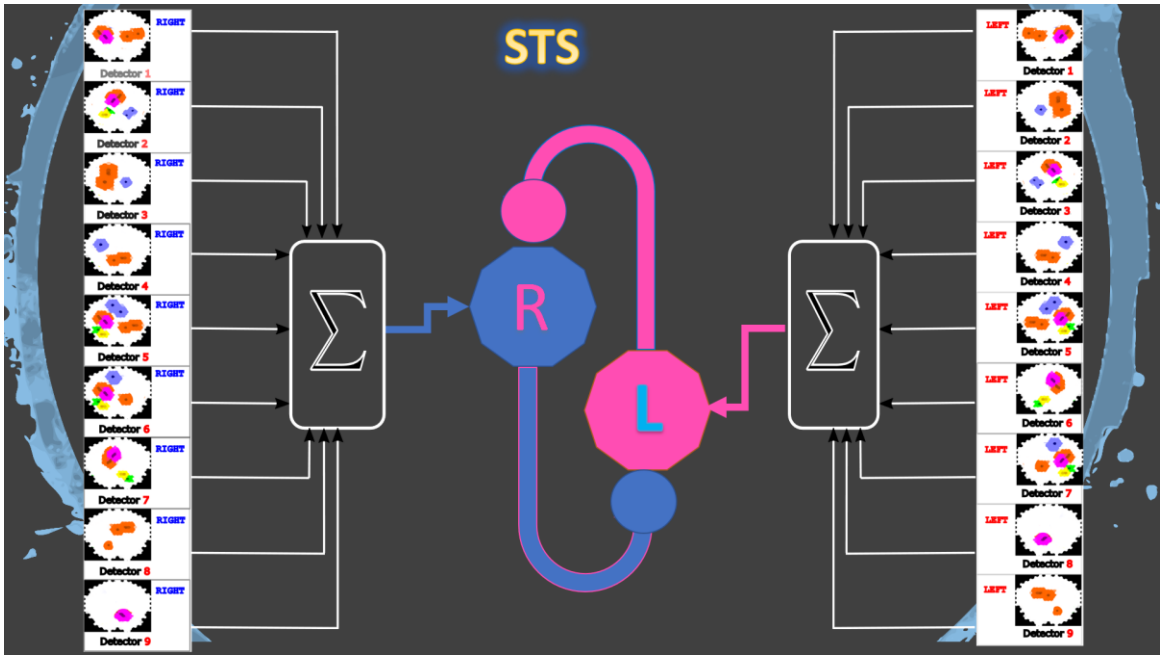

Figure01-16: The anatomy of the interaction between two decision making neurons (or group of neurons). The round headed shape connections (blue and pink) represent the existing mutual inhibitions. “R” marks the neuron (or group of neurons) that gets activated if the decision is “to the right” and “L” marks the neuron (or group of neurons) that gets activated in case the decision is “to the left”.

SAT and Our Model. Although the speed/accuracy trade-off is a very significant element to the decision-making process, the psychophysical data that the model is based on do not incorporate it. There was no design in the experiment to integrate different levels of urgency in the first place. Apparently, given such data modeling, the SAT at the implementational level will be incredibly insightful and challenging at the same time.

Article 1

"Descriptive Risk-averse Bayesian Decision-making," a Model for Complex Biological Motion Perception in the Human Dorsal Pathway

Khashayar Misaghian, J.E. Lugo and Jocelyn Faubert (2018)

Faubert Lab, School of Optometry, Université de Montréal, C. P. 6128, Montreal, Quebec, Canada.

Abstract

Biological motion perception is integral not only to survival but also to the social life of human beings. Identifying the underlying mechanisms and their associated neurobiological substrates has been a matter of investigation and debate for some time. Although, in general, it is believed that the integration of local motion and dynamic-form cues in the brain empowers the visual system to perceive/recognize biological motion stimuli, some recent studies have been insinuating the importance of dynamic form cues in such a process. Inspired by the previous, neurophysiologically plausible biological motion perception models, a new descriptive risk-averse Bayesian simulation model, capable of discerning the ball's direction from a set of complex biological motion soccer kick stimuli, is proposed. The model only represents the dorsal pathway as a motion information processing section of the visual system according to the two-stream theory. The stimuli used have been obtained from a previous psychophysical study on athletes in our lab. Furthermore, the acquired psychophysical data from that study have been used to re-enact human behavior using our simulation model. By adjusting the model parameters, the psychometric function of athlete subjects has been mimicked. The correlation analysis between human and simulation data shows a significant and robust correlation between angular thresholds and slopes of the psychometric functions of both groups. Although it is established that the visual system optimally integrates all available information in the decision-making process, the results conform to the speculations favouring motion cue importance over dynamic form by testing the limits when biological motion perception only depends on motion information processing.

Keywords: Biological motion, Bayesian, Dorsal pathway, Hierarchical simulation model

Introduction

Human's robust ability to recover information (e.g., identity or type of activity) about a moving living thing from sparse input is known as Biological Motion Perception. This sparse input has been created and introduced by Johansson in 1973, using only light points placed on the individual's strategic joints. Biological motion perception is critical to survival and social interactions of humans and primates and plays a significant role in their activities. In this regard, there has been an emphasis on the visual analysis of human action in multiple studies with the primary focus on the kinematic information of the movements (such as the type of activity and emotional states), the motor role in the perception of actions, and the neural mechanisms (Blake & Shiffrar, 2007; Giese & Poggio, 2003)

The many psychophysical, neurophysiological and functional imaging experiments conducted on movement perception resulted in a wide range of experimental data and findings. Activation of the "dorsal pathway," specialized in motion information processing, the form pathway (ventral pathway) and where the two streams converge at superior temporal sulcus (STS) are counted as the highlights of the discoveries as mentioned earlier (Beintema & Lappe, 2002; Mather et al., 1992).

Furthermore, significant accumulation of experimental data and the necessity for a compelling theoretical framework emphasized the specific demand for a neurophysiologically plausible computational model for biological motion perception (Blake & Shiffrar, 2007).

Based on the assumption that the visual system stores prototypical patterns in the perception/cognition process, a hierarchical feed-forward model has been proposed (Giese & Poggio, 2003). The model entailed two parallel processing modules simulating the ventral (form) and dorsal streams (optic flow). The study concluded that local motion analysis taking place in the dorsal pathway is the most critical factor in pattern detection (Blake & Shiffrar, 2007; Casile & Giese, 2005; Giese & Poggio, 2003), contradicting an earlier study by Beintema and Lappe (Beintema & Lappe, 2002). Only recently has it been suggested that the multitude of contingencies are at work simultaneously, to integrate either local motion or dynamic form analysis to make the perception/recognition of the actions in the presence of internal and external noise as robust as possible (Blake & Shiffrar, 2007).

While behavioural evidence implies the existence of low-level filters capable of capturing motion cues to detect biological motion as pure-motion detection mechanisms (Chang & Troje, 2008; Troje & Westhoff, 2006), developmental studies also show a natural predilection towards biological motion in human infants and newborn chicks while suggesting the lack of such sensitivity to biological form cues. To be precise, unlike motion, the visual system processes the biological and non-biological dynamic form in the same fashion, and there is no specialized substrate in the brain for dealing explicitly with biological form (Bardi et al., 2011; Vallortigara et al., 2005). Thereafter, in 2014, to validate the behavioural results from their study and hypothesis, Thurman and Lu proposed a Bayesian template-matching model, which integrated form features of the stimuli using some weighting scheme, asserting that the dynamic form analysis pathway (ventral pathway) works for both biological and non-biological motion in a similar Bayesian fashion. This result suggests the absence of a specialized substrate for the processing of dynamic biological form (Thurman & Lu, 2014).

Further investigations of the neural correlates involved in the perception of body movement show an extensive cortical network (Grosbras et al., 2012). Even though the biological motion perception incorporates both form and motion (Kourtzi et al., 2008) and, therefore, the cortical regions linked to both cues get activated, it is unclear that the contribution of those areas is all of causal nature (Gilaie-Dotan et al., 2015). Recently, to address whether the activations of the ventral pathway during the biological motion detection are functionally integral to the perception process, one study examined six patients with focally (compromised) injured ventral visual cortex in multiple regions. Not only did they all manage to recognize the point light stimuli, but their thresholds were also not significantly different from the control group's thresholds. More interestingly, they significantly outperformed subjects with impairment in other regions critical to biological motion perception (Gilaie-Dotan et al., 2015).

In regard to the question of modeling and simulating this phenomenon more explicitly, one could always picture the detection of biological motion as a sequential ? decision-making task. Like many other natural scenarios, biological motion perception also occurs in the presence of uncertainty, which stems from the inherent uncertainty of the subject's generative model and the noise of the input process (Bitzer, Park, Blankenburg, & Kiebel, 2014). Uncertainty begets risk, so it is essential to deem human decision making to be subjected to this factor and,

therefore, not always economically rational. In that light, a more plausible model could most certainly benefit from taking the risk factor into account (Kahneman & Tversky, 2013). In recent years, the risk-sensitive decision-making problem has been brought to researchers' attention and been investigated in different areas including neuroeconomics and cognitive sciences (Braun et al., 2011; Dayan & Niv, 2008; Nagengast et al., 2010; Niv et al., 2012; Shen et al., 2014).

Here, we intend to propose a feed-forward risk-sensitive Bayesian simulation model. The suggested model is hierarchical and appropriates the earlier assumption of stored prototypical patterns in STS located in the temporal lobe of the brain. Moreover, to model the motion pattern neurons, which are the decision-making neurons and also believed to be located in STS, a dynamic model called the mutual inhibition network had been utilized (Lugo et al., 2018). The presented model has been challenged with a stimulus of higher complexity, namely a soccer kick, only to detect the direction of the ball from the subject's point of view. Furthermore, as for the proof of concept of the Gilaie and Dotan study in 2015, the ventral pathway has not been implemented (Gilaie-Dotan et al., 2015). Finally, the behavioral data that had been collected previously in our lab was used to validate the performance of the proposed model, in a sense that the model has been tuned to different modes only to replicate the behavior of 11 athlete subjects. The simulated psychometric function parameters show a significant correlation with those of athlete human subjects (Romeas & Faubert, 2015).

Model

The neural model devised for our simulations is inspired by the biologically plausible model proposed by Poggio and Giese (2003) and by Cassile and Giese (2005) (Casile & Giese, 2005; Giese & Poggio, 2003). Our simulation model appropriates three assumptions of the models, as mentioned earlier: 1. Dorsal stream (Optic flow) like other visual pathways consists of hierarchies of neural detectors to extract optic-flow features. 2. This model adopts a predominantly feed-forward architecture. 3. The visual system stores prototypical patterns and uses them for perception/recognition (**Figure 2-1**)

The neural hierarchy of the dorsal stream is as follow:

Local Motion Energy Detectors. These detectors are sensitive to different motion directions and have small receptive fields (≈0.4 deg). For the present study, the simulations have implemented receptive fields which are sensitive to four different directions: right, left, up and down and, for the sake of simplicity, no diagonal direction has been implemented. These detectors have been deployed in a 36x31 assembly of receptive fields according to Smith et. Al (1994). It is reported that these selectively acting neurons reside in monkey visual cortex in area V1/2 and area MT (A. T. Smith & Snowden, 1994).

To simplify things, we calculated the optical flow of every two consecutive frames of the stimulus so that the activity of all the assigned motion detectors in the 36x31 assembly could have been approximated at each time point (every 500 msec) using the obtained vector field. The more detailed explanation of the implementation of this level can be found in (Casile & Giese, 2005).

Opponent-motion detectors. These detectors are sensitive to opponent motions like expansions, contractions, and rotations. For example, a neuron specialized in vertical contraction detection gets activated by the occurrence of such opposite motion in the two adjacent subfields located in its receptive field (A. T. Smith & Snowden, 1994). The opponent motion detector pools the responses of the local motion detectors of the same direction preference into one subfield using a maximum operator. In the case of vertical contraction, the detector pools the rightward motion in the left subfield and leftward motion from the adjacent subfield. The output of the Opponent motion is made up of the multiplication of these maxima (The square root of this multiplicative pooling) (Allman et al., 1985). Utilization of the/a maximum operator in the opponent motion-sensitive neurons simulation is rooted in the discovery of the same sort of computation in the visual cortex of monkeys and cats (Gawne & Martin, 2002; Lampl, Ferster, Poggio, & Riesenhuber, 2004). Moreover, the pooling process entails the spatial invariance within the respective receptive fields (Riesenhuber & Poggio, 1999).

Imaging studies suggest that opponent-motion detectors probably exist in the kinetic occipital area (KO/V3B) of humans (Orban et al., 1995; Orban et al., 1992).

Similar to Cassile's 2005 study, we implemented the four types of vertical and horizontal, contraction and expansions using 5x5 assemblies of detectors to generate 100 simulated features

at each time point (every 500 msec). For more descriptive details one must refer to (Casile & Giese, 2005).

Complex Global Optical-Flow Patterns. The third hierarchy level is made up of neurons capable of discerning momentarily complex optic flow patterns. The other critical factor to which these neurons must be responsive is the temporal order of the input that they are receiving. In other words, each detector is tuned to a certain optic flow pattern of a certain temporal order. In previous attempts to model optic flow detectors with this characteristic, a network of laterally coupled neurons has been proposed. It is through these asymmetrical connections that the active neuron at one moment excites the neurons tuned to the future optic flow patterns and inhibits the rest of the detectors encrypting earlier patterns (Mineiro & Zipser, 1998). In this manner, the assumed dynamic of the optic flow pattern neuron sensitive to the ith frame (the optic flow that comes from the $i-1$ and ith frames) of one stimulus sequence is as follow (Casile & Giese, 2005):

$$\tau_{OFP}\dot{H}_i(t) = -H_i(t) + G_i(t) + \sum_m w(i-m)f(H_i(t)) \quad (1)$$

Where $H_i(t)$ is the activity of the ith neuron, the $\tau_{OFP} = 150\,ms$ is the time constant of the global optic flow pattern detection dynamic, $w(m)$ is an asymmetrical weight kernel, $f(H)$ is a step threshold function, and $G_i(t)$ is considered as the instantaneous feed-forward input of the neuron. As mentioned before, one of the fundamental assumptions about the model is the prototypical matching performed by the neuron. It is only the result of this template matching process that constitutes the aforementioned feed-forward input. In previously proposed models, for each key feature-vector derived from the stimulus video sequence, namely template, a Gaussian radial basis function has been designated and tuned it. Thus, when the detector receives its input from the previous level, depending on how similar it is to the center of the corresponding Gaussian function, the instantaneous feed-forward input gets generated. For a detailed description of this, the reader is referred to Giese and Poggio (2003) and Casile and Giese (2005) (Casile & Giese, 2005; Giese & Poggio, 2003). While our model holds the exact laterally connected dynamics for the optical flow detectors, it uses far fewer neurons and a different strategy to generate the instantaneous feed-forward input, $G_i(t)$.

In our model, the feed-forward input $G_i(t)$ is deemed to be a product of a multiclass Bayesian classification scheme. Here, the most classical minimization of classification error did not seem to serve the purpose; instead, minimizing the average risk method, which includes different significances for different errors, shows more efficiency. To be more precise, false classification of the represented frame into one of the future vital feature-vectors must have less gravity compared to one related to an older template (Theodoridis, 2010). The logic behind it can be explained by the goalkeeper example; meaning that if a goalkeeper decides that the frame observed in a scene belongs to one of the future states of the sequence, the chance to save the ball is less compromised as opposed to classifying that scene into one of the earlier-encoding templates.

The same stimuli have been used in previous experiments in our lab (Romeas & Faubert, 2015). Each stimulus sequence is comprised of 90 frames. For every two consecutive frames (after passing through the first two levels), a feature-vector of 140 elements would be generated and fed to the optical flow pattern detection stage. There exists a stimulus for every angle of deviation from the center in order to train or test the model. We considered nine stages for each kicking sequence. Our classification problem consists of 18 classes, nine classes for the rightward kick and nine for the leftward. Each class represents one specific stage of the kicking process, i.e., the 1st class associated with right-ward kick means we are in the first stage of the kicking process (first ten frames) and the 3rd class associated with a left-ward kick is the right decision when the stimulus reaches somewhere between frames 31 to 40. Therefore, our problem is an 18-class, $\omega_i,\ i = 1, \dots, 18$ classification problem, where $R_j, j = 1, \dots, 18$ makes up the regions of the feature space. An error happens when the feature-vector u which pertains to the region R_i gets misclassified in class ω_k while $i \neq k$ and so, a loss term λ_{ki}will be assigned to this incorrect decision. In this manner, a Loss matrix could be formed that its element λ_{ki} constitutes the penalty for action k (here: classification in class ω_k) when the actual state is i (the feature-vector fed to the layer). It can be shown that the average risk is minimized when (Theodoridis, 2010):

$$(2) \qquad u \in R_i \ \ if \sum_{k=1}^{18} \lambda_{ki} p(u|\omega_k) p(\omega_k) < \sum_{k=1}^{18} \lambda_{kj} p(u|\omega_k) p(\omega_k) \quad \lambda_{ll} = 0, \quad \forall\, j \neq i$$

which indicates, that u originates from the region R_i when it has the lowest weighted sum and classifies in class ω_i.

$p(u|\omega_k)$ is the likelihood of the feature-vector given the class ω_k, and $p(\omega_k)$ is the prior probability of the class ω_k. In our model, we assume that the likelihood of feature-vectors of each region R_i follows a Gaussian distribution $\mathcal{N}(\mu_i, \Sigma_i)$, in which, μ_i is the mean vector, and Σ_i is the covariance matrix. Moreover, the priors, $p(\omega_k)$, are predefined for each class ω_k separately where $\sum_{k=1}^{18} p(\omega_k) = 1$.

In this manner, the detector tuned to class ω_i receives a positive non-zero feed-forward input, $G_i(t)$, at each time step whenever $u(t)$ belongs to the feature region, R_i.

To describe it in the cellular level, when one input matches the saved template of one neuron, all other neurons with different classes see that as a sizeable weighted quantity added to their risk sum while the loss term $\lambda_{ii} = 0$ relieves the matching neuron from adding that large signal to its risk sum. In other words, the neuron with the matching template inhibits the feed-forward input of other neurons.

The consensus is that the complex optic flow pattern neurons are likely to be found in disparate areas of the superior temporal sulcus (Decety & Grèzes, 1999; Oram & Perrett, 1994; Perrett et al., 1985; Vaina et al., 2001).

Complete Biological Motion Pattern Detectors (Motion Pattern Detectors). Discrimination of complete biological motion patterns occurs in motion pattern neurons, which make up the fourth and highest level of the model. The complete biological actions in our study comprise of leftward kick and rightward kick. The sum of the activities of the optic flow pattern detectors that belong to one particular action serves as an input to the motion pattern detector associated with that very action. It is the activities of these motion pattern detectors which constitute the decision response or more generally the behaviour of the biological motion detection system (Casile & Giese, 2005; Giese & Poggio, 2003). Moreover, imaging studies account for the possibility of the existence of motion pattern neurons in STS (Grossman et al., 2000; Vaina et al., 2001), and perhaps also in FFA (Grossman et al., 2000).

A non-linear, excitatory and inhibitory network has been adapted, to simulate these motion pattern detectors, which has been used initially to describe neuronal polarity under various circumstances (Lugo et al., 2018). In this mechanism, which is known as mutual or global

inhibition, the element with the highest excitatory input suppresses the activity of those whose activities have not passed their thresholds in a nonlinear and reciprocated fashion (Lugo et al., 2018; Wilson, 1999).

The fact that mathematical models similar to the mutual inhibition one have shown success in the simulation of humans' decision neuronal networks (Wilson, 1999) is the reason behind this choice of model.

Robust Mutual Inhibition Model. Initially, the mutual inhibition model (Lugo et al., 2018) explains the response of decision making neurons using the following nonlinear dynamic below:

$$\tau \frac{dT}{dt} = -T + S\big(P_T(D)\big) \tag{3}$$

$$\tau \frac{dD}{dt} = -D + S(P_D(D,T)) \tag{4}$$

Where T is the activity of whichever neuron getting excited first by the activity of the previous hierarchy level and D is the activity of the rest of the neurons. τ is a time constant and $S()$ is a modified Michaelis-Menten function (Wilson, 1999) which is especially useful in designing excitatory-inhibitory networks (Lugo et al., 2018):

$$S(P) = \begin{Bmatrix} \frac{MP^2}{\sigma^2 + P^2} & P \geq 0 \\ 0 & P < 0 \end{Bmatrix} \tag{5}$$

where M is the maximum information threshold for the excitatory-inhibitory activity and σ almost always marks the information, threshold point where the function hits half of its maximum. P_T and P_D are the information thresholds available to $T - type$ and $D - type$ neurons, respectively:

$$P_T(D) = E_T - kND \tag{6}$$

$$P_D(D,T) = E_D - k(N-1)D - kT \tag{7}$$

where N is the number of neurons and the constant k is the inhibitory feedback gain. Also, E_T and E_D represent the external inputs generated from the previous hierarchy level. The number

of equations to solve depends on how many decision-making neurons are involved in the process. For instance, if we want decision-making agents to pick one choice out of N choices, we would need to solve one equation (6) and $N-1$ equations (7). Thus, $N=2$, since, in our model, the decision is between left and right kicks. For more information and mathematical details, one must refer to Lugo et al. (2018) (Lugo et al., 2018).

The original mutual inhibition model dictates that only the non-negative information thresholds, P_T or P_D, would contribute to the activity of the decision neurons and, when negative, the neuron activity attenuates exponentially according to the linear first-order dynamic that it follows in the absence of any input and interconnection between other neurons. Although this implementation maintains some degree of robustness, it falls short facing the high variation signals coming from the third hierarchy layer. To reduce the level of sensitivity, we modified the system to neglect the negative changes. In other words, when neurons are disconnected as a result of negative information thresholds, detectors' activities will be as follows:

$$\tau\frac{dT}{dt}=\begin{Bmatrix}-T & T\leq 0\\ 0 & T>0\end{Bmatrix} \quad (8)$$

$$\tau\frac{dD}{dt}=\begin{Bmatrix}-D & D\leq 0\\ 0 & D>0\end{Bmatrix} \quad (9)$$

Modeling of the Internal Noise. To simulate uncertainty in the decision-making process, we assumed that the output of each optic flow pattern neuron is drawn from a Gaussian distribution, $\mathcal{N}(H_i(t),\Delta t\delta^2)$, where $H_i(t)$ is the ideal activity of the optic flow neuron in the absence of the added internal noise of the variance, δ^2. In our model, this implementation can be construed as the generative input process of the 4th layer due to the physiological noise in the visual pathway. It also can be shown that in the particular case of the constant priors for generating feed-forward input, $G_i(t)$, such exercise mirrors the uncertainty in the internal generative models of the 3rd layer. In this case, the added noise represents the error between the internal generative model and the feature input that the decision-making agent receives.

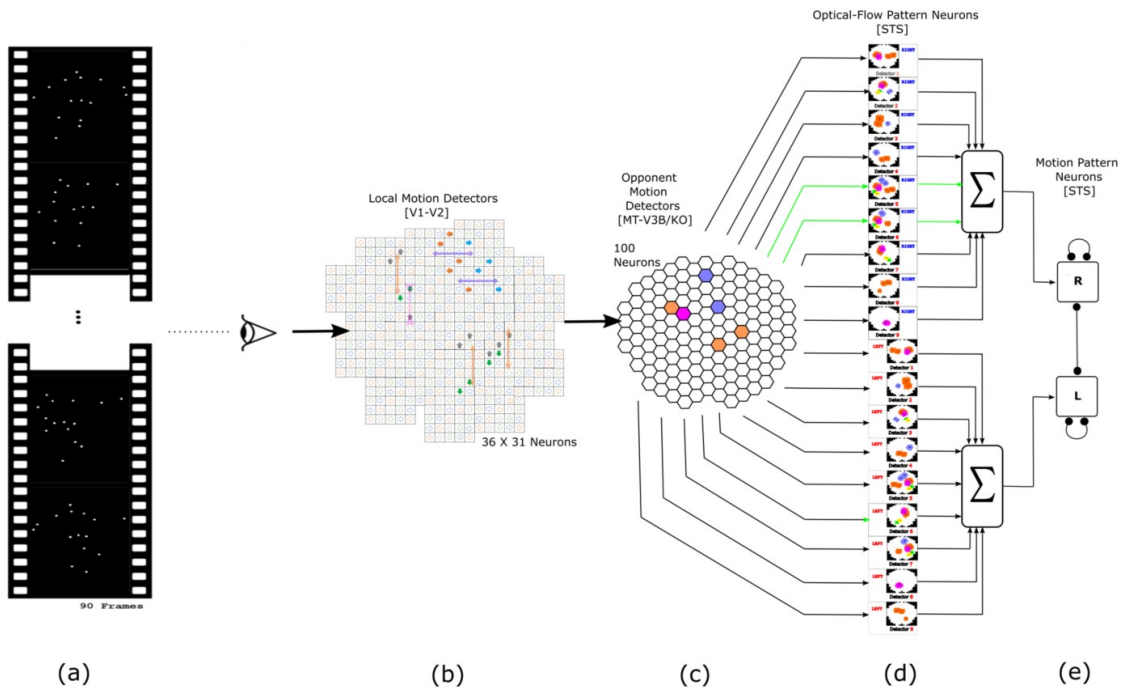

Figure02-1: Schematic of the model in one hypothetical point in time, from left to right: (a) the reel of biological motion stimulus (b) local motion detectors as ensemble of 1116 neurons positioned in a 36 by 31 arrangement, are firing due to the motions they have experienced during two consecutive frames, represented by the cells with filled-color arrows (blue: right, orange: left, grey: up, and green: down), the larger, two-headed, colorful arrows were drawn to display the types of opponent motions that would be sensed on the next level (cyan: horizontal expansion, orange: vertical expansion, and magenta: vertical contraction) (c) opponent motion detectors, the ensemble of 100 neurons to detect horizontal expansion, horizontal contraction, vertical expansion, and vertical contraction, the activated detectors are marked with color-filled hexagons with their corresponding color (cyan: horizontal expansion, orange: vertical expansion, and magenta: vertical contraction), (d) optical-flow pattern detectors, an arrangement of 18 neurons following a one-dimensional mean-field dynamics, each neuron incorporates a statistical template (displayed as colorful map) that represents a specific part of the manifold of the kicking sequences (for example neuron number 2 contains a template for the seconds 11 to 20 of the kick-to-right sequence, while neuron number 10 would have a larger instantaneous input for the seconds 1 to 10 of the kick to the left stimulus). Green arrows are highlighting the contribution of two cells to the evidence integration at that hypothetical point due to the

similarity of the evidence signal and their template (e) thresholding stage, two decision neurons for the right and left decisions (marked by capital letters R and L on the square cells with soft edges) are following our mutual inhibition dynamics receiving their corresponding inputs from integration stage, the straight and curve lines with rounded heads highlight the inhibitory interaction between the neurons and the auto-inhibition, respectively. No activity could be seen by either of the neurons since at that hypothetical point in time, neither made a decision yet.

Methods

All implementations of the simulation model have been executed in Matlab, and for the data fitting and statistical analyses, R Studio platform has been used.

Stimuli and Data. To simulate the same conditions of the psychophysics study (Romeas & Faubert, 2015) for which we propose a simulation model, we adopted the same original point light soccer kick captured by Mixamo studio. The stimulus comprises 15 dots representing the head and the human body's major joints (shoulders, hips, elbows, wrists, knees, and ankles). The stimulus is comprised of 90 frames with a duration length of 4.5 seconds. By rotating the original stimulus around the Z-axis, we were able to create the stimuli for leftward and rightward point-light soccer kicks with different angles. In the psychophysics study, subjects were exposed to the stimuli with deviations of 2, 4, 8 and 15◦ angles either towards the left-hand side or right-hand side of the viewer. For training and cross-validation of the model, the utilized data is comprised of all shooting angles within the range of 1° to 20°. This range is the angular range in a penalty kick from the goalie's point of view. As a real-world example, a penalty kick resembles a wide range of situations. Nonetheless, in a regulated and constrained condition, it provides a framework to estimate an angular range within which one can assume the human brain has been trained. In other words, we believe that this angular range is the approximate range that constructs the prototypical patterns in one's visual system.

A k-fold cross-validation (k=5) procedure has been used to validate our model (Jung & Hu, 2015). Thenceforth, the model has been trained in the range of 7° to 20°moreover, tested for angles 2°, 4°, 8° and $15^{\circ}$to recreate the behavioral test conditions.

Local Motion Energy and Opponent Motion Neurons. The methods to implement the 1st and the 2nd hierarchy level of the present simulation model have been borrowed from the previous studies (Casile & Giese, 2005; Giese & Poggio, 2003).

Optic Flow Pattern Neurons. For each direction (left or right), we installed nine optical flow pattern detectors. Each detector is selective for 10 consecutive frames out of 90; for example, neuron H_1^{Left} is selective for frames 1 to 10 of the left side shooting and H_6^{Right} is selective for the frames 41 to 50 of the right-side shooting. Each neuron incorporates an internal generative model, $p(u|\omega_k), k = 1,..,18$, assumed to be of the Gaussian form, $\mathcal{N}(\mu_k, \Sigma_k)$. The mean, μ_k, and covariance matrix, Σ_k, of each template is computed using feature vectors derived from 10 frames of multiple stimuli with different degrees of deviation. For instance, H_6^{Right} is trained using feature vectors from frames 61 to 70 of the shootings with 7° to 20° degrees of deviation to the right-hand side of the observer. Concisely, H_6^{Right} is supposedly selective for frames 61 to 70 regardless of the deviation of the shooting.

While the feed-forward input to each optic flow neuron is derived from the previous layer output, the dynamic of the neurons of this level, following (1), is solved using Euler's method. To provide the input for the next hierarchy level, an independent Gaussian noise has been added to the activity of each of the optical flow detectors.

Below, the activity of these neurons in the absence of the internal noise to the stimulus representing a kick with 9°degrees of deviation to the right is demonstrated (Figure 2-2).

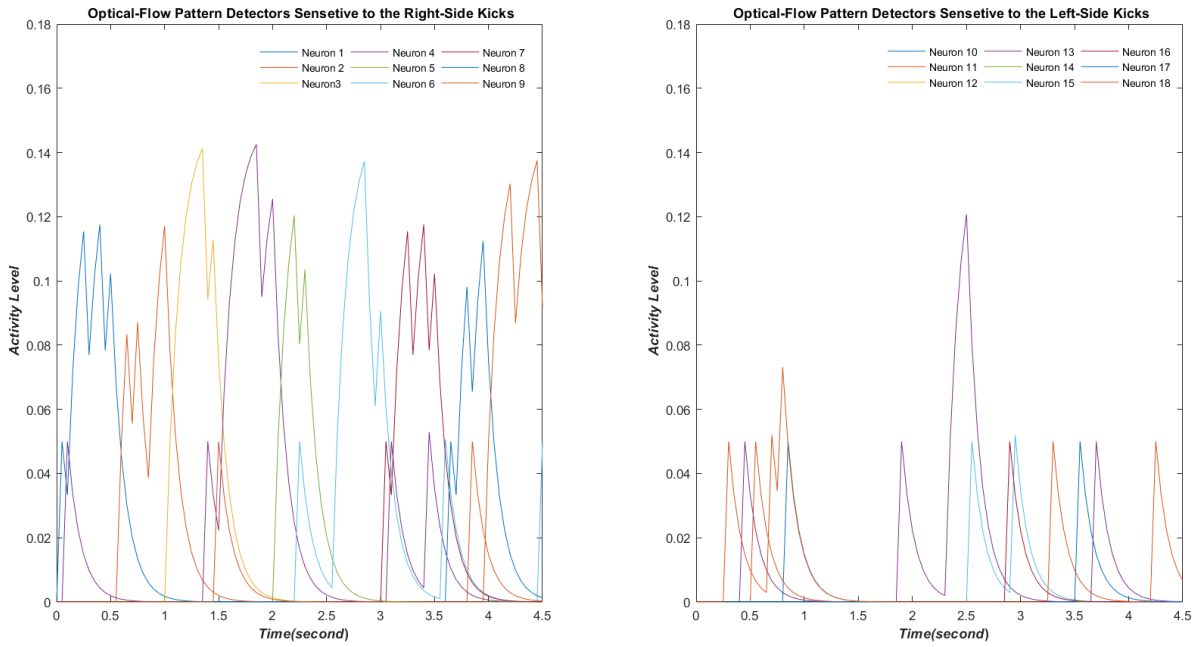

Figure02-2: The activity of these neurons in the absence of the internal noise to the stimulus representing a kick with 9° degrees of deviation to the right. Neurons 1 to 9 are responsive to the right-side kicks and neurons 11 to 18 are sensitive to the left-side kicks.

Motion-Pattern Neurons. At the decision-making layer, two motion pattern neurons have been implemented, One for the leftward kick motion and the other one for the rightward kick motion. As described in the previous section we modeled the dynamic of these detectors using robust mutual inhibition method. The fourth-order Runge-Kutta has been utilized to solve the nonlinear system dynamics.

Also, the activity of these decision-making neurons as members of the thresholding stage when the stimulus is a sequence of a 9° degrees to the right kick, while the internal noise is not present, is depicted in figure 2-3, below:

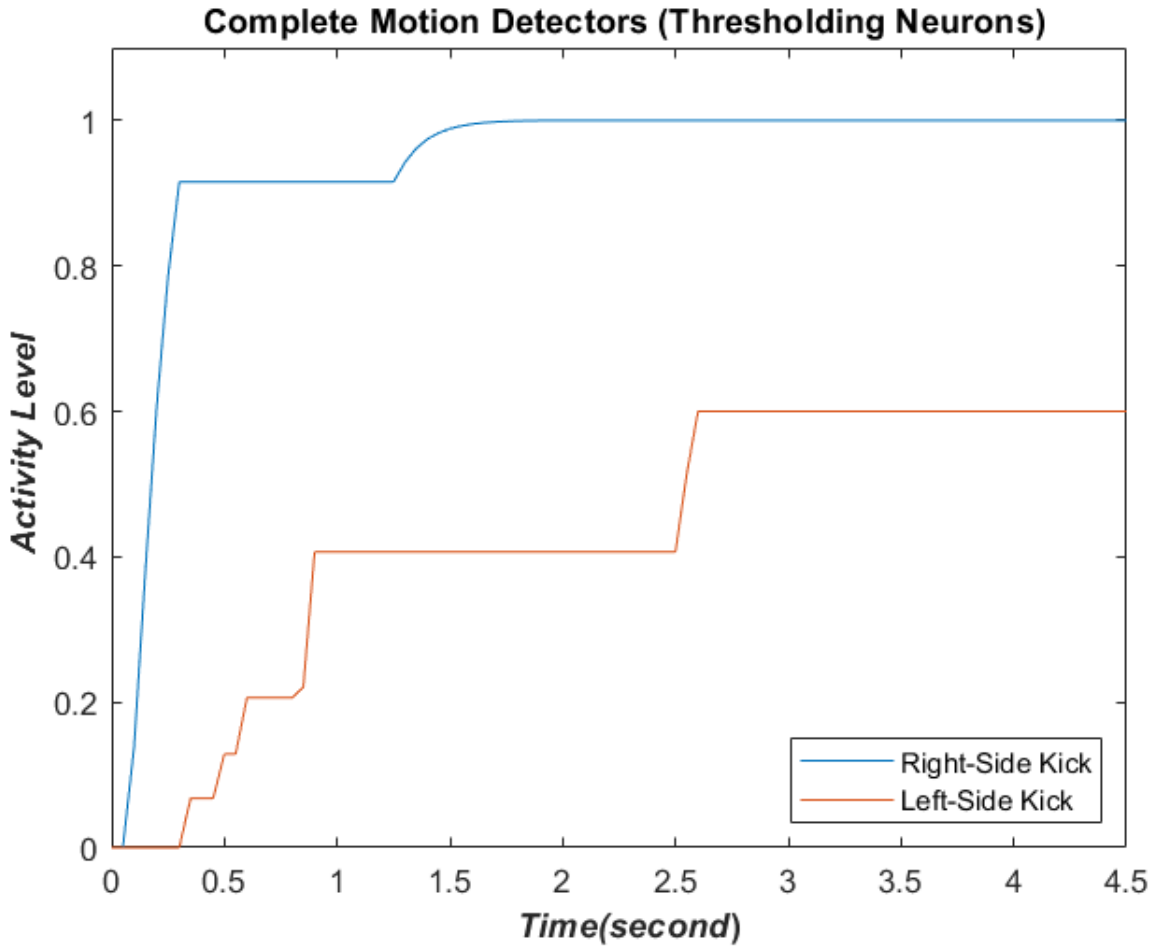

Figure02-3: The neuron responsive to the right-side kick (blue) is highly activated, while the inhibition in the other neuron is evident.

Simulating Human Behaviour. In the behavioral study, Romeas and Faubert (2015) utilized a forced-choice paradigm task to decide the direction of the ball (left or right) by only relying on the biological motion signal (Romeas & Faubert, 2015). Each subject was exposed to a total of 1080 randomized stimulus sequences of left and right shooting with deviations of $2^{\circ}, 4^{\circ}, 8^{\circ}$ and 15° angles (120 times for each angle at each side). Accordingly, for each subject, a psychometric function to relate human behaviour to the angular deviation was determined (Romeas & Faubert, 2015). Here, to simulate those performances, three parameters of our simulation model were adjusted to mimic the behaviours of 35 athlete subjects from the psychophysical study.

Just like the behavioural study, for each angle and side, the simulation model has been exposed to the particular stimulus 120 times in order to generate an error percentage quantity. Additionally, this has been repeated 30 times, and the corresponding psychometric function has been determined using the simulated results.

The three variables for tuning the model to 35 athlete subjects were:

1. The standard deviation of the added internal noise, δ.
2. The time constant, τ.
3. The inhibitory feedback gain, k.

Results

While the previously proposed models, trained with similar data, performed very poorly for detecting the point-light kicking sequences, our model efficiently showed outstanding performance facing the stimuli. The 5-fold cross-validation of our model resulted in 87.5% average success.

The model performance demonstrated remarkable robustness in the presence of a wide range of imposed internal noise, δ. Besides noise being a prominent adjuster of our model, the degree of inhibition occurring between two decision making neurons, represented by k, along with their intrinsic latency, represented by τ, prove to be critical factors to bring the model into different functional states. Grid search computation has been performed for different ranges of internal noise, δ, mutual inhibition gain, k, and intrinsic latency of the decision neurons (thresholding stage), to generate the results. Here we present a part of the results from solving the model for

different parameters as an effort to get an insight into how each parameter could contribute to the model's decision-making behavior (**Table 2-1**). Increase in neurons' dynamic time constant, τ always results in better performance, meaning lower angular thresholds and steeper slopes, while an increase in the inhibitory gain, k shows a different trait.

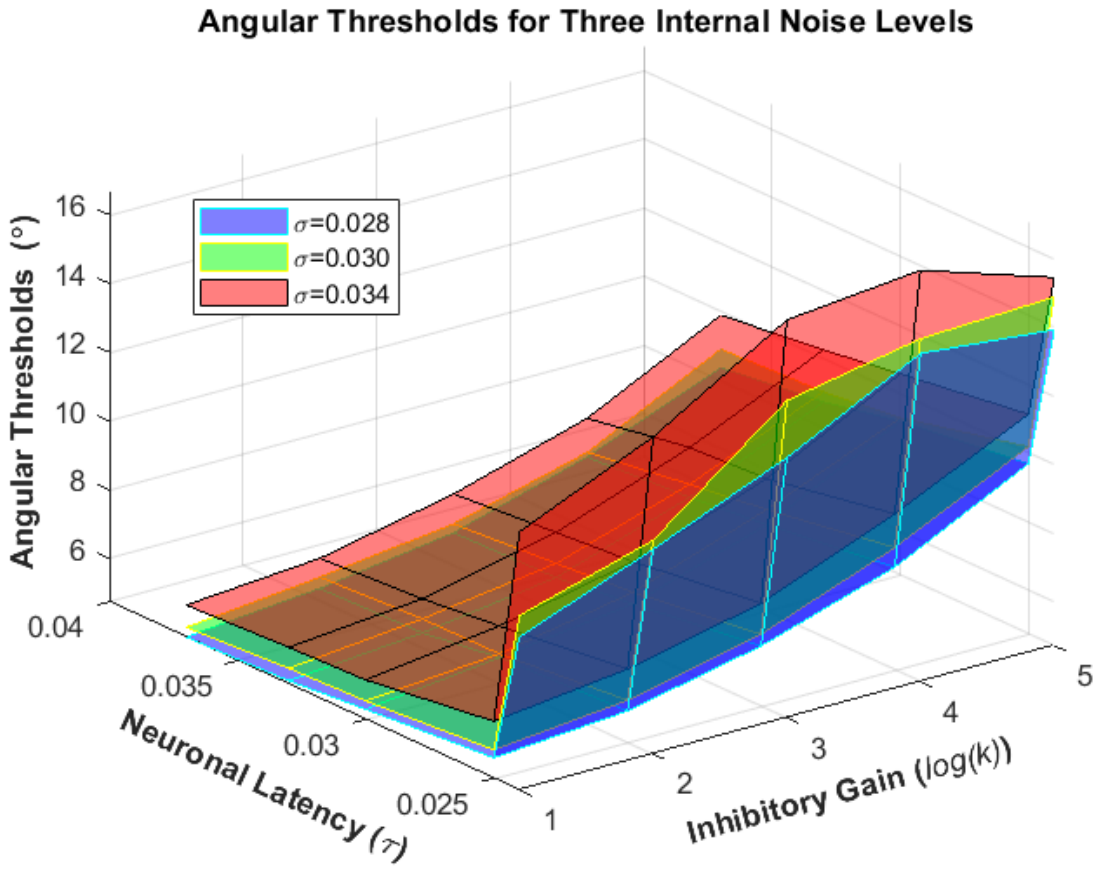

Figure 2-4: The psychometric function angular thresholds resulted from running the model for exemplary ranges of neuronal latency ($\tau = 0.024,\ 0.025,\ 0.03,\ 0.033,\ 0.037\ sec$) and inhibitory gain ($k = 2, 4, 8, 16, 32$) for three noise levels ($\delta = 0.028, 0.030, 0.034$)

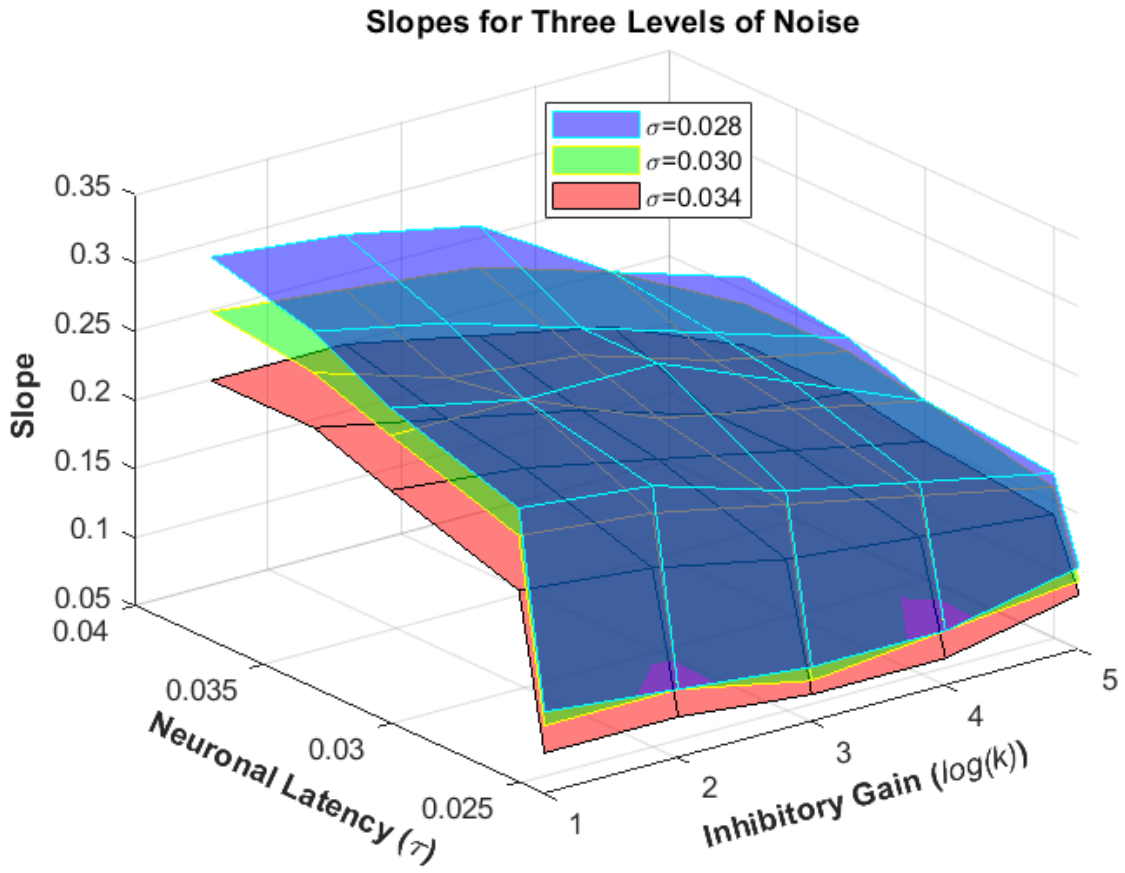

Figure 2-5: The psychometric function slopes resulted from running the model for exemplary ranges of neuronal latency ($\tau = 0.024,\ 0.025,\ 0.03,\ 0.033,\ 0.037\ sec$) and inhibitory gain ($k = 2, 4, 8, 16, 32$) for three noise levels ($\delta = 0.028, 0.030, 0.034$)

At first, the increase of inhibition gain, k leads to deterioration of performance (higher threshold, flatter slope) but this changes after k passes the value of 8. However, the phenomenon seems less evident for δ =0.030. At that noise level, the angular thresholds are not decreasing and just increasing at a lower rate; however, one must notice the slopes taking on a new trend becoming steeper which only means reaching higher accuracy in smaller angular deviations.

Unsurprisingly, the betterment of the performance does not come free of cost. Analyzing the activity of decision neurons shows it takes far more time for the winning neuron to reach the highest point of its activity when the inhibitory gain, k, is too large, and that could only be interpreted as longer processing time.

Human Results Vs. Simulation Results. By adjusting the parameters mentioned above: internal noise, δ, mutual inhibition time constant, τ, and inhibitory gain, k, the behaviour of 35 athlete subjects has been mimicked. The parameters and the associated simulated angular thresholds and slopes versus the experimental values have been reported below in **table 2-2**. Subjects are grouped by similar angular thresholds and slopes and each group is simulated by one set of parameters. Such an approach helps to acquire a more generalized understanding of subjects' behaviours as groups.

Moreover, a ranked assembly of experimental angular thresholds versus their simulated counterparts has been plotted in **figure 2-2**, and the corresponding slopes to the angular thresholds have been plotted versus their corresponding simulated slopes in **figure 2-3**. The two figures provide a more discernable comparison between experimental and simulation results.

Correlation analysis shows a significant positive correlation between experimental and simulated angular threshold values, with the Spearman correlation coefficient $r_s = 0.991, p - value = 7.08E - 31$ $(p < 0.001)$ and another significant positive correlation between simulated and experimental slope values with Spearman correlation coefficient $r_s = 0.963,\ p - value = 2.70E - 20 (p < 0.001)$.

Table 2-1: by tuning the k, τ and δ Parameters the angular thresholds (75%) and the slopes of athletes' psychometric functions have been simulated

Subjects	*Angular Thresholds from Experiment*	*Angular Thresholds from Simulation*	*Slopes from Experiment*	*Slopes from Simulation*	*Inhibitory Gain (k)*	*Time Constant (τ)*	*Noise (δ)*
C12	4.041±1.05	**5.209±0.200**	0.261±0.03	**0.260±0.0048**	4	0.0245	0.022
A10	4.176±1.08	〃	0.252±0.028	〃	〃	〃	〃
B04	4.506±1.1	〃	0.246±0.027	〃	〃	〃	〃
B01	4.805±1.12	〃	0.243±0.026	〃	〃	〃	〃
A15	5.321±1.14	**5.448±0.205**	0.242±0.025	**0.251±0.0047**	2	0.033	0.032
B05	5.361±1.04	**5.425±0.193**	0.284±0.028	**0.279±0.005**	4	0.037	0.03
B09	6.602±1.41	**6.871±0.268**	0.188±0.02	**0.181±0.0036**	4	0.025	0.034
A11	6.637±1.52	〃	0.171±0.019	〃	〃	〃	〃
A06	6.609±1.21	**6.556±0.232**	0.233±0.022	**0.218±0.004**	8	0.033	0.032
A01	7.000±1.51	**7.228±0.263**	0.175±0.019	**0.188±0.0036**	8	0.03	0.034
C07	7.097±1.42	〃	0.192±0.02	〃	〃	〃	〃
C11	7.165±1.39	〃	0.197±0.02	〃	〃	〃	〃
B14	7.692±1.79	**7.664±0.363**	0.147±0.017	**0.130±0.0031**	1	0.024	0.026
B08	7.753±1.8	〃	0.146±0.017	〃	〃	〃	〃
A02	7.837±1.86	〃	0.141±0.017	〃	〃	〃	〃
A13	7.873±1.69	〃	0.159±0.018	〃	〃	〃	〃
B11	8.132±2	**8.509±0.421**	0.132±0.017	**0.115±0.003**	1	0.024	0.028
C13	8.594±2.08	〃	0.128±0.016	〃	〃	〃	〃
C04	9.173±1.77	**9.275±0.337**	0.158±0.017	**0.151±0.003**	16	0.025	0.034
B03	9.191±2.64	**9.198±0.438**	0.103±0.016	**0.113±0.0029**	2	0.024	0.028
C06	9.543±2.34	**9.818±0.496**	0.118±0.016	**0.102±0.0028**	2	0.024	0.03
B07	9.589±2.86	〃	0.096±0.015	〃	〃	〃	〃
C08	9.747±1.69	**9.791±0.313**	0.170±0.017	**0.168±0.0031**	32	0.033	0.032
A03	10.49±1.56	**11.131±0.376**	0.130±0.011	**0.144±0.0028**	32	0.025	0.34
A04	10.801±2.2	〃	0.132±0.015	〃	〃	〃	〃
A07	10.843±2.25	〃	0.128±0.015	〃	〃	〃	〃
A05	10.77±2.71	**10.696±0.529**	0.105±0.015	**0.098±0.0028**	4	0.024	0.028
C01	10.83±2.6	〃	0.110±0.015	〃	〃	〃	〃
A08	12.132±2.75	**12.315±0.606**	0.109±0.015	**0.091±0.0027**	8	0.024	0.028
B02	12.173±2.67	〃	0.113±0.015	〃	〃	〃	〃
B06	12.525±2.81	〃	0.108±0.014	〃	〃	〃	〃
B13	12.86±3.93	**12.258±0.664**	0.078±0.014	**0.083±0.0027**	2	0.024	0.034
A14	16.617±4.88	**17.978±1.105**	0.071±0.013	**0.06±0.0025**	8	0.024	0.036
A09	17.194±5.84	〃	0.061±0.013	〃	〃	〃	〃
C02	17.787±5.35	〃	0.068±0.013	〃	〃	〃	〃

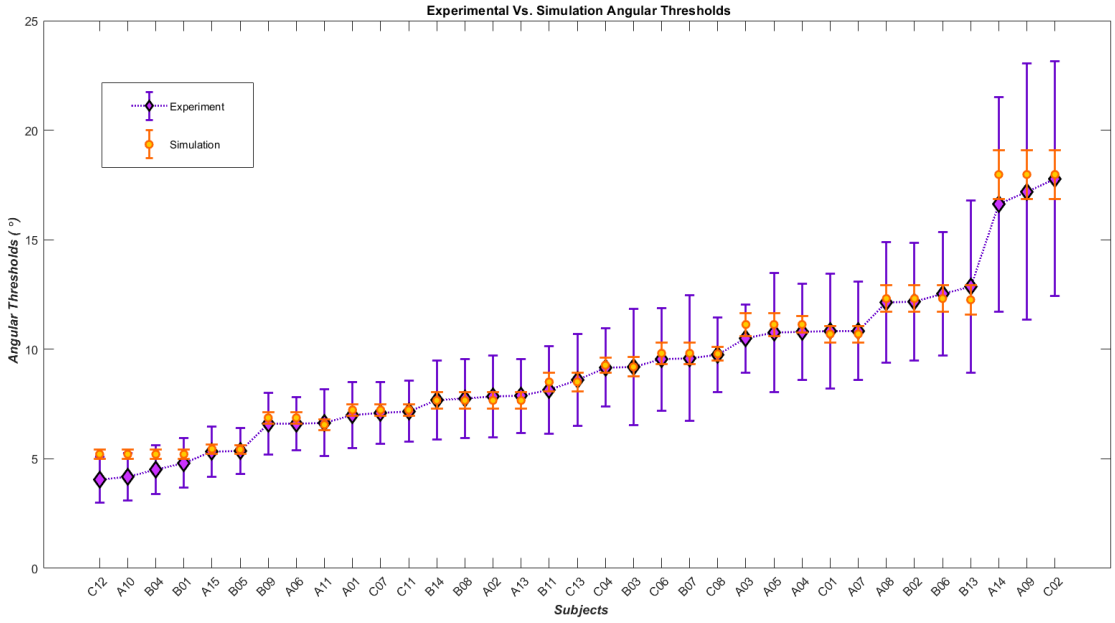

Figure 2-6: diamonds represent the angular thresholds (75%) calculated from the psychometric function of the subjects in the experimental tests and the black dots display the angular thresholds generated by simulation.

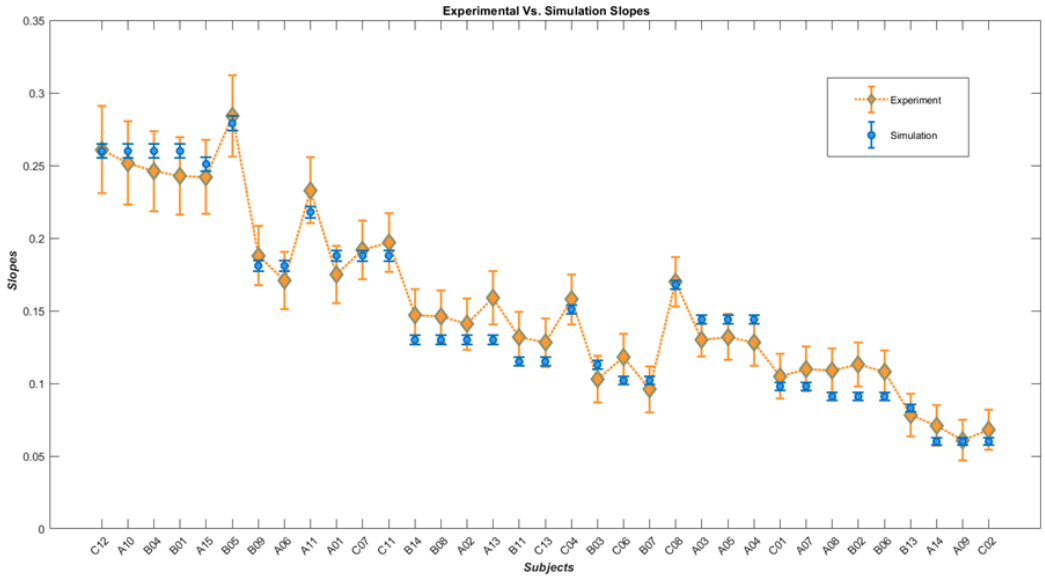

Figure02-7 : Diamonds represent the slopes of the subjects' psychometric functions while black dots demonstrate the simulated slopes

Discussion

We applied our descriptive risk-averse Bayesian decision-making approach to the 3rd layer and the mutual inhibition method to the 4th layer of the hierarchies, and unlike their predecessor proposed methods (Casile & Giese, 2005; Giese & Poggio, 2003), the model showed notable success to simulate human behaviour in the sense of mimicking their psychometric function. Therefore, despite all the existing limitations of the model, mirroring the behaviour of 11 athletic subjects has been accomplished. Moreover, we deem the model has not unleashed its full capacity, and those potentials are yet to be implemented which would make the model encompass the behaviour of all the subjects. One other future work at hand is to integrate the reaction time into the present model.

It is generally agreed that the human visual system exploits a mixture of all sorts of motion and form cues to detect the biological motion and neither the optical flow features nor the form features in and of themselves are adequate for the biological motion recognition (Blake & Shiffrar, 2007). Here, by the proposed model, we aimed to investigate and test the extent of the optic flow features sufficiency to discern a complex biological motion stimulus. The results seem to corroborate the findings in the Gliaie and Dotan (2015) study, which does not find the form cues integral to biological motion detection (Gilaie-Dotan et al., 2015). Also, our findings are in line with the claim in the Thurman and Lu (2014) study suggesting that the ventral pathway processes the dynamic biological and non-biological forms in the same fashion (Thurman & Lu, 2014).

However, there are limitations to be considered and discussed. One imposed constraint is the fact that each opponent motion neuron in our model only looks at two horizontally abutting receptive fields while in reality some of these neurons are wired to pool the signals from two distant receptive fields, enabling the visual system to process more global relative motions in a moving scene (A. T. Smith & Snowden, 1994). Furthermore, for the sake of simplification, like in the previous studies, the activity of the local motion neurons have been approximated by the computation of the optical flow from the stimulus animation (Casile & Giese, 2005). Also, both the first and second layers have been presumed to be noise free. Additionally, while the existence of rotation detectors have been substantiated in the human visual system (A. T. Smith

& Snowden, 1994), in our model, opponent motion detection level only provides the next level with expansion and contraction cues while rotation cues are an additional source of information from which the decision making parts of the model could benefit. Again, online learning is another capacity that needs to be implemented.

Additionally, it has been shown that executive function deficit leads to slower cognitive processing speed and longer time for completing tasks (Hill, 2004). Moreover, disorders such as anxiety disorder, major depressive disorder, attention deficit hyperactivity disorder, and autism impair the executive function (Hosenbocus & Chahal, 2012). Furthermore, one introduced model has suggested that some forms of autism are caused by an increased ratio of excitation/inhibition in sensory, mnemonic and some other systems because of genetics and environmental factors affecting one's neural system (Rubenstein & Merzenich, 2003). In our model, the increase in the processing time appearing in large inhibitory gains (which affects the excitation/inhibition ratio of the motion pattern neuronal system) could be construed as noticeable compliance of the present model with current findings.

The present model uses fixed prototypes, parameters, and priors to perceive and make decisions. A more comprehensive model could benefit from online learning and adaptation capacities. To implement such capabilities in the current platform and empower it to detect biological motion through online learning also lies in our plan for future work.

Funding

This work was supported by an NSERC-Essilor Research Chair, the NSERC discovery grant, and FESP- ÉOUM.

Article 2

"Extended Descriptive Risk-averse Bayesian Model" a More Comprehensive Approach in Simulating Complex Biological Motion Perception

Khashayar Misaghian, J.E. Lugo and Jocelyn Faubert (2018)

Faubert Lab, School of Optometry, University of Montreal, C. P. 6128, Montreal, Quebec, Canada.

Abstract

The importance of biological motion perception in different aspects of human lives such as survival, their social life, and interactions is a well-established consensus. So, it comes as no surprise that to determine its mechanisms and affiliated neurobiological substrates has been a subject of interest for quite a while. Previously, we proposed a descriptive risk-averse Bayesian simulation model, which represented the dorsal pathway as a motion information processor of the visual system (assimilating two-stream theory). This approach has been inspired by recent studies questioning the degree of impact of dynamic form cues in biological motion perception and was developed based on earlier neurophysiologically plausible model assumptions. The model was trained to distinguish the soccer ball's direction (invisible) from a set of complex biological motion soccer-kick stimuli used in an earlier psychometric study in our lab. The goal was to simulate the accuracy behaviour of the athlete subjects from our previous study by recreating their psychometric functions with the model. However, the model was not capable of simulating the subjects' reaction times in a neurophysiologically credible manner, and a few subjects could not be simulated. Therefore, in the present work, incorporating neural adaptation using our novel disremembering strategy in the decision-making level enabled the model to simulate the reaction times of the athlete subjects. Also, similar to earlier works, in our previous model, the rotational optic flow patterns have not been taken into account for decision making. Therefore, in the present extended version, the receptive fields to detect rotational optic flow have been implemented leading to the simulation of a new subject and the betterment of correlation between simulation and experimental coefficients. Such finding sheds light on the criticality of how rotational optic flow could contribute to the decision-making process while providing some insight on how different individuals perform at different levels. The correlation analysis of human versus simulation data shows a significant, almost perfect correlation between experimental and simulated angular thresholds and slopes, respectively, and also a significant and strong relation between athlete subjects and simulations average reaction times.

Keywords: Biological motion, Bayesian, Dorsal pathway, Hierarchical simulation model, Reaction Time

Introduction

The consistent flowing motions exclusive to biological agents are known as biological motion phenomenon. Biological motion tends to disclose a variety of information, ranging from the identity of a predator to the intent of a person in a social context. To accurately perceive those cues under somewhat suboptimal conditions could preserve the physiological or social survival of an observer (Blake & Shiffrar, 2007; Johansson, 1973). Biological motion could be efficiently recognized from point-light displays which are a number of lit points representing significant joints of the biological agent (Gilaie-Dotan et al., 2015; Johansson, 1973). The body of research in this domain is vast and diverse, but it mainly has been targeting three prominent themes: kinematic information captured by the visual system, underlying neural mechanisms of the biological motion perception (Blake & Shiffrar, 2007; Giese & Poggio, 2003) and brain's sensory and motor areas participation in biological motion perception (Saygin, 2012).

On account of the massive number of imaging, neurophysiological and psychophysical studies on the subject it appears that there exists a unanimous agreement on the prominent activated areas of the brain during the biological motion perception process. Dorsal and ventral pathways of the visual system along with the site of their convergence in the superior temporal sulcus (STS) are considered the major activated areas during the process (Beintema & Lappe, 2002; Mather et al., 1992).

Naturally, after a while, the accretion of data from biological motion experiments and also the need for a sound theoretical framework necessitated a computational model that could explain the biological motion perception specifically in a neurophysiologically plausible fashion (Blake & Shiffrar, 2007). Therefore, founded on the idea of formation and presence of saved prototypical patterns in the visual system Giese et al. proposed a feedforward multi-level architecture with one stream for dynamic form detection and one stream to detect the optic flow, simulating the dorsal and ventral pathways of the visual system (Giese & Poggio, 2003). Using this simulation model in their study, they concluded that it is the dorsal pathway (motion analysis stream) which has the most impact for biological motion perception (Blake & Shiffrar, 2007; Casile & Giese, 2005; Giese & Poggio, 2003). Such finding was at variance with the earlier study on the matter by Beintema and Lappe (Beintema & Lappe, 2002). Later, it was argued

that the perception/recognition of the biological motion requires the synergy between two pathways in order to achieve the most robust response (Blake & Shiffrar, 2007).

Meanwhile, developmental studies apprise of exclusive predisposition towards motions emanated from biological agents in human infants and newborn fowls while no exclusivity has been distinguished about organic shapes and forms over non-biological ones (Bardi et al., 2011; Vallortigara et al., 2005). Also, the existence of some low-level motion capturing filters specialized in biological motion has been indicated by behavioral data (Chang & Troje, 2008; Troje & Westhoff, 2006). Consequently, Thurman and Lu (2014) showed that the ventral pathway processes the biological and non-biological dynamic forms similarily, challenging the existence of any substrate, specialized in processing dynamic biological form exclusively (Thurman & Lu, 2014).

Although, further examinations of the neural correlates show the activation of some cortical regions linked to form and motion cues in addition to the ventral and dorsal pathways in the event of biological motion perception, the nature of those activations could not be appraised as causal in nature (Gilaie-Dotan et al., 2015; Grosbras et al., 2012; Kourtzi et al., 2008). Consequently, one study has investigated six patients with compromised visual cortex who had focal injuries in multiple regions of their ventral pathway. Accordingly, all subjects were capable of recognizing the point-light stimuli while maintaining not significantly different thresholds compared to intact subjects. Surprisingly, they exceded other patients who had injuries in other areas of the brain critical to biological motion perception (Gilaie-Dotan et al., 2015).

To explore the potentials and the limits of the dorsal pathway, considering the connotations from all recent findings and the apparent need to address the biological motion perception in a more realistic context, the necessity of a more effective biologically plausible computational framework appears desirable(Misaghian et al., 2018).

In a more pragmatic approach, Misaghian et al. proposed a biologically plausible simulation model which could anticipate the direction of the ball from a wide range of biological motion stimuli of a soccer player, adopted from Romeas et al. (2015), while previous approaches showed no promise when confronted with these stimuli (Romeas & Faubert, 2015). Founded on

the very assumption that the visual system recognizes and makes a decision using stored prototypical patterns (Giese & Poggio, 2003), our model managed to replicate the psychometric functions of 11 athlete subjects from a behavioural study accurately, (Misaghian, Lugo, & Faubert, 2018; Romeas & Faubert, 2015). The model is comprised of hierarchies parallel to the motion pathway hierarchy levels in the visual system (Casile & Giese, 2005; Giese & Poggio, 2003) while incorporating a descriptive risk-averse Bayesian scheme for pattern recognition and a more robust version of a mutual inhibition network for decision making (Misaghian et al., 2018). Despite the model's success, it could not contain all the subjects' performances from the psychophysical study (Romeas & Faubert, 2015) and lacked the circuitry to characterize the subjects' reaction times.

The present study intends to augment the scope of the model above in the sense that it could represent all subjects' behaviors from the Romeas et al (2015) (Romeas & Faubert, 2015). study in both accuracy and reaction time domains. In the enhanced model the integration of rotational detectors at the opponent-motion detection level extends the model's ability to explain observers' performance more comprehensively by exploring the role of the rotational cues (A. T. Smith & Snowden, 1994; Tanaka & Saito, 1989) in the decision-making process. In the meantime, modification of our robust mutual inhibition model that represents the motion pattern detection level empowers our simulation model to estimate the reaction time of the observers without compromising the results of the previous work (Misaghian et al., 2018).

Model

The descriptive risk-averse Bayesian model mentioned above is a feed-forward model consisting of hierarchies of neurons representing the dorsal stream as follows:

Local Motion Energy Detectors. Neurons at this level are sensitive to motion directions with small receptive fields (≈0.4 deg). At this level, the descriptive risk-averse Bayesian model directly incorporates sensitivity to four relative directions in 2D (up/down/left/right). The receptive fields are arranged in a 36x31 grid with some overlapping according to (A. T. Smith & Snowden, 1994). For the sake of simplification, the activity of local motion detectors is approximated using the vector fields obtained from the calculation of optical flow in all consecutive frames of the stimulus. A more detailed description can be found in Casile and Giese's paper (2005) (Casile & Giese, 2005). The presence of such neurons has been reported in areas V1/2 and area MT of monkey's visual cortex(A. T. Smith & Snowden, 1994).

Opponent-Motion Detectors. The second level of the hierarchy pertains to neurons that are sensitive to expansions, contractions, and rotations occurring in the contiguous subfields of their receptive fields (A. T. Smith & Snowden, 1994). It is believed that, within each subfield, Such detector "max-pools" the responses of the corresponding local energy neurons from the lower level and the output signal is a product of the maxima, suggesting spatial invariance within the receptive field (Allman et al., 1985; Gawne & Martin, 2002; Lampl et al., 2004; Riesenhuber & Poggio, 1999). It has been suggested that opponent-motion detection neurons might reside in the human brain's KO/V3B area (Orban et al., 1995; Orban et al., 1992).

In this study clockwise and counterclockwise rotation detectors have been implemented in addition to the previous horizontal and vertical contraction and expansion sensors to explore their role in the process of biological motion perception in light of previous findings (Misaghian et al., 2018).

Here, two 5x4 assemblies, accounting for clockwise and counterclockwise detectors, introduce 20 new rotation detectors to the previous arrangement of 100 contraction and expansion detectors (Casile & Giese, 2005; Misaghian et al., 2018).

Complex Global Optic Flow Pattern Detectors. Detectors in the next hierarchy level do possess receptive fields of more than 0.8 degrees (which cover the whole stimulus) and recognize complex optic flow patterns in the right temporal order. More accurately, detectors at this level are tuned to a specific optic flow pattern of a particular temporal order. Here, to simulate the third hierarchy level, the same structure as the previous study has been maintained (Misaghian et al., 2018).

The 18 neurons at this level of our model are asymmetrically and laterally connected. These connections are arranged in a way that the active neuron excites the neurons tuned to the future templates and inhibits the ones tuned to the past (Casile & Giese, 2005; Giese & Poggio, 2003; Mineiro & Zipser, 1998).

The dynamic of a detector sensitive to the optic flow pattern in the ith frame (the optic flow risen from the $i-1$ to ith frame) of one stimulus sequence is as follows (Casile & Giese, 2005):

$$\tau_{OFP}\,\dot{H}_i(t) = -H_i(t) + G_i(t) + \sum_m w(i-m) f(H_i(t))$$

Where $H_i(t)$ is the activity of the detector i, $\tau_{OFP} = 150\,ms$, is also the time constant of the global optic flow pattern layer dynamic, $w(m)$ is a weight kernel, $f(H)$ is a step threshold function, and the instantaneous template matching performed by the neuron is modeled as the feed-forward input $G_i(t)$. Here, the feed-forward input is generated by our previously designed descriptive risk-averse Bayesian classifier. Refer to Misaghian et al. (2018) for a thorough description of this approach(Misaghian et al., 2018) .

Different areas in the superior temporal sulcus have been known to be the most probable locations of the complex optic flow pattern neurons (Decety & Grèzes, 1999; Oram & Perrett, 1994; Perrett et al., 1985; Vaina et al., 2001)

Complete Biological Motion Pattern Detectors (Motion Pattern Detectors). The robust mutual inhibition model from Misaghian et al. (2018) had possessed no mechanism to explain the reaction time of the athlete subjects from Romeas and Faubert's study 2015 study (Misaghian et al., 2018; Romeas & Faubert, 2015). Here, by introducing, the disremembering strategy into the robust mutual inhibition model, motion pattern neurons are enabled to make consistent decisions but, this time, within a similar reaction time frame.

Neural adaptation refers to the decrease in the responsiveness of neurons exposed to a constant stimulus over time. For example, in the visual system, perception of an image or a motion

gradually diminishes or vanishes if there is no micro-saccadic eye movement (Martinez-Conde, Macknik, & Hubel, 2004). Moreover, the effect of adaptation phenomena has also been investigated and characterized in the context of decision making (Mayo & Smith, 2017; Theodoni, Kovács, Greenlee, & Deco, 2011). Complete motion pattern neurons as decision-making neurons are no exceptions and could not stay activated perpetually. Our disremembering strategy serves to implement the ephemeral nature of neural activation in our model.

Robust Mutual Inhibition Model with Adaptation. The mutual inhibition model (Lugo et al., 2018) has the dynamic below and explains the response of decision making neurons:

$$\tau \frac{dT}{dt} = -T + S\big(P_T(D)\big) \tag{3}$$

$$\tau \frac{dD}{dt} = -D + S(P_D(D,T)) \tag{4}$$

where, T is the activity of a primarily excited neuron and D represents the activity of other neurons. τ is a time constant and $S()$ is a modified Michaelis-Menten function (Wilson, 1999) which has been proven advantageous in excitatory-inhibitory network model design. Also, P_T and P_D are the information thresholds (Lugo et al., 2018). When information thresholds are negative and, as a result, the neurons lateral connections are off, the robust mutual inhibition model sets the negative output of the neurons into zero. For more information on the mechanism of robust mutual inhibition one must refer to Misaghian et al. (2018) (Misaghian et al., 2018).

To actualize the neural adaptation in our model, we add the following terms as an input to the dynamic of both T and D neurons:

$$Dis_T = u(t-\tau_a) * \big[T - S\big(P_T(D)\big) - kT\big] \tag{5}$$

$$Dis_D = u(t-\tau_a) * \big[D - S\big(P_D(D,T)\big) - kD\big] \tag{6}$$

where, $u()$ is the unit step function, τ_a marks the time point when adaptation starts and k is just a weighting coefficient. As one can see, at τ_a, the disremembering inputs to the differential equations get switched on and the dynamic of each neuron reduces to a simple exponential decline, driving the neuron out of excitation state.

Modeling Internal Noise. Like our previous study, to model the uncertainty, output of each optic flow pattern neuron is considered to be elicited from $\mathcal{N}(H_i(t), \Delta t\delta^2)$, where $\mathcal{N}()$ is a Gaussian process with the mean, $H_i(t)$, as the activity of the optic flow neuron i without noise and δ^2 being the variance of the added internal noise (Misaghian et al., 2018).

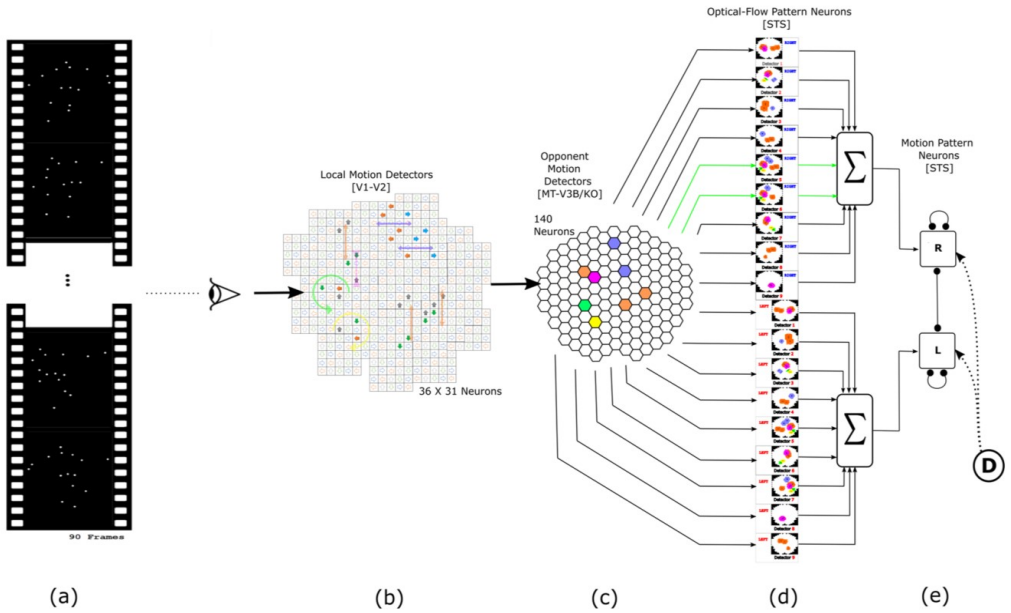

Figure 3-1: Schematic of the model in one hypothetical point in time, from left to right: (a) the reel of biological motion stimulus (b) local motion detectors as ensemble of 1116 neurons positioned in a 36 by 31 arrangement, are firing due to the motions they have experienced during two consecutive frames, represented by the cells with color-filled arrows (blue: right, orange: left, grey: up, green: down), the larger, two-headed or curved, colorful arrows were drawn to display the types of opponent motions that would be sensed on the next level (cyan: horizontal expansion, orange: vertical expansion, magenta: vertical contraction, green: counter-clockwise rotation, and yellow: clockwise rotation) (c) opponent motion detectors, the ensemble of 140 neurons to detect horizontal expansion, horizontal contraction, vertical expansion, and vertical contraction, the activated detectors are marked with color-filled hexagons with their corresponding color (cyan: horizontal expansion, orange: vertical expansion, magenta: vertical contraction, green: counter-clockwise rotation, and yellow: clockwise rotation), (d) optical-flow pattern detectors, an arrangement of 18 neurons following a one-dimensional mean-field dynamics, each neuron incorporates a statistical template (displayed as colorful map) that

represents a specific part of the manifold of the kicking sequences (for example neuron number 2 contains a template for the seconds 11 to 20 of the kick-to-right sequence, while neuron number 10 would have a larger instantaneous input for the seconds 1 to 10 of the kick to the left stimulus). Green arrows are highlighting the contribution of two cells to the evidence integration at that hypothetical point due to the similarity of the evidence signal and their template (e) thresholding stage, two decision neurons for the right and left decisions (marked by capital letters R and L on the square cells with soft edges) are following our mutual inhibition dynamics receiving their corresponding inputs from integration stage, the straight and curve lines with rounded heads highlight the inhibitory interaction between the neurons and the auto-inhibition, respectively. No activity could be seen by either of the neurons since at that hypothetical point in time, neither made a decision yet. Also, the dotted curved arrows and the circle with the letter D, are the representatives of the disremembering mechanism.

Methods

The simulation model has been implemented in Matlab, and the data and statistical analyses have been performed within R Studio framework. The original point light soccer kick from Romeas and Faubert (2015) has been adopted to maintain the similarity between the simulation model and human subjects (Romeas & Faubert, 2015). The stimulus is a 90-frame animation with 4.5-sec length demonstrating bright point lights, representative of human body significant joints, with a dark background. The leftward and rightward kicks have been synthesized by rotating the stimulus above about the Z-axis for different angles. While it is possible to rotate the stimulus to any arbitrary degree, the existing psychometric data only contain the human response from the deviations of 2° , 4°, 8° and 15° for either direction (Romeas & Faubert, 2015). Cross-validation and training data have been chosen from a whole range of 1° to 20° of deviation for both sides. This range spans all the possible degrees of deviation from a soccer goalkeeper point of view, considering the ball's distance from the goal and the physical goal width. The penalty kick is one realistic example where such a task is required by a soccer player.

The model has been validated using k-fold cross validation (k=5). Furthermore, the range of 7° to 20° has been used for training. Also, the model has been tested for the angles from the psychophysical study (Misaghian et al., 2018; Romeas & Faubert, 2015).

Local Motion Energy and Opponent Motion Neurons. While the 1st hierarchy level of local motion energy detectors have been correctly implemented as in Casile and Giese (2005), the new version of our model incorporates the clockwise and counterclockwise detectors in addition to previously implemented vertical and horizontal expansion and contraction neurons in its 2nd level (Casile & Giese, 2005; Misaghian et al., 2018). We implemented 20 receptive fields for each clockwise and counterclockwise detection, encompassing the 36x31 local motion detection grid of the lower layer. Each rotation receptive field is connected to 4 contiguous and overlapping subfields allowing the rotation detector to pick up the highest rotational activity using the max-pooling strategy. Each subfield is comprised of 14x14 local motion sensors making up a 4x5 receptive field arrangement for either of clockwise and counterclockwise rotation in the opponent-motion detection level. To clarify the mechanism of the detection, let us consider one clockwise rotation receptive field: as mentioned, there are four subfields connected to each detector: the upper-left, the upper-right, the lower-left and the lower right. Because our local motion detection level only detects the four fundamental right, left, up and down directions, the clockwise rotation could only manifest itself under two conditions depicted in Figure 3-2, and either of these situations get the clockwise rotation detection neuron excited.

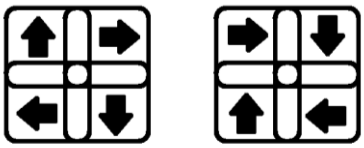

Figure 3-2 : Subfields in one clockwise rotation receptive field of our model

Optic Flow Pattern Neurons. The architecture of the 3rd hierarchy level has remained unchanged from the previous model introduced in Misaghian et al. (2018) (Misaghian et al., 2018). Briefly, there exist nine detectors for each direction, and each detector is sensitive to 10 sequential frames out of 90 frames of the stimulus which sums it up to 18 neurons in the optic flow pattern level. For more detailed information on this one could refer to (Misaghian et al., 2018).

Motion Pattern Neurons. Two complete motion pattern neurons have been assigned, to differentiate between the leftward kick and rightward kick stimuli. The robust mutual Inhibition model with the ability to adapt and disremember has been utilized to model the interactive dynamics of these decision-making neurons. To solve this nonlinear differential system, we have employed the 4th order Runge-Kutta method.

Operating the Simulator. In the behavioral study of our interest, a forced-choice paradigm task has been devised to detect the direction of the ball (left or right) from the biological motion stimuli (Romeas & Faubert, 2015). Therefore, subjects performed the task for a total of 960 times, facing the randomly ordered stimuli of left and right shooting with $2^{\circ}, 4^{\circ}, 8^{\circ}$ and 15° degrees of deviation (120 times for each side and each angle). Subsequently, in our previous study, the tuning of three parameters of the model was adequate to replicate the psychometric function of 35 athlete subjects which described their precision in terms of angular deviation (Misaghian et al., 2018). The three mentioned parameters are the standard deviation of the internal noise, δ, the time constant, τ, and the inhibitory feedback gain, k. In the present extended model, the new parameter τ_a, which characterizes the starting time point of the adaptation process is the parameter which enables our model to simulate the reaction time of human subjects. More precisely, each reaction time from each trial is calculated by averaging the time points within which the winning decision signal is at its maximum. It is our intention to tune our model in a way that can generate the angular threshold and the slope of each subject along with its average reaction time and this must be achieved by modifying four parameters instead of the previous three:

1. The standard deviation of the added internal noise, δ .
2. The time constant, τ .
3. The inhibitory feedback gain, k, and

4. The time point of adaptation onset, τ_a

Results

Extended Model Reaction Time Output. For a wide range of parameters, $k, \tau \; and \; \delta$, the model has been run for a constant parameter value of $\tau_a = 1.22 \; sec$ and the angular thresholds, slopes and reaction times have been calculated accordingly. Part of the results has been presented below to give an insight into how the reaction time would vary as a function of all four parameters (**Table 3-1**). Each measured reaction time in the psychometric data (Romeas & Faubert, 2015) is a sum of motor time plus the actual reaction time (time lapse between exposure to the stimulus and the initiation of the motor response). Thus, it is worth mentioning, that the motor time (time elapsed from motor response initiation and button being pushed) has been approximated to zero in this study. This approximation has been made, considering the motor time being only a fraction of the reaction time in our task, one being in the order of tens of milliseconds (Botwinick & Thompson, 1966) and the other one's average being one second. Adding to previous findings, the increase in neurons' time constant, τ, not only contributes to smaller angular thresholds and steeper slopes but also leads to a decrease in the reaction time. In other words, better performance. Furthermore, while an increase in inhibitory gain, k, deteriorates and then ameliorates the response accuracy of the model after certain inhibition gain value, it always leads to higher reaction time. As one could see in the **Table 3-1,** shaded cells show how doubling the inhibitory gain, k, results in a lower angular threshold and a steeper slope while the reaction times of both conditions are unrealistically large which is normal considering k being too large for both conditions. It is the consensus, that slower cognitive processing speed could be a result of executive function deficit because of disorders such as autism and attention deficit hyperactivity disorder (Hill, 2004; Hosenbocus & Chahal, 2012). Also, it has been suggested that some forms of autism are believed to be caused by a high ratio of excitation/inhibition in neuronal systems (Rubenstein & Merzenich, 2003).

Intriguingly, having within-range accuracy with such high reaction time when k is large stands in line with an autistic behaviour, corroborating the implications from our previous work, suggesting these states of our model could be associated with what occurs in some forms of autism (Hill, 2004; Hosenbocus & Chahal, 2012; Misaghian et al., 2018; Rubenstein & Merzenich, 2003).

Furthermore, the increase in internal noise level, δ, results in a higher angular threshold, flatter slope and faster reaction time or overall worse performance of the simulation model.

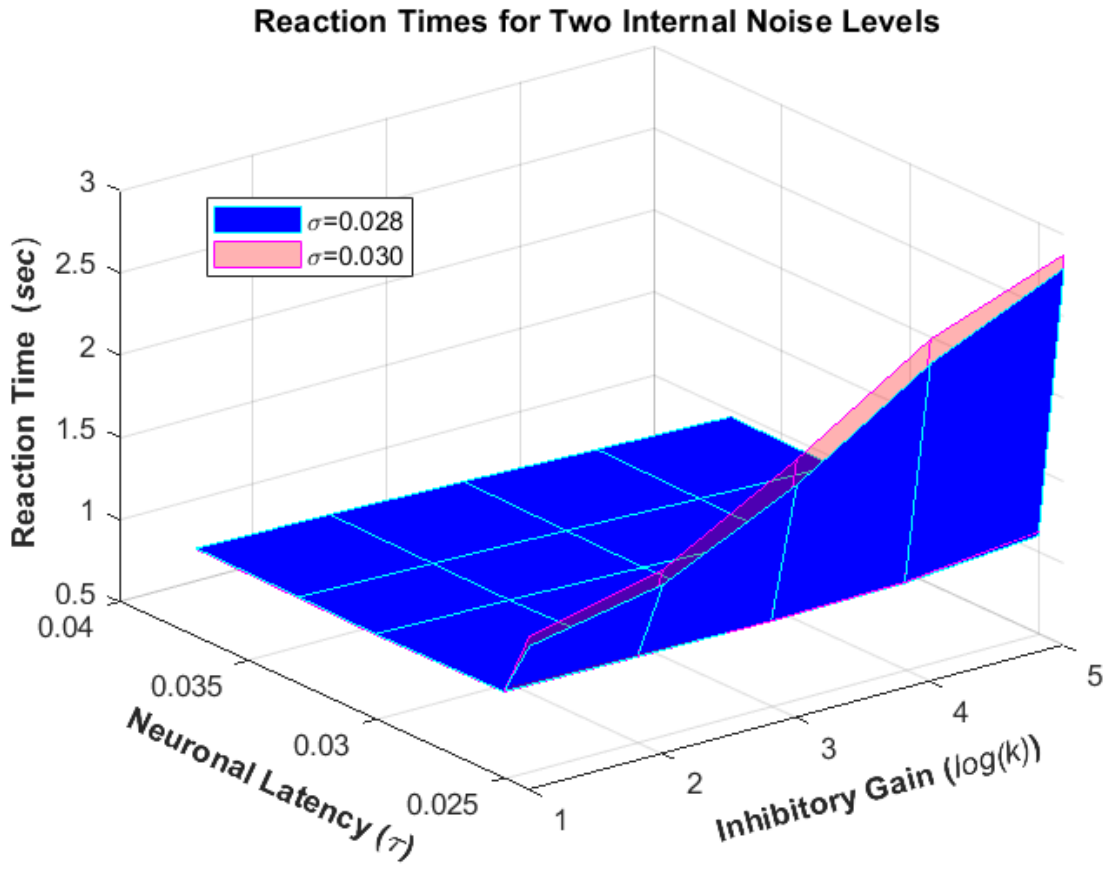

Figure 3-3: The reaction times resulted from running the model for exemplary ranges of neuronal latency ($\tau = 0.024,\ 0.025,\ 0.03,\ 0.033,\ 0.037\ sec$) and inhibitory gain ($k = 2, 4, 8, 16, 32$) for three noise levels ($\delta = 0.028, 0.030, 0.034$)

Also, the table below demonstrates the mentioned reaction times of the simulated observer along with its corresponding angular thresholds and slopes for the mentioned ranges of τ and k.

Table 3-1: For $\tau_a = 1.22$, the angular threshold and slope of the psychometric function and the average reaction time of the model for different values of τ and k, for two noise levels ($\delta = 0.030$ and $\delta = 0.034$) have been calculated and reported below.

Threshold	τ				
$\delta = 0.030$	**0.024**	**0.025**	**0.03**	**0.033**	**0.037**
2	9.82	5.57	5.28	5.20	5.02
4	10.96	5.96	5.60	5.59	5.43
8	13.97	6.83	6.34	6.15	5.93
16	**14.72**	8.30	7.69	7.40	6.96
32	**14.88**	10.18	9.31	9.04	8.91

k

Threshold	τ				
$\delta = 0.034$	**0.024**	**0.025**	**0.03**	**0.033**	**0.037**
2	12.26	6.40	5.89	5.81	5.67
4	13.97	6.87	6.41	6.17	5.98
8	16.32	7.73	7.23	7.05	6.80
16	**16.71**	9.28	8.59	8.47	7.95
32	**15.45**	11.13	10.59	10.26	9.90

k

Slope	τ				
$\delta = 0.030$	**0.024**	**0.025**	**0.03**	**0.033**	**0.037**
2	0.10	0.23	0.26	0.28	0.29
4	0.10	0.22	0.26	0.25	0.28
8	0.08	0.20	0.22	0.24	0.27
16	**0.09**	0.18	0.20	0.21	0.24
32	**0.10**	0.16	0.18	0.19	0.19

k

Slope	τ				
$\delta = 0.034$	**0.024**	**0.025**	**0.03**	**0.033**	**0.037**
2	0.08	0.19	0.22	0.24	0.24
4	0.08	0.18	0.21	0.22	0.24
8	0.07	0.16	0.19	0.20	0.22
16	**0.07**	0.15	0.17	0.17	0.20
32	**0.09**	0.14	0.15	0.16	0.16

k

RT	τ				
$\delta = 0.030$	**0.024**	**0.025**	**0.03**	**0.033**	**0.037**
2	1.375	1.028	1.019	1.030	1.039
4	1.530	1.021	1.006	1.014	1.025
8	1.915	1.016	0.985	0.994	1.006
16	**2.433**	1.027	0.957	0.968	0.981
32	**2.793**	1.096	0.938	0.948	0.960

k

RT	τ				
$\delta = 0.034$	**0.024**	**0.025**	**0.03**	**0.033**	**0.037**
2	1.434	1.025	1.014	1.022	1.034
4	1.622	1.019	0.996	1.007	1.019
8	2.070	1.017	0.976	0.986	0.996
16	**2.581**	1.033	0.948	0.960	0.974
32	**2.876**	1.121	0.928	0.937	0.951

k

Integration of Rotation Detection in Opponent Motion Hierarchy Level. One other aspect of our extended model, as mentioned above, is the integration of rotation detection receptive fields in the opponent-motion hierarchy level. In doing so, as anticipated, feeding the rotation features in addition to expansion/contraction features to the third layer leads to a better performance in all computed states of the model with no exception, meaning a lower angular threshold and steeper slope (no significant change in reaction time). It is needless to say that the opponent motion detectors were trained with rotation included training data, with the same fashion reported in Misaghian et al. (2018) (Misaghian et al., 2018).

Interestingly, by turning on the rotation receptive fields, the simulation of the performance of subject B10 which was not attainable in the previous setup (Misaghian et al. 2018) has been achieved leaving us with only two non-simulated subjects from our entire athlete subject pool. One credible interpretation of this finding could be that, when it comes to biological motion perception, it is highly probable that the visual system of different individuals deploys a different combination of its expansion/contraction and rotation receptive fields. In more general words, because of the various factors, the representation of the neural hierarchies of the visual system could be diverse at different levels, including the opponent motion detection layer (Kriegeskorte & Douglas, 2018). Therefore, one could deduce that, by knowing the right combination of operating expansion/contraction and rotation receptive fields the two non-simulated subjects could be mimicked. Implementing the capacity for the model to deploy the appropriate combination would be an exciting subject of future work.

Human Results Vs. Simulation Results. The simulated angular thresholds and slopes along with the average reaction time and the four parameters which drive the model in those states versus the corresponding experimental values have been reported in **table 3-2**. Similar to our previous work (Misaghian et al., 2018), we grouped the subjects based on the similarity of their angular threshold, slopes and reaction times and used grid-search to simulate those groups and determine the corresponding parameters. It is worth noting that there were some subjects with no similarity to any other subjects and that they were accounted for as a group with a single member. Moreover, this grouping approach only makes it easier to gain much more generalized insight into the overall behaviour of subjects. While it is entirely possible to pinpoint each subject with a slightly different set of parameters, one could see that it could only defeat the purpose of generalization.

Since the reaction time is the new output feature of our model, a plot of the groups' average reaction times against the corresponding simulated values is depicted in **Figure 3-4**, below.

Analysis of the correlation reveals significant positive correlations between experimental and corresponding simulated variables: Spearman's correlation coefficient between experimental and simulated angular thresholds is $r_s = 0.984, p - value = 2.01E - 27$ $(p < 0.001)$, between experimental and simulated slope, is $r_s = 0.955,\ p - value = 1.22E - 19 (p < 0.001)$ and finally between experimental and simulated average reaction time is $r_s = 0.513,$ $p - value = 0.0014$ $(p < 0.005)$. Higher variation of reaction times from subject to subject and our approach to simulate subjects in groups for the sake of generalization is the reason that the correlation value between experimental and simulated average reaction times shows a distinct relationship. However, if we look into the correlation between simulated average times and the subjects' average of each group the relationship proves to be strong: $r_s = 0.70,\ p - value = 0.002 (p < 0.005)$.

Table 3-2: by tuning the k, τ, δ and τ_a the angular thresholds (75%) and the slopes of athletes' psychometric functions along with their average reaction times have been simulated.

Rotation detectors are active for simulating B10

Subjects	Angular Thresholds from Experiment	**Angular Thresholds from Simulation**	Slopes from Experiment	**Slopes from Simulation**	Reaction Time from Experiment	**Reaction Time from Simulation**	Inhibitory Gain (k)	Time Constant (τ)	Noise (δ)	adaptation onset (τ_a)
'C12'	4.041±1.06	**5.252±0.20**	0.261±0.030	**0.263±0.0049**	0.994±0.07	**1.148±0.0005**	4	0.025	0.022	1.22
'A10'	4.176±1.08	〃	0.252±0.029	〃	0.929±0.04	〃	〃	〃	〃	〃
'B04'	4.506±1.11	〃	0.246±0.028	〃	1.194±0.05	〃	〃	〃	〃	〃
'B01'	4.805±1.13	〃	0.243±0.027	〃	1.443±0.06	〃	〃	〃	〃	〃
'A15'	5.321±1.15	**5.317±0.19**	0.242±0.025	**0.276±0.005**	1.131±0.08	**1.106±0.0002**	2	0.033	0.032	1.34
'B05'	5.361±1.05	**5.201±0.18**	0.284±0.028	**0.307±0.0055**	1.165±0.01	**1.146±0.0002**	4	0.037	0.030	1.40
'B09'	6.602±1.42	**6.872±0.27**	0.188±0.021	**0.180±0.0036**	1.001±0.03	**1.020±0.0003**	4	0.025	0.034	1.22
'A11'	6.637±1.52	〃	0.171±0.023	〃	1.013±0.05	〃	〃	〃	〃	〃
'A06'	6.609±1.22	**6.793±0.25**	0.233±0.020	**0.200±0.0038**	0.989±0.03	**0.883±0.0002**	8	0.033	0.032	1.10
'A01'	7.000±1.52	**6.909±0.25**	0.175±0.02	**0.205±0.0038**	1.007±0.01	**1.089±0.0003**	8	0.030	0.034	1.40
'C07'	7.097±1.42	〃	0.192±0.02	〃	1.169±0.07	〃	〃	〃	〃	〃
'C11'	7.165±1.39	〃	0.197±0.02	〃	1.146±0.08	〃	〃	〃	〃	〃
'B14'	7.692±1.80	**7.701±0.36**	0.147±0.018	**0.131±0.0032**	1.005±0.04	**1.076±0.0009**	1	0.024	0.026	0.96
'B08'	7.753±1.81	〃	0.146±0.018	〃	0.923±0.06	〃	〃	〃	〃	〃
'A02'	7.837±1.87	〃	0.141±0.018	〃	1.133±0.04	〃	〃	〃	〃	〃
'A13'	7.873±1.69	〃	0.159±0.018	〃	1.203±0.08	〃	〃	〃	〃	〃
'B11'	8.132±2.00	**8.459±0.39**	0.132±0.017	**0.124±0.0031**	1.065±0.02	**1.116±0.0009**	1	0.024	0.028	1.00
'C13'	8.594±2.09	〃	0.128±0.017	〃	1.147±0.05	〃	〃	〃	〃	〃
'C04'	9.173±1.78	**9.685±0.35**	0.158±0.017	**0.148±0.003**	0.887±0.03	**0.880±0.0003**	16	0.025	0.034	1.04
'B03'	9.191±2.64	**9.292±0.45**	0.103±0.016	**0.111±0.0029**	1.141±0.07	**1.181±0.0012**	2	0.024	0.028	1.00
'C06'	9.543±2.34	**9.709±0.41**	0.118±0.016	**0.123±0.0029**	0.899±0.05	**1.078±0.001**	2	0.024	0.030	0.90
'B07'	9.589±2.86	〃	0.096±0.016	〃	1.264±0.07	〃	〃	〃	〃	〃
'C08'	9.747±1.70	**9.838±0.32**	0.170±0.017	**0.167±0.0031**	0.947±0.05	**0.944±0.0003**	32	0.033	0.032	1.22
'A03'	10.490±1.56	**12.076±0.43**	0.130±0.011	**0.130±0.0028**	0.964±0.04	**0.858±0.0006**	32	0.025	0.340	0.88
'A04'	10.801±2.20	〃	0.132±0.016	〃	0.757±0.05	〃	〃	〃	〃	〃
'A07'	10.843±2.26	〃	0.128±0.016	〃	0.871±0.05	〃	〃	〃	〃	〃
'A05'	10.770±2.72	**10.747±0.41**	0.105±0.015	**0.130±0.0029**	1.098±0.06	**1.068±0.0014**	4	0.024	0.028	0.80
'C01'	10.830±2.61	〃	0.110±0.016	〃	0.909±0.06	〃	〃	〃	〃	〃
'A08'	12.132±2.76	**12.722±0.45**	0.109±0.015	**0.124±0.0027**	0.793±0.03	**0.962±0.0013**	4	0.024	0.032	0.66
'B02'	12.173±2.68	〃	0.113±0.015	〃	0.936±0.05	〃	〃	〃	〃	〃
'B06'	12.525±2.82	〃	0.108±0.015	〃	0.888±0.06	〃	〃	〃	〃	〃
'B13'	12.860±3.94	**11.549±0.49**	0.078±0.015	**0.109±0.0028**	1.032±0.06	**1.067±0.0011**	2	0.024	0.034	0.84
***'B10'**	13.160±3.02	**13.363±0.56**	0.103±0.015	**0.101±0.0027**	1.044±0.06	**1.208±0.0009**	64	0.025	0.036	1.15
'A14'	16.617±4.89	**17.319±0.74**	0.071±0.014	**0.088±0.0025**	1.058±0.06	**1.154±0.0017**	4	0.024	0.038	0.60
'A09'	17.194±5.84	〃	0.061±0.014	〃	1.014±0.04	〃	〃	〃	〃	〃
'C02'	17.787±5.36	〃	0.068±0.014	〃	0.842±0.04	〃	〃	〃	〃	〃

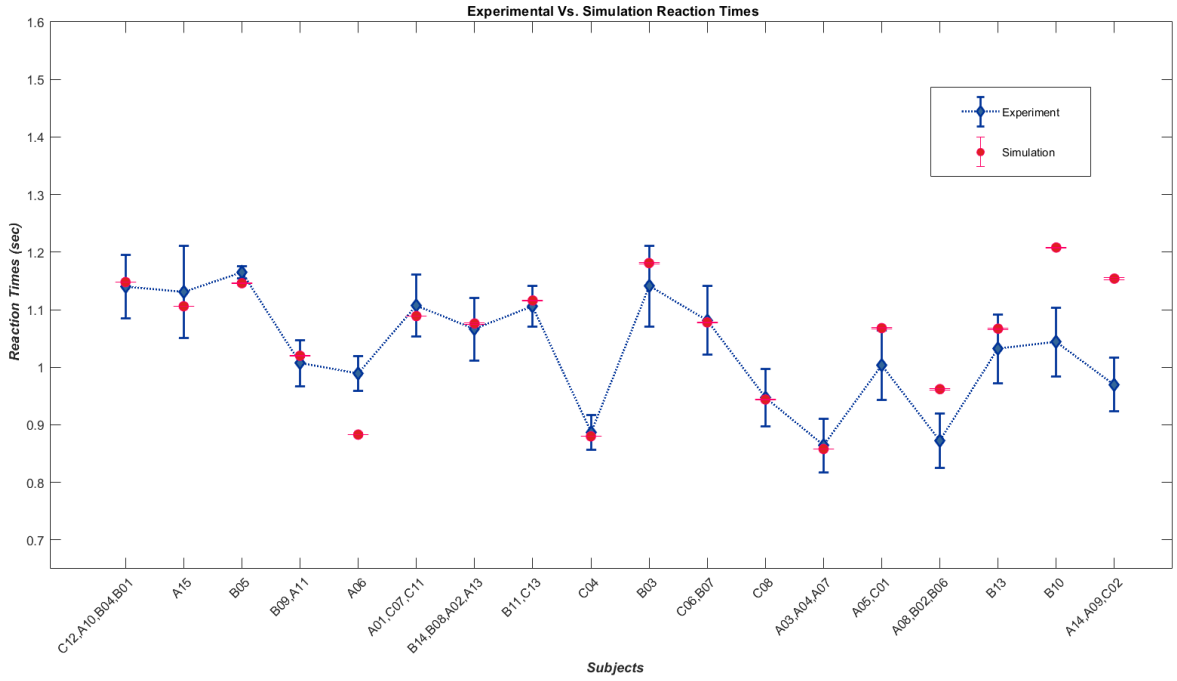

Figure 3-4: Diamonds represent the average reaction time of athlete sub-groups performing the tasks in the psychometric experiment (Romeas & Faubert, 2015) while dots demonstrate the average reaction times acquired from the model simulating those sub-groups.

Discussion

To achieve better performance by including the rotational optic flow detectors into the mix, obviously, was not a counterintuitive result because, most of the time, more information leads to better decisions. However, the interesting finding was the discovery of a more flexible and wider range of angular threshold-to-slope relationships in psychometric curves that enables the model to encompass a noticeably bigger spectrum of behaviours. There were three subjects out of 38 in the subject pool whose behaviour could not be simulated before (Misaghian et al., 2018). The fact that such accuracy behaviours (psychometric functions) exist in the human data is a reliable indicator of a missing factor or factors in the previous setups. Moreover, managing to simulate one of these subjects by including the rotational features postulates that the utilization of such features is essential but that they most likely differ from individual to individual. Unfortunately, the extent of it could not be estimated by our simulation model.

Furthermore, empowering the model to have a reaction time using our physiologically plausible strategy not only seemed necessary for a thorough simulation model but also appeared to be a source of new information and disambiguation. For instance, the earlier setup could achieve similar behaviours with different tunings, and it was only possible to pick the right set of parameters by examining the characteristics of the decision signals. However, in the extended model, the reaction time of the model was showing which tuning complies with human behavior. Also, as mentioned in the results section, the same accuracy behavior but with much more longer reaction time could be deemed as a result of executive function deficit and analyzing the model's parameters showed that such states occur when the mutual inhibition is high. Interestingly, it has been suggested that some forms of autism could be the result of an increased ratio of excitation/inhibition in sensory, mnemonic and some other systems (Rubenstein & Merzenich, 2003).

There exist numerous limitations to the present model. For example, the opponent-motion neuron in the model only receives signals from adjoining receptive fields, and there is no detector to pool the signals from two distant receptive fields. Hence, it is unable to incorporate any global relative motion in a moving scene (A. T. Smith & Snowden, 1994). Also, both the first and second layers have been presumed to be noise-free and also no process noise has been introduced to the model. That is going to be considered in the future work.

Furthermore, the feedforward assumption in our model imposes fixed prototypes, parameters, and priors which apparently is far from what happens in the live human visual system. A more inclusive model must also be capable of learning and updating. Therefore, the integration of such capacities lies in our future work.

Funding

This work was supported by an NSERC-Essilor Research Chair, the NSERC discovery grant, and FESP- ÉOUM.

Conclusion

Complying with the law of parsimony or Ockham's razor, the descriptive simulation model of biological motion perception adopts certain assumptions:

- Maintaining feedforward architecture while the brain always updates and learns:

In general, intelligence is regarded as the capacity to perceive, infer the information and preserve it as knowledge for further use (Gottfredson, 1997). If this cognitive process involves working memory, it is called fluid intelligence (i.e., pattern recognition and problem-solving) and if it depends on long term memory it is known as crystallized intelligence (i.e., the ability to deduce using words or numbers) (Cattell, 1963; Ross & Martin, 2006; Tullo, Faubert, & Bertone, 2018). Moreover, what resides in the first level of the working memory is nothing but an activated subset of representations in long-term memory. The second level of the working memory could retain up to four of these activated representations (Cowan, 1998). Therefore in both cases of fluid or crystallized processes, we are dealing with already formed representations that are prone to minor changes and updates. In our simulation model, the fixed prototypical templates count for the aforementioned memory representations; therefore, the feed-forward fixed architecture assumption only falls short if we want the model to learn any body movement automatically from the ground up or to update the prototypes in case of significant variations of the body movements after the representations are formed.

- Resorting to the two-stream theory and modeling the motion pathway while there exists an ongoing debate on the validity of such theory (Whitwell, Milner, & Goodale, 2015)

- Excluding the mirror neurons in the implementation of the model, while one group of neurons which is considered to be a part of the mirror neuron system and reside in superior temporal sulcus (STS), does not discharge amid the execution of action but is selectively responsive to biological motion (Grossman et al., 2000)

There is no doubt that these items must be addressed and integrated into future work. As for the next step, to excel the model into an online and Omni-learner could be considered a significant leap forward.

Online Learning

One primary assumption of the model is that the model adopted a feed-forward architecture for the sake of simplicity. While such a constraint created a controlled setup to address the concerns of this study, in reality, it is expected that the network learns and updates its knowledge according to what it is being exposed to and the variations of the exposure in time. Such a platform is one step closer to the idea of a universal biological motion detector like the one in the visual system.

As mentioned in previous chapters, our approach is a statistical risk-sensitive framework with a pre-tuned risk matrix. Now, for making our network capable of online learning, it only makes sense that we only pursue those algorithms that cater to our solution. In the realm of machine learning, reinforcement learning wherein an agent learns to do specific actions that result in the highest reward is a subset of unsupervised learning whose method of learning conforms to cause and effect. Q-learning as a form of reinforcement learning has shown promise in modeling reward-based human decision making and dopamine mediated reward prediction mechanisms (Schultz, 2002; Schultz, Dayan, & Montague, 1997; Shen, 2015).

To give a brief background on Q-learning, here we introduce some concepts:

- Environment: The plot within which the problem happens
- Agent: an autonomous actor that performs actions under certain assumptions
- Action: any possible performance that the agent could perform (like a link in a graph)
- State: the situation within which the agent could preside (like a node in a graph)
- Reward: the immediate gain that the environment awards the agent for its last action (like a weight assigned to each link)
- Policy: the strategy that dictates the next action by the agent based on the current state
- Value: expected long-term gain of any state using a specific policy

- Action value: also called Q-value similar to value but only depends on the action, which means the expected long-term gain from taking a particular action in a particular state using specific policy

If we assume, in a certain environment, one of the states is the goal, the objective of the agent with a clean slate is to arrive at that state when put into the mentioned environment. For instance, to assign one state as the goal could be achieved by associating a reward value or weight to each possible action. For example, if there is one state from which the agent could go to the goal state in the next step that action has a reward value of 100, but, any action that does not lead to the goal state has zero reward value. One could suggest that the reward is a matrix that relates the states to actions with elements of the matrix being the reward values. In that matrix besides the values of zero and 100, when some action does not exist, we merely assign a negative reward value to it. Now, the Action value matrix, Q, with an unknown number of elements and also initialized to a zero matrix with a single value of zero (expands when new states discovered), represents the brain of our agent who knows nothing. With a simple transition formula:

$$Q(state, action) = Reward(state, action) + \gamma \times Max(Q(next\ state, all\ actions))$$

Each element of the Q would be calculated by adding a learning term to the corresponding value in the reward matrix. The updating term is the maximum value from the Q for all possible actions in the next state multiplied by learning rate, γ.

By initializing the agent in a random state and Q to a zero matrix, the algorithm could start. At each step the agent randomly chooses to go to one of the possible states, then we calculate the value of the element in the Q by adding the corresponding element of the reward matrix element to the maximum value of all possible actions in the next state in the Q multiplied by an updating factor (figure 1). What is explained above characterizes one iteration of the learning process. Upon convergence, one can assume that the agent knows the optimal path to the goal, meaning from whichever initial state the path that sums up the highest value is the path to take (McCullock, 2012).

In the framework of our biological motion perception model, the agent would be the third layer that recognizes the different stages of the motion, the state space is the stimuli (all kinds of body movement) moved through the first and second layers, and the action space would

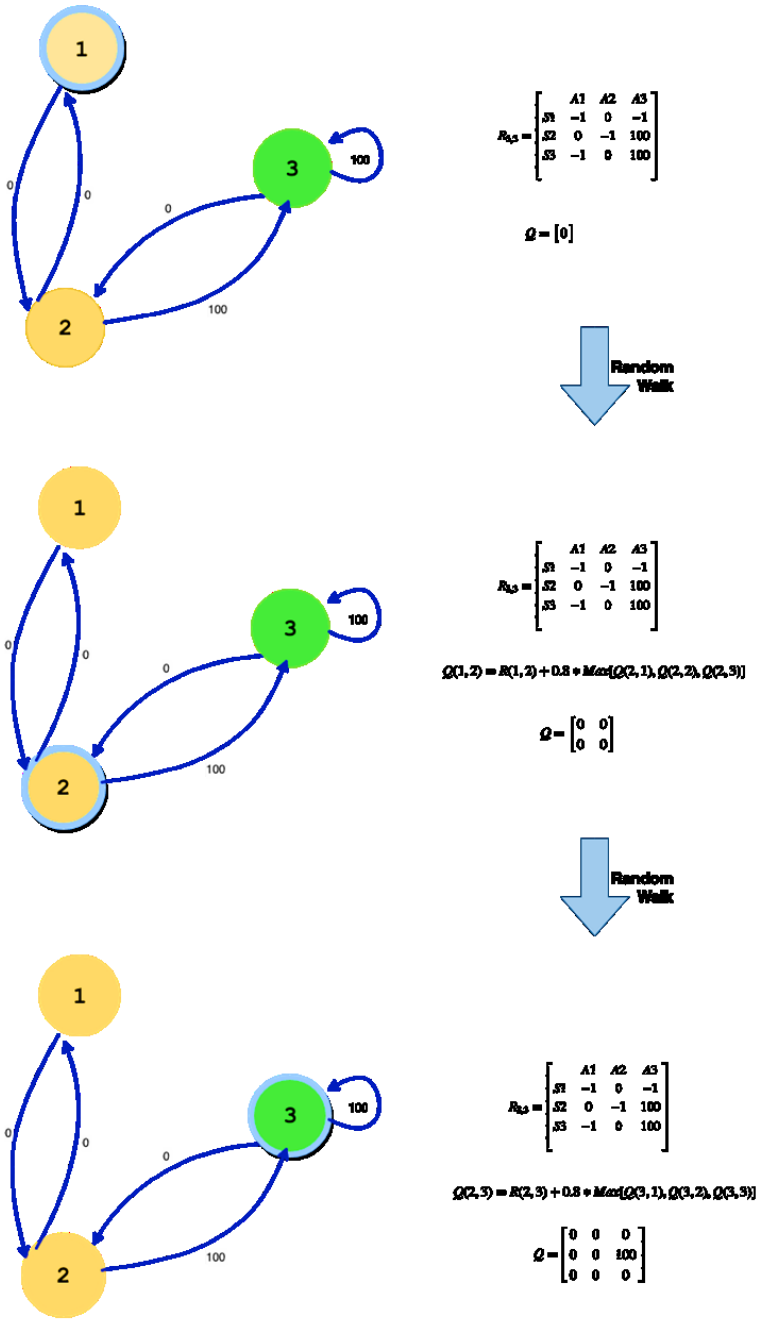

Figure 4-1 : A simple example of one episode of the Q-learning algorithm for a 3 state system with an absorbing goal

be the classification of the observations into their corresponding temporal stages. At every run, we set up a new environment with a new initial state. At each step, for a given sequence in the stimulus, we get an action from the agent based on which the environment returns reward and a new state. This set of state, action, reward, and next states shapes up our Q-value according to the mentioned updating rule. A stabilized converged Q-value is the policy that enables the agent to make the best classification given observation for maximum reward. To attain accurate Q-values, one could resort to deep neural networks. Hence, the term deep Q-learning (Surma, 2018).

To model systems with unknown transition probabilities like human behaviour one study has proposed a risk-sensitive Q-learning algorithm for implementing the sequential decision making in humans and asserted that by a careful choice of utility function this algorithm could offer a risk-sensitive framework for decision making with noisy rewards which fall perfectly into our question's scenario (Shen, 2015).

More on Autism

We showed that the increase in the inhibitory gain, k, causes a change of the performance. Surprisingly, after exceeding a certain value, the system performs better in exchange for noticeably longer reaction time. Whereas, slower cognitive processing speed is believed to be one repercussion of executive function deficit caused by a multitude of disorders such as ADHD or autism (Hill, 2004; Hosenbocus & Chahal, 2012). Therefore, we found this trait of our model in concurrence with the findings by Rubenstein and Mezernich (2003) which suggested that some forms of autism are believed to be caused by a high ratio of excitation/inhibition in neuronal systems (Rubenstein & Merzenich, 2003). It is worth noticing that we are referring to the slower reaction time in cognitive function of individuals with autistic spectrum disorder and not the slowed-down motor time caused by the compromised proprioception for some ASD individuals (Schmitz, Daly, & Murphy, 2007).

Reaction Time Approximation

Previously, we mentioned that the motor time (MT) had been approximated to zero in this study. One could define the Reaction time as the amount of time between exposure to a

stimulus and the initiation of the motor response to that stimulus by the individual (Wong et al., 2015). It has been reported that the mean reaction time for young adults is around 160 milliseconds for a simple auditory stimulus detection task and about 190 milliseconds for visual stimulus detection task and, expectedly, this number goes up for Go/No-go, choice reaction time (CRT) and discrimination reaction time tasks (Kosinski, 2008; Taoka, 1989). Also, in a simple reaction time test (the simple task of lifting a finger in response to an auditory stimulus), by recording the EMG signals of the subjects' hands, it has been shown that unlike reaction time (premotor time), motor time is highly uncorrelated with the reaction time. Also, the same study reported that the mean range of the MT is something between 38 milliseconds and 42 milliseconds (Botwinick & Thompson, 1966). Thus, considering the average time lapse needed for pushing the button and the complexity of our task which begets a long RT (approximately 1 second), our approximation is rendered sufficiently feasible.

Applications of the Extended Descriptive Risk-averse Bayesian Model

As a functioning simulator, the present simulation model could have multiple usages. One that has attracted the attention of the industry is that this virtual brain model could help to predict the impact of the lens-induced distortions, caused by various lens designs, on human decision-making.

Therefore, the producers of ophthalmic lenses would be able to evaluate and estimate the impact of their designs on real-life situations in advance. An example of such situations is to determine if the person approaching from straight ahead goes to the left or right of the observer in order to avoid a collision or to detect more subtle movements. This application could be accomplished by inserting the lens design model between the biological motion stimulus and the simulation model as presented in the figure below. By implementing the process before the production, the lens manufacturer could spare a large part of the expenses and time that is typically invested into the assessment stage.

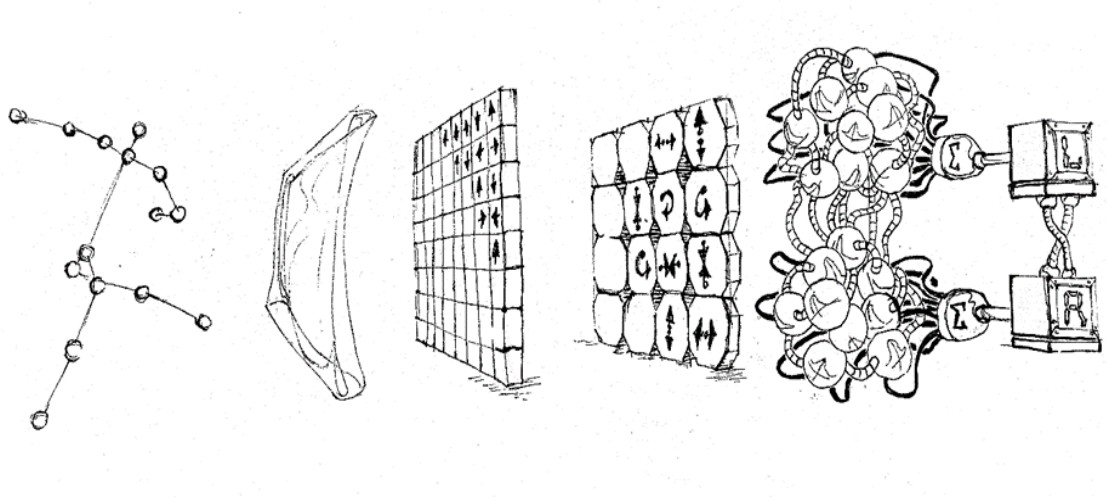

Figure04-2 : From left to right: animated visual input, the lens design model, local motion detection layer, opponent motion detection layer, global pattern detection layer, complete biological motion detection layer

As a proof of concept, a 2.3 dioptre barrel-type distortion has been imposed on the soccer kick biological motion stimulus as a visual input to the simulation model tuned to two participants from our subject pool. Below, one can see the change in the thresholds and the slopes of the psychometric functions of these subjects:

- subject B03's threshold of 9.3° alters to 17.9° moreover, its slope of 0.12 becomes 0.06
- subject A05's threshold of 10.7° alters to 42.3° moreover, its slope of 0.11 becomes 0.013

Moreover, there exist several other applications like in robotic vision for recognition of human gestures, surveillance systems for specification determination and in sports, for monitoring the performance and, finally, in motion-based tracking systems.

To conclude, to have a virtual brain in order to determine the impact of ophthalmic lens designs on decision-making outcomes for socially relevant actions unlocks possibilities that are not presently accessible. The presently existing limitations of the simulation model are related to the type of action we have studied. However, using more data, it could be extended to numerous human actions of interest in the future.

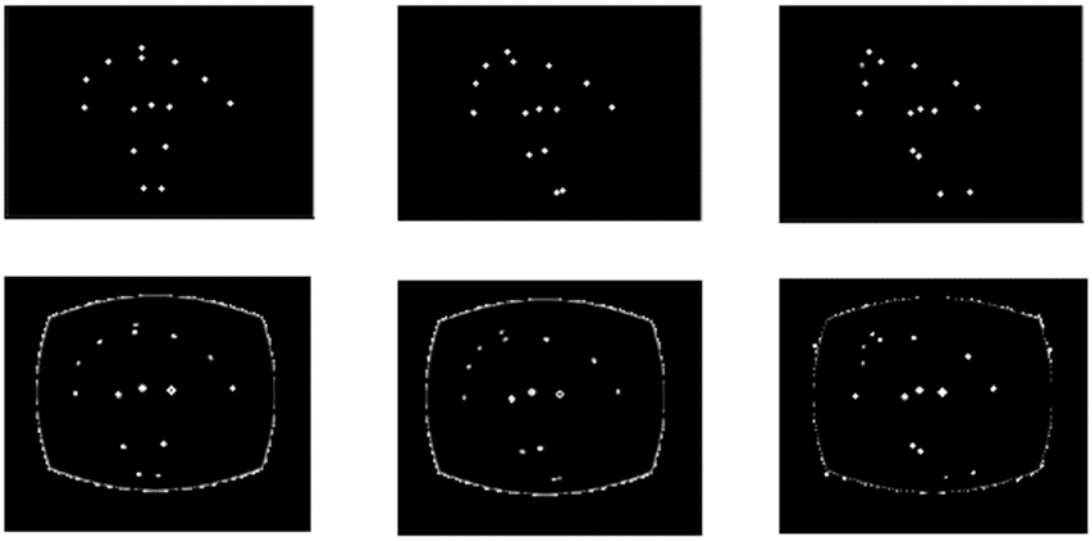

Figure 4-3 : Above are three frames from one stimulus and below are the corresponding aberrated frame with barrel aberration of 2.3 diopters

References

Albantakis, L., & Deco, G. (2009). The encoding of alternatives in multiple-choice decision-making. *BMC Neuroscience, 10*(1), P166.

Albright, T. D. (1993). Cortical processing of visual motion. *Rev Oculomot Res, 5*, 177-201.

Allais, M., & Hagen, G. (2013). *Expected Utility Hypotheses and the Allais Paradox: Contemporary Discussions of the decisions under uncertainty with Allais' Rejoinder* (Vol. 21): Springer Science & Business Media.

Allman, J., Miezin, F., & McGuinness, E. (1985). Direction-and velocity-specific responses from beyond the classical receptive field in the middle temporal visual area (MT). *Perception, 14*(2), 105-126.

Bardi, L., Regolin, L., & Simion, F. (2011). Biological motion preference in humans at birth: role of dynamic and configural properties. *Developmental science, 14*(2), 353-359.

Basso, M. A., & Wurtz, R. H. (1997). Modulation of neuronal activity by target uncertainty. *Nature, 389*(6646), 66.

Basso, M. A., & Wurtz, R. H. (1998). Modulation of neuronal activity in superior colliculus by changes in target probability. *Journal of Neuroscience, 18*(18), 7519-7534.

Bastos, A. M., Usrey, W. M., Adams, R. A., Mangun, G. R., Fries, P., & Friston, K. J. (2012). Canonical microcircuits for predictive coding. *Neuron, 76*(4), 695-711.

Beintema, J. A., & Lappe, M. (2002). Perception of biological motion without local image motion. *Proceedings of the National Academy of Sciences, 99*(8), 5661-5663. doi:10.1073/pnas.082483699

Bichot, N. P., & Schall, J. D. (1999). Saccade target selection in macaque during feature and conjunction visual search. *Visual neuroscience, 16*(1), 81-89.

Bitzer, S., Park, H., Blankenburg, F., & Kiebel, S. J. (2014). Perceptual decision making: drift-diffusion model is equivalent to a Bayesian model. *Frontiers in Human Neuroscience, 8*, 102.

Blake, R., & Shiffrar, M. (2007). Perception of human motion. *Annu Rev Psychol, 58*, 47-73. doi:10.1146/annurev.psych.57.102904.190152

Bogacz, R., Brown, E., Moehlis, J., Holmes, P., & Cohen, J. D. (2006). The physics of optimal decision making: a formal analysis of models of performance in two-alternative forced-choice tasks. *Psychological review, 113*(4), 700.

Bogacz, R., Wagenmakers, E.-J., Forstmann, B. U., & Nieuwenhuis, S. (2010). The neural basis of the speed–accuracy tradeoff. *Trends in neurosciences, 33*(1), 10-16.

Bollimunta, A., & Ditterich, J. (2011). Local computation of decision-relevant net sensory evidence in parietal cortex. *Cerebral cortex, 22*(4), 903-917.

Botwinick, J., & Thompson, L. W. (1966). Premotor and motor components of reaction time. *Journal of Experimental Psychology, 71*(1), 9-15. doi:10.1037/h0022634

Boussaoud, D., & Wise, S. (1993). Primate frontal cortex: effects of stimulus and movement. *Experimental Brain Research, 95*(1), 28-40.

Braun, D. A., Nagengast, A. J., & Wolpert, D. (2011). Risk-sensitivity in sensorimotor control. *Frontiers in Human Neuroscience, 5*, 1.

Britten, K. H., Shadlen, M. N., Newsome, W. T., & Movshon, J. A. (1992). The analysis of visual motion: a comparison of neuronal and psychophysical performance. *Journal of Neuroscience, 12*(12), 4745-4765.

Britten, K. H., Shadlen, M. N., Newsome, W. T., & Movshon, J. A. (1993). Responses of neurons in macaque MT to stochastic motion signals. *Visual neuroscience, 10*(6), 1157-1169.
Brockmann, E. N., & Anthony, W. P. (2002). Tacit Knowledge and Strategic Decision Making. *Group & Organization Management, 27*(4), 436-455. doi:10.1177/1059601102238356
Bruce, C. J., & Goldberg, M. E. (1985). Primate frontal eye fields. I. Single neurons discharging before saccades. *Journal of neurophysiology, 53*(3), 603-635.
Carpenter, R. H., & Williams, M. (1995). Neural computation of log likelihood in control of saccadic eye movements. *Nature, 377*(6544), 59.
Casile, A., & Giese, M. A. (2005). Critical features for the recognition of biological motion. *Journal of Vision, 5*(4), 6-6. doi:10.1167/5.4.6
Cattell, R. B. (1963). Theory of fluid and crystallized intelligence: A critical experiment. *Journal of educational psychology, 54*(1), 1.
Chang, D. H., & Troje, N. F. (2008). The local inversion effect in biological motion perception is acceleration-based. *Journal of Vision, 8*(6), 911-911.
Churchland, A. K., Kiani, R., & Shadlen, M. N. (2008). Decision-making with multiple alternatives. *Nat Neurosci, 11*(6), 693.
Colby, C. L., & Goldberg, M. E. (1999). Space and attention in parietal cortex. *Annu Rev Neurosci, 22*(1), 319-349.
Commons, W. (2017). File: Drift Diffusion Model Unbiased Source Decision Making Examples.png --- Wikimedia Commons{,} the free media repository. Retrieved from "https://commons.wikimedia.org/w/index.php?title=File:Drift_Diffusion_Model_Unbiased_Source_Decision_Making_Examples.png&oldid=254788499". "https://commons.wikimedia.org/w/index.php?title=File:Drift_Diffusion_Model_Unbiased_Source_Decision_Making_Examples.png&oldid=254788499"
Commons, W. (2018). File: Marr's Levels of Analysis.svg --- Wikimedia Commons{,} the free media repository.
Coombes, S. (2010). Large-scale neural dynamics: simple and complex. *NeuroImage, 52*(3), 731-739.
Cowan, N. (1998). *Attention and memory: An integrated framework* (Vol. 26): Oxford University Press.
Creutzfeldt, O. D. (1977). Generality of the functional structure of the neocortex. *Naturwissenschaften, 64*(10), 507-517.
Dayan, P., & Niv, Y. (2008). Reinforcement learning: the good, the bad and the ugly. *Current Opinion in Neurobiology, 18*(2), 185-196.
Decety, J., & Grèzes, J. (1999). Neural mechanisms subserving the perception of human actions. *Trends in cognitive sciences, 3*(5), 172-178.
Deneve, S., Latham, P. E., & Pouget, A. (1999). Reading population codes: a neural implementation of ideal observers. *Nat Neurosci, 2*(8), 740.
Denève, S., & Machens, C. K. (2016). Efficient codes and balanced networks. *Nat Neurosci, 19*(3), 375.
Diedrichsen, J., & Kriegeskorte, N. (2017). Representational models: A common framework for understanding encoding, pattern-component, and representational-similarity analysis. *PLoS computational biology, 13*(4), e1005508.
Ding, L., & Gold, J. I. (2012). Separate, causal roles of the caudate in saccadic choice and execution in a perceptual decision task. *Neuron, 75*(5), 865-874.

Dobransky, P. (1999). *Mind OS: The Operating system of the Human Mind*
Dorris, M. C., & Munoz, D. P. (1998). Saccadic probability influences motor preparation signals and time to saccadic initiation. *Journal of Neuroscience, 18*(17), 7015-7026.
Fitts, P. M. (1966). Cognitive aspects of information processing: III. Set for speed versus accuracy. *Journal of Experimental Psychology, 71*(6), 849.
Forstmann, B. U., Anwander, A., Schäfer, A., Neumann, J., Brown, S., Wagenmakers, E.-J., . . . Turner, R. (2010). Cortico-striatal connections predict control over speed and accuracy in perceptual decision making. *Proceedings of the National Academy of Sciences, 107*(36), 15916-15920.
Frank, M. J. (2006). Hold your horses: a dynamic computational role for the subthalamic nucleus in decision making. *Neural Networks, 19*(8), 1120-1136.
Furman, M., & Wang, X.-J. (2008). Similarity effect and optimal control of multiple-choice decision making. *Neuron, 60*(6), 1153-1168.
Gawne, T. J., & Martin, J. M. (2002). Responses of primate visual cortical neurons to stimuli presented by flash, saccade, blink, and external darkening. *Journal of neurophysiology, 88*(5), 2178-2186.
Giese, M. A., & Poggio, T. (2003). Neural mechanisms for the recognition of biological movements. *Nat Rev Neurosci, 4*(3), 179-192. doi:http://www.nature.com/nrn/journal/v4/n3/suppinfo/nrn1057_S1.html
Gilaie-Dotan, S., Saygin, A. P., Lorenzi, L. J., Rees, G., & Behrmann, M. (2015). Ventral aspect of the visual form pathway is not critical for the perception of biological motion. *Proceedings of the National Academy of Sciences, 112*(4), E361-E370.
Gold, J. I., & Shadlen, M. N. (2000). Representation of a perceptual decision in developing oculomotor commands. *Nature, 404*(6776), 390.
Gold, J. I., & Shadlen, M. N. (2001). Neural computations that underlie decisions about sensory stimuli. *Trends in cognitive sciences, 5*(1), 10-16.
Gold, J. I., & Shadlen, M. N. (2007). The neural basis of decision making. *Annu. Rev. Neurosci., 30*, 535-574.
Gottfredson, L. S. (1997). Mainstream science on intelligence: An editorial with 52 signatories, history, and bibliography. In: Citeseer.
Graham, N. V. S. (1989). *Visual pattern analyzers* (Vol. 16): Oxford University Press.
Green, D. M., & Swets, J. A. (1966). *Signal detection theory and psychophysics* (Vol. 1): Wiley New York.
Green, N., Biele, G. P., & Heekeren, H. R. (2012). Changes in neural connectivity underlie decision threshold modulation for reward maximization. *Journal of Neuroscience, 32*(43), 14942-14950.
Grosbras, M. H., Beaton, S., & Eickhoff, S. B. (2012). Brain regions involved in human movement perception: A quantitative voxel-based meta-analysis. *Human brain mapping, 33*(2), 431-454.
Grossman, E., Donnelly, M., Price, R., Pickens, D., Morgan, V., Neighbor, G., & Blake, R. (2000). Brain areas involved in perception of biological motion. *Journal of cognitive neuroscience, 12*(5), 711-720.
Heitz, R. P., & Schall, J. D. (2012). Neural mechanisms of speed-accuracy tradeoff. *Neuron, 76*(3), 616-628.
Hill, E. L. (2004). Executive dysfunction in autism. *Trends in cognitive sciences, 8*(1), 26-32.

Hosenbocus, S., & Chahal, R. (2012). A review of executive function deficits and pharmacological management in children and adolescents. *Journal of the Canadian Academy of Child*
Adolescent Psychiatry
21(3), 223.
Johansson, G. (1973). Visual perception of biological motion and a model for its analysis. *Perception & psychophysics, 14*(2), 201-211.
Johnson, K. (1980a). Sensory discrimination: decision process. *Journal of neurophysiology, 43*(6), 1771-1792.
Johnson, K. (1980b). Sensory discrimination: neural processes preceding discrimination decision. *Journal of neurophysiology, 43*(6), 1793-1815.
Jung, Y., & Hu, J. (2015). AK-fold averaging cross-validation procedure. *Journal of nonparametric statistics, 27*(2), 167-179.
Kable, J. W., & Glimcher, P. W. (2009). The neurobiology of decision: consensus and controversy. *Neuron, 63*(6), 733-745.
Kahneman, D., & Tversky, A. (2013). Prospect theory: An analysis of decision under risk. In *Handbook of the fundamentals of financial decision making: Part I* (pp. 99-127): World Scientific.
Kim, J. N., & Shadlen, M. N. (1999). Neural correlates of a decision in the dorsolateral prefrontal cortex of the macaque. *Nat Neurosci, 2*(2), 176.
Kosinski, R. J. (2008). A literature review on reaction time. *Clemson University, 10*.
Kourtzi, Z., Krekelberg, B., & Van Wezel, R. J. (2008). Linking form and motion in the primate brain. *Trends in cognitive sciences, 12*(6), 230-236.
Kriegeskorte, N. (2015). Deep neural networks: a new framework for modeling biological vision and brain information processing. *Annual review of vision science, 1*, 417-446.
Kriegeskorte, N., & Douglas, P. K. (2018). Cognitive computational neuroscience. *Nat Neurosci*, 1.
Lampl, I., Ferster, D., Poggio, T., & Riesenhuber, M. (2004). Intracellular measurements of spatial integration and the MAX operation in complex cells of the cat primary visual cortex. *Journal of neurophysiology, 92*(5), 2704-2713.
Lo, C.-C., & Wang, X.-J. (2006). Cortico–basal ganglia circuit mechanism for a decision threshold in reaction time tasks. *Nat Neurosci, 9*(7), 956.
Lugo, J. E., Mejia-Romero, S., Doti, R., Ray, K., Kothari, S. L., Withers, G. S., & Faubert, J. (2018). A simple dynamic model that accounts for regulation of neuronal polarity. *Journal of Integrative Neuroscience, 17*(4).
Marr, D. (1982). Vision: A computational investigation into the human representation and processing of visual information.
Marr, D., & Poggio, T. (1976). From understanding computation to understanding neural circuitry.
Martinez-Conde, S., Macknik, S. L., & Hubel, D. H. (2004). The role of fixational eye movements in visual perception. *Nature Reviews Neuroscience, 5*(3), 229.
Mather, G., Radford, K., & West, S. (1992). Low-Level Visual Processing of Biological Motion. *Proceedings of the Royal Society of London. Series B: Biological Sciences, 249*(1325), 149-155. doi:10.1098/rspb.1992.0097
Mayo, J. P., & Smith, M. A. (2017). Neuronal Adaptation: Tired Neurons or Wired Networks? *Trends in neurosciences, 40*(3), 127-128.

McCullock, J. (2012). A Painless Q-Learning Tutorial. Retrieved from http://mnemstudio.org/path-finding-q-learning-tutorial.htm

Miller, E. K., Erickson, C. A., & Desimone, R. (1996). Neural mechanisms of visual working memory in prefrontal cortex of the macaque. *Journal of Neuroscience, 16*(16), 5154-5167.

Mineiro, P., & Zipser, D. (1998). Analysis of direction selectivity arising from recurrent cortical interactions. *Neural Computation, 10*(2), 353-371.

Misaghian, K., Lugo, J. E., & Faubert, J. (2018). *Descriptive risk-averse Bayesian decision-making" as a model for complex biological motion perception in the human dorsal pathway*. In preparation.

Moran, R. J., Pinotsis, D. A., & Friston, K. J. (2013). Neural masses and fields in dynamic causal modeling. *Frontiers in computational neuroscience, 7*, 57.

Mountcastle, V. B., Talbot, W. H., Sakata, H., & Hyvärinen, J. (1969). Cortical neuronal mechanisms in flutter-vibration studied in unanesthetized monkeys. Neuronal periodicity and frequency discrimination. *Journal of neurophysiology, 32*(3), 452-484.

Nagengast, A. J., Braun, D. A., & Wolpert, D. M. (2010). Risk-sensitive optimal feedback control accounts for sensorimotor behavior under uncertainty. *PLoS computational biology, 6*(7), e1000857.

Nayebi, A., Bear, D., Kubilius, J., Kar, K., Ganguli, S., Sussillo, D., . . . Yamins, D. L. (2018). *Task-Driven convolutional recurrent models of the visual system.* Paper presented at the Advances in Neural Information Processing Systems.

Newell, A. (1994). *Unified theories of cognition*: Harvard University Press.

Newsome, W. T., & Pare, E. B. (1988). A selective impairment of motion perception following lesions of the middle temporal visual area (MT). *Journal of Neuroscience, 8*(6), 2201-2211.

Niv, Y., Edlund, J. A., Dayan, P., & O'Doherty, J. P. (2012). Neural prediction errors reveal a risk-sensitive reinforcement-learning process in the human brain. *Journal of Neuroscience, 32*(2), 551-562.

Oram, M. W., & Perrett, D. I. (1994). Responses of anterior superior temporal polysensory (STPa) neurons to "biological motion" stimuli. *Journal of cognitive neuroscience, 6*(2), 99-116.

Orban, G. A., Dupont, P., De Bruyn, B., Vogels, R., Vandenberghe, R., & Mortelmans, L. (1995). A motion area in human visual cortex. *Proceedings of the National Academy of Sciences, 92*(4), 993-997.

Orban, G. A., Lagae, L., Verri, A., Raiguel, S., Xiao, D., Maes, H., & Torre, V. (1992). First-order analysis of optical flow in monkey brain. *Proceedings of the National Academy of Sciences, 89*(7), 2595-2599.

Parker, A. J., & Newsome, W. T. (1998). Sense and the single neuron: probing the physiology of perception. *Annu Rev Neurosci, 21*(1), 227-277.

Perrett, D. I., Smith, P. A. J., Mistlin, A. J., Chitty, A. J., Head, A. S., Potter, D. D., . . . Jeeves, M. A. (1985). Visual analysis of body movements by neurones in the temporal cortex of the macaque monkey: a preliminary report. *Behavioural brain research, 16*(2-3), 153-170.

Platt, M. L., & Glimcher, P. W. (1999). Neural correlates of decision variables in parietal cortex. *Nature, 400*(6741), 233.

Poggio, T. (2012). The levels of understanding framework, revised. *Perception, 41*(9), 1017-1023.
Poldrack, R. A. (2006). Can cognitive processes be inferred from neuroimaging data? *Trends in cognitive sciences, 10*(2), 59-63.
Purcell, S. W., Hair, C. A., & Mills, D. J. (2012). Sea cucumber culture, farming and sea ranching in the tropics: Progress, problems and opportunities. *Aquaculture, 368*, 68-81.
Ratcliff, R., & McKoon, G. (2008). The diffusion decision model: theory and data for two-choice decision tasks. *Neural computation, 20*(4), 873-922.
Recanzone, G. H., Guard, D. C., & Phan, M. L. (2000). Frequency and intensity response properties of single neurons in the auditory cortex of the behaving macaque monkey. *Journal of neurophysiology, 83*(4), 2315-2331.
Riesenhuber, M., & Poggio, T. (1999). Hierarchical models of object recognition in cortex. *Nat Neurosci, 2*(11), 1019.
Roitman, J. D., & Shadlen, M. N. (2002). Response of neurons in the lateral intraparietal area during a combined visual discrimination reaction time task. *Journal of Neuroscience, 22*(21), 9475-9489.
Romeas, T., & Faubert, J. (2015). Soccer athletes are superior to non-athletes at perceiving soccer-specific and non-sport specific human biological motion. *Frontiers in Psychology, 6*, 1343. doi:10.3389/fpsyg.2015.01343
Romeas, T., Guldner, A., & Faubert, J. (2016). 3D-Multiple Object Tracking training task improves passing decision-making accuracy in soccer players. *Psychology of Sport and Exercise, 22*, 1-9. doi:http://dx.doi.org/10.1016/j.psychsport.2015.06.002
Romo, R., Brody, C. D., Hernández, A., & Lemus, L. (1999). Neuronal correlates of parametric working memory in the prefrontal cortex. *Nature, 399*(6735), 470.
Romo, R., Hernández, A., Zainos, A., Brody, C. D., & Lemus, L. (2000). Sensing without touching: psychophysical performance based on cortical microstimulation. *Neuron, 26*(1), 273-278.
Romo, R., Hernández, A., Zainos, A., & Salinas, E. (1998). Somatosensory discrimination based on cortical microstimulation. *Nature, 392*(6674), 387.
Ross, D. A., & Martin, A. (2006). The origin of mind: Evolution of brain, cognition, and general intelligence. *American Journal of Psychiatry, 163*(9), 1652-1653.
Roxin, A., & Ledberg, A. (2008). Neurobiological models of two-choice decision making can be reduced to a one-dimensional nonlinear diffusion equation. *PLoS computational biology, 4*(3), e1000046.
Rubenstein, J., & Merzenich, M. M. (2003). Model of autism: increased ratio of excitation/inhibition in key neural systems. *Genes, Brain and Behavior, 2*(5), 255-267.
Salzman, C. D., Murasugi, C. M., Britten, K. H., & Newsome, W. T. (1992). Microstimulation in visual area MT: effects on direction discrimination performance. *Journal of Neuroscience, 12*(6), 2331-2355.
Sanders, J. I., Hangya, B., & Kepecs, A. (2016). Signatures of a statistical computation in the human sense of confidence. *Neuron, 90*(3), 499-506.
Saygin, A. P. (2012). Sensory and motor brain areas supporting biological motion perception: Neuropsychological and neuroimaging studies. 371-389.
Schall, J. D. (2001). Neural basis of deciding, choosing and acting. *Nature Reviews Neuroscience, 2*(1), 33.

Schall, J. D., & Bichot, N. P. (1998). Neural correlates of visual and motor decision processes. *Current Opinion in Neurobiology, 8*(2), 211-217.
Schmitz, N., Daly, E., & Murphy, D. (2007). Frontal anatomy and reaction time in Autism. *Neuroscience Letters, 412*(1), 12-17.
Schoemaker, P. J. (1982). The expected utility model: Its variants, purposes, evidence and limitations. *Journal of economic literature*, 529-563.
Schultz, W. (2002). Getting formal with dopamine and reward. *Neuron, 36*(2), 241-263.
Schultz, W., Dayan, P., & Montague, P. R. (1997). A neural substrate of prediction and reward. *Science, 275*(5306), 1593-1599.
Scolari, M., Byers, A., & Serences, J. T. (2012). Optimal deployment of attentional gain during fine discriminations. *Journal of Neuroscience, 32*(22), 7723-7733.
Seung, H. S., & Sompolinsky, H. (1993). Simple models for reading neuronal population codes. *Proceedings of the National Academy of Sciences, 90*(22), 10749-10753.
Shadlen, M. N., & Kiani, R. (2013). Decision making as a window on cognition. *Neuron, 80*(3), 791-806.
Shadlen, M. N., & Newsome, W. T. (1996). Motion perception: seeing and deciding. *Proceedings of the National Academy of Sciences, 93*(2), 628-633.
Shen, Y. (2015). *Risk-sensitive Markov Decision Processes.* (doctor rerum naturalium). Technischen Universität Berlin,
Shen, Y., Tobia, M. J., Sommer, T., & Obermayer, K. (2014). Risk-sensitive reinforcement learning. *Neural computation, 26*(7), 1298-1328.
Simen, P. (2012). Evidence accumulator or decision threshold–which cortical mechanism are we observing? *Frontiers in Psychology, 3*, 183.
Simen, P., Cohen, J. D., & Holmes, P. (2006). Rapid decision threshold modulation by reward rate in a neural network. *Neural Networks, 19*(8), 1013-1026.
Smith, A. T., & Snowden, R. J. (1994). *Visual detection of motion*: Academic Press.
Smith, P. L., & Ratcliff, R. (2004). Psychology and neurobiology of simple decisions. *Trends in neurosciences, 27*(3), 161-168.
Snyder, L. H., Batista, A. P., & Andersen, R. A. (2000). Intention-related activity in the posterior parietal cortex: a review. *Vision research, 40*(10-12), 1433-1441.
Sporns, O. (2007). Brain connectivity. *Scholarpedia, 2*, 4695. Retrieved from http://www.scholarpedia.org/article/Brain_connectivity
Standage, D., Blohm, G., & Dorris, M. C. (2014). On the neural implementation of the speed-accuracy trade-off. *Frontiers in neuroscience, 8*, 236.
Standage, D., & Paré, M. (2011). Persistent storage capability impairs decision making in a biophysical network model. *Neural Networks, 24*(10), 1062-1073.
Stephan, K. E., & Friston, K. J. (2010). Analyzing effective connectivity with functional magnetic resonance imaging. *Wiley Interdisciplinary Reviews: Cognitive Science, 1*(3), 446-459.
Surma, G. (2018). Cartpole - Introduction to Reinforcement Learning (DQN - Deep Q-Learning). Retrieved from towardsdatascience.com/cartpole-introduction-to-reinforcement-learning-ed0eb5b58288
Tanaka, K., & Saito, H. A. (1989). Analysis of motion of the visual field by direction, expansion/contraction, and rotation cells clustered in the dorsal part of the medial superior temporal area of the macaque monkey. *Journal of neurophysiology, 62*(3), 626-641.

Taoka, G. T. (1989). Brake reaction times of unalerted drivers. *ITE journal, 59*(3), 19-21.
Theodoni, P., Kovács, G., Greenlee, M. W., & Deco, G. (2011). Neuronal adaptation effects in decision making. *Journal of Neuroscience, 31*(1), 234-246.
Theodoridis, S. (2010). *Introduction to pattern recognition : a MATLAB approach*. Amsterdam: Academic Press.
Thurman, S. M., & Lu, H. (2014). Bayesian integration of position and orientation cues in perception of biological and non-biological forms. *Frontiers in Human Neuroscience, 8*, 91. doi:10.3389/fnhum.2014.00091
Troje, N. F., & Westhoff, C. (2006). The inversion effect in biological motion perception: Evidence for a "life detector"? *Current Biology, 16*(8), 821-824.
Tullo, D., Faubert, J., & Bertone, A. (2018). The characterization of attention resource capacity and its relationship with fluid reasoning intelligence: a multiple object tracking study. *Intelligence, 69*, 158-168.
Usher, M., & McClelland, J. L. (2001). The time course of perceptual choice: the leaky, competing accumulator model. *Psychological review, 108*(3), 550.
Vaina, L. M., Solomon, J., Chowdhury, S., Sinha, P., & Belliveau, J. W. (2001). Functional neuroanatomy of biological motion perception in humans. *Proceedings of the National Academy of Sciences*
98(20), 11656-11661.
Vallortigara, G., Regolin, L., & Marconato, F. (2005). Visually inexperienced chicks exhibit spontaneous preference for biological motion patterns. *PLoS biology, 3*(7), e208.
Von Neumann, J., Morgenstern, O., & Kuhn, H. W. (2007). *Theory of games and economic behavior (commemorative edition)*: Princeton university press.
Wang, X. J. (2002). Probabilistic decision making by slow reverberation in cortical circuits. *Neuron, 36*(5), 955-968.
Wang, X. J. (2008). Decision making in recurrent neuronal circuits. *Neuron, 60*(2), 215-234.
Wang, X. J. (2012). Neural dynamics and circuit mechanisms of decision-making. *Current Opinion in Neurobiology, 22*(6), 1039-1046.
Whitwell, R. L., Milner, A. D., & Goodale, M. A. (2015). The two visual systems hypothesis: new challenges and insights from visual form agnosic patient DF. *Arm and Hand Movement: Current Knowledge and Future Perspective, 5*(255), 98.
Wickelgren, W. A. (1977). Speed-accuracy tradeoff and information processing dynamics. *Acta psychologica, 41*(1), 67-85.
Wilson, H. R. (1999). Spikes, decisions, and actions: the dynamical foundations of neurosciences.
Wong, A. L., Haith, A. M., & Krakauer, J. W. (2015). Motor planning. *The Neuroscientist, 21*(4), 385-398.

Annex I: Model Outputs for Ranges of All Parameters

As the output of the model, the angular threshold, the slope and the reaction time has been computed for different ranges of parameters, $k, \tau \; and \; \delta$, the model has been run for a constant parameter value of $\tau_a = 1.22 \; sec$. In the tables below "SD" is the standard deviation of the internal noise (δ), "Tau" is the time constant (τ), "k" is the inhibitory feedback gain (k) and "TauA" is the time when adaptation starts (τ_a). The outputs are for the rotation-off condition unless indicated otherwise.

Threshold						
SD=0.28						
k/Tau	0.0238	0.024	0.025	0.03	0.033	0.037
2		9.197664	5.336503	5.04255	4.840897	4.744169
4		10.6964	5.651746	5.490651	5.182649	5.096875
8	16.85817	12.31467	6.486838	5.996146	5.737578	5.665996
16		14.28962	7.72746	7.254823	7.023524	6.815714
32		13.93415	9.692215	9.212861	8.737363	8.361226
Slope						
SD=0.28						
k/Tau	0.0238	0.024	0.025	0.03	0.033	0.037
2		0.113052	0.254628	0.284279	0.311952	0.333829
4		0.098356	0.244615	0.26296	0.294649	0.321853
8	0.06408	0.090725	0.213841	0.255491	0.262199	0.2982
16		0.08876	0.19051	0.215353	0.231348	0.24347
32		0.107469	0.170732	0.184602	0.200075	0.210914
RT						
SD=0.28	TauA=1.22					
k/Tau	0.0238	0.024	0.025	0.03	0.033	0.037
2		1.353221	1.026973	1.022712	1.032164	1.042237
4		1.497359	1.01993	1.006413	1.018348	1.029181
8	2.07263	1.848327	1.015681	0.988631	1.000207	1.00965
16		2.353995	1.022339	0.962445	0.97369	0.986381
32		2.726345	1.08692	0.939905	0.951588	0.963768

Threshold

SD=0.30

k/Tau	0.0238	0.024	0.025	0.03	0.033	0.037
2		9.818355	5.572589	5.276817	5.200037	5.024327
4	15.52754	10.95955	5.963591	5.597452	5.58571	5.425188
8	18.03722	13.96506	6.827265	6.335999	6.145875	5.925539
16		14.72345	8.299454	7.686642	7.399865	6.964347
32		14.88309	10.18108	9.309029	9.035201	8.910117

Slope

SD=0.30

k/Tau	0.0238	0.024	0.025	0.03	0.033	0.037
2		0.101679	0.231018	0.256602	0.277914	0.292677
4	0.067909	0.095588	0.221492	0.256027	0.253839	0.279148
8	0.060368	0.081558	0.197813	0.217659	0.237907	0.270065
16		0.08605	0.177634	0.197	0.211577	0.239028
32		0.098457	0.160104	0.178489	0.188514	0.190639

RT

SD=0.30 TauA=1.22

k/Tau	0.0238	0.024	0.025	0.03	0.033	0.037
2		1.374671	1.02771	1.018876	1.029551	1.038786
4	1.745106	1.529833	1.021327	1.00599	1.014472	1.025188
8	2.15216	1.915206	1.015998	0.985379	0.994378	1.005593
16		2.432881	1.027326	0.956882	0.968061	0.980932
32		2.793	1.096267	0.937695	0.948128	0.959711

Threshold

SD=0.32

k/Tau	0.0238	0.024	0.025	0.03	0.033	0.037
2	13.77285	10.63042	5.948867	5.673493	5.447783	5.458618
4	17.82864	12.26712	6.44257	5.998894	5.752032	5.663438
8	19.79285	15.26717	7.262721	6.744773	6.556027	6.315479
16		15.86156	8.705413	7.952382	7.893298	7.528021
32		15.042	10.72309	10.10217	9.790671	9.399096

Slope

SD=0.32

k/Tau	0.0238	0.024	0.025	0.03	0.033	0.037
2	0.072913	0.10086	0.199398	0.228581	0.251764	0.259913
4	0.055488	0.085456	0.196842	0.230259	0.247588	0.253931
8	0.05645	0.071952	0.178734	0.198864	0.218022	0.231969
16		0.079999	0.162328	0.188988	0.194631	0.194631
32		0.096955	0.154813	0.157765	0.16814	0.17607

RT

SD=0.32	TauA=1.22					
k/Tau	0.0238	0.024	0.025	0.03	0.033	0.037
2	1.5673	1.397142	1.025497	1.016617	1.024827	1.034829
4	1.802622	1.575956	1.020388	1.001828	1.011001	1.023062
8	2.244682	1.997408	1.014841	0.980023	0.988714	1.000737
16		2.514902	1.029418	0.95435	0.962444	0.978297
32		2.841894	1.108206	0.932323	0.941686	0.954792

Threshold

SD=0.34

k/Tau	0.0234	0.0235	0.0238	0.024	0.025	0.03	0.033	0.037
0.5	26.04025046				6.026699089			
1	31.05527662	22.94449074						
2			15.86212919	12.25782571	6.401044206	5.894937185	5.813227631	5.671442048
4			18.70755768	13.97207374	6.871074951	6.412694163	6.173939798	5.978884373
8			21.61145844	16.32418223	7.73404209	7.227720629	7.046449537	6.795070439
16				16.71376121	9.275310169	8.585520937	8.474794536	7.949813794
32				15.4491377	11.13088719	10.59331628	10.26492392	9.896368657
64				15.9493597	13.44320848	12.51420123	12.43958556	12.15062332

Slope

SD=0.34

k/Tau	0.0234	0.0235	0.0238	0.024	0.025	0.03	0.033	0.037
0.5	0.037786571				0.195469731			
1	0.031884199	0.043532551						
2			0.062134829	0.082699084	0.187360785	0.222609027	0.236419165	0.238308982
4			0.055887914	0.075268041	0.181560805	0.209892796	0.218916881	0.236060457
8			0.050748892	0.067899487	0.162471863	0.18830491	0.196393501	0.219149673
16				0.07423423	0.15139445	0.168538926	0.173152716	0.195031271
32				0.094809381	0.143633761	0.153896898	0.160483108	0.164625517
64				0.105170582	0.130740016	0.141374893	0.142660867	0.144270715

RT

SD=0.34 TauA=1.22

k/Tau	0.0234	0.0235	0.0238	0.024	0.025	0.03	0.033	0.037
0.5	1.798960938				1.033139757			
1	1.86449566	1.757355903						
2			1.596083333	1.434205729	1.025394097	1.013573785	1.022244792	1.034171007
4			1.844083333	1.622039063	1.019449653	0.996434028	1.006876736	1.019079861
8			2.315454861	2.069783854	1.01706684	0.976282118	0.986235243	0.996454861
16				2.581341146	1.032777778	0.948445313	0.960373264	0.97402691
32				2.876326389	1.120559896	0.927696181	0.936998264	0.951432292
64				2.886463542	1.271202257	0.919350694	0.929057292	0.937887153

Threshold		
SD=0.35		
k/Tau	0.0234	0.0235
0.5	35.41457	23.55513
1	34.75212	30.00713
2	46.73145	32.78787
4	51.85078	44.689
Slope		
SD=0.35		
k/Tau	0.0234	0.0235
0.5	0.026912	0.041811
1	0.028418	0.031384
2	0.021194	0.030766
4	0.019944	0.02279
RT		
SD=0.35		
k/Tau	0.0234	0.0235
0.5	1.840424	1.72482
1	1.913123	1.795263
2	2.065134	1.952413
4	2.379926	2.260973

Threshold				
SD=0.36				
k/Tau	0.0234	0.0235	0.0238	0.024
0.5	33.40041			
1	36.23791	25.79852		
2	40.76853	31.98546	16.75126	
4	59.43271	40.80413		14.17264
8				17.78255
Slope				
SD=0.36				
k/Tau	0.0234	0.0235	0.0238	0.024
0.5	0.029067			
1	0.028036	0.0387		
2	0.025078	0.032689	0.059942	
4	0.017576	0.025055		0.07571
8				0.062458

RT				
SD=0.36	TauA=1.22			
k/Tau	0.0234	0.0235	0.0238	0.024
0.5	1.85592			
1	1.944779	1.81361		
2	2.100295	1.970632	1.631792	
4	2.42594	2.277661		1.665456
8				2.131043

Threshold						
SD=0.37						
k/Tau	0.0234	0.0235	0.0238	0.024	0.025	0.03
0.5	32.91093					
1	47.91844	26.80331	15.67928			6.169073
2	48.62642	33.72745	17.54302			6.39065
4	69.3816	43.3165				
8						
16						9.280559
Slope						
SD=0.37						
k/Tau	0.0234	0.0235	0.0238	0.024	0.025	0.03
0.5	0.030125					
1	0.020417	0.037992	0.065093			0.205144
2	0.02086	0.030335	0.057043			0.193823
4	0.014459	0.023745				
8						
16						0.153828
RT						
SD=0.37	TauA=1.22					
k/Tau	0.0234	0.0235	0.0238	0.024	0.025	0.03
0.5	1.859872					
1	1.954814	1.826126	1.518168			1.017628
2	2.119239	1.988892	1.647724			1.008941
4	2.443091	2.313084				
8						
16						0.942225

Threshold							
SD=0.38							
k/Tau	0.0234	0.0235	0.0236	0.0238	0.025	0.03	0.033
0.5	32.51423				6.650587	6.386482	
1	36.65452	26.78533	23.58953	15.90159			6.418915
2	52.27162	33.75394	30.20205	19.10257			
4	73.01815	58.49941	33.43291	22.32362		7.194801	
Slope							
SD=0.38							
k/Tau	0.0234	0.0235	0.0236	0.0238	0.025	0.03	0.033
0.5	0.030962				0.179394	0.186303	
1	0.027708	0.039189	0.041185	0.061043			0.188688
2	0.019958	0.031139	0.033522	0.052846			
4	0.013925	0.016791	0.030452	0.048202		0.177758	
RT							
SD=0.38	TauA=1.22						
k/Tau	0.0234	0.0235	0.0236	0.0238	0.025	0.03	0.033
0.5	1.874886				1.032575	1.021787	
1	1.951345	1.831886	1.723938	1.530787			1.025449
2	2.146878	2.010883	1.893503	1.663383			
4	2.502425	2.36184	2.192076	1.971137		0.992323	

Threshold						
SD=0.028					ROTATION: ON	
k/Tau	0.023	0.024	0.025	0.03	0.033	0.037
2		8.422681				
4		9.550793		4.901833		
8		11.27742				
Slope						
SD=0.28						
k/Tau	0.023	0.024	0.025	0.03	0.033	0.037
2		0.140878				
4		0.121165		0.328095		
8		0.108359				
RT						
SD=0.28	TauA=1.22					
k/Tau	0.023	0.024	0.025	0.03	0.033	0.037
2		1.357878				
4		1.4912		1.010036		
8		1.781836				

Threshold						
SD=0.030					ROTATION:ON	
k/Tau	0.023	0.024	0.025	0.03	0.033	0.037
2		9.20318				
4						4.870994
8			6.105788			
16		13.36789				
Slope						
SD=0.30						
k/Tau	0.023	0.024	0.025	0.03	0.033	0.037
2		0.12729				
4						0.341674
8			0.238425			
16		0.092837				
RT						
SD=0.30	TauA=1.22					
k/Tau	0.023	0.024	0.025	0.03	0.033	0.037
2		1.381705				
4						1.027491
8			1.007914			
16		2.313459				

Threshold					
SD=0.032				ROTATION:ON	
k/Tau	0.023	0.025	0.03	0.033	0.037
2				5.036455	4.953634
4					
8				5.910174	
16					
32				8.556405	
Slope					
SD=0.32					
k/Tau	0.023	0.025	0.03	0.033	0.037
2				0.310352	0.324894
4					
8				0.25423	
16					
32				0.170468	
RT					
SD=0.32	TauA=1.22				
k/Tau	0.023	0.025	0.03	0.033	0.037
2				1.025159	1.035743
4					
8				0.994075	
16					
32				0.952406	

Threshold				
SD=0.034			ROTATION:ON	
k/Tau	0.023	0.024	0.025	0.03
2		10.1927		
4			6.098976	
8				6.541491
16		14.64847	8.214337	
32			10.53772	
Slope				
SD=0.34				
k/Tau	0.023	0.024	0.025	0.03
2		0.109074		
4			0.219381	
8				0.231781
16		0.082493	0.164951	
32			0.127072	

RT				
SD=0.34	TauA=1.22			
k/Tau	0.023	0.024	0.025	0.03
2		1.433964		
4			1.013773	
8				0.997075
16		2.493138	1.030563	
32			1.118101	

Annex II: Models Schematics

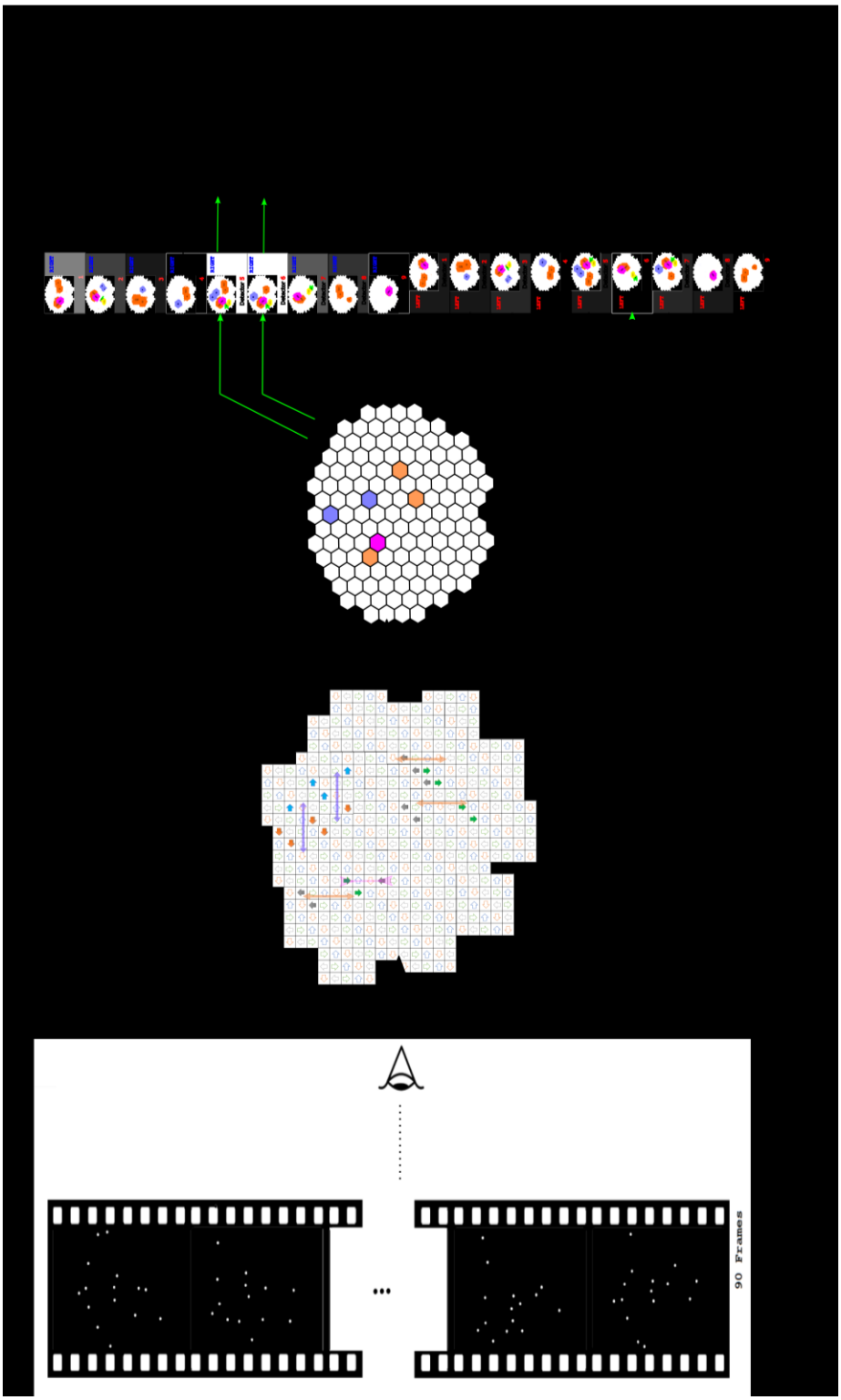

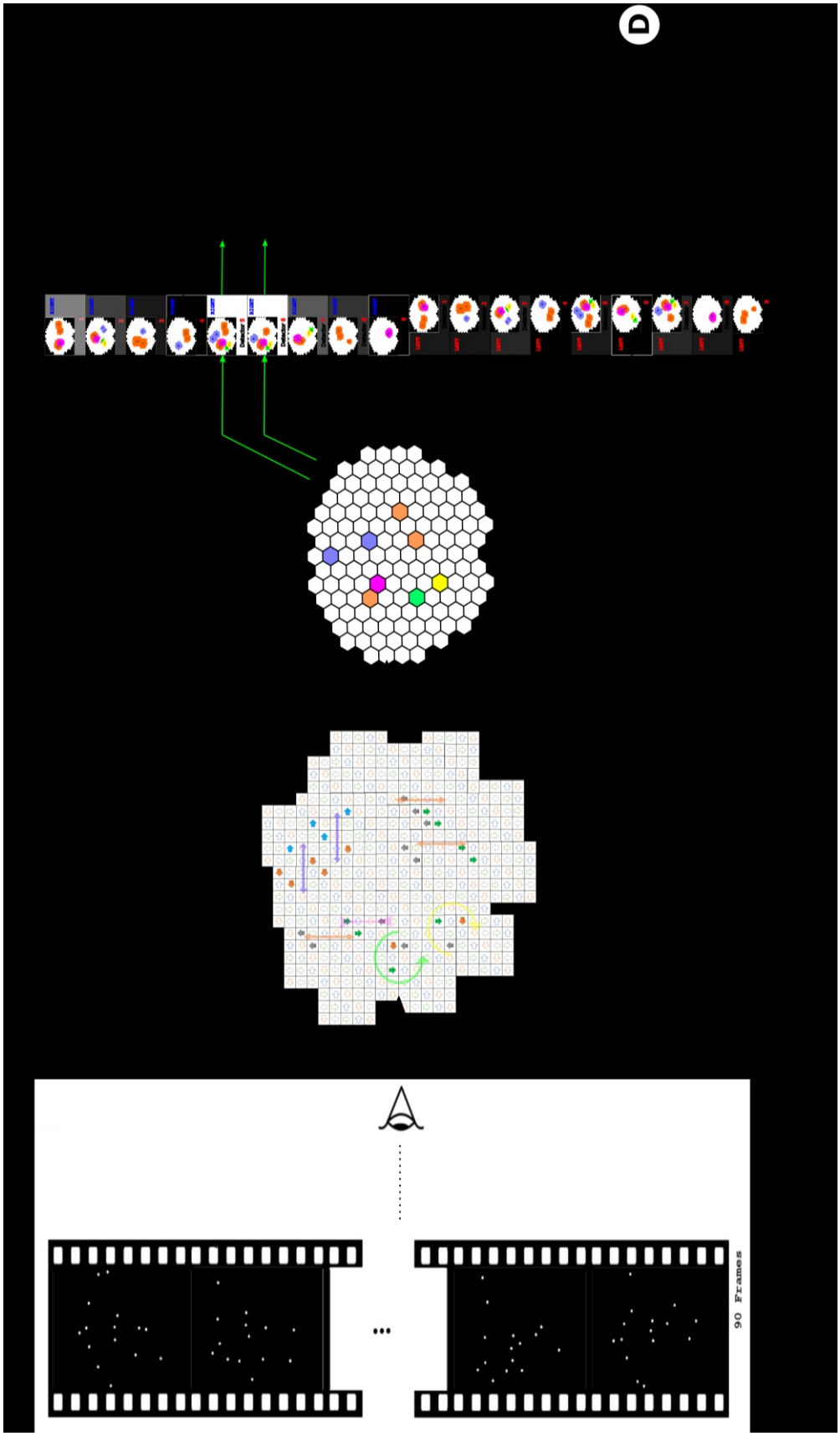
90 Frames